Graduate School ETD Form 9
(Revised 12/07)

PURDUE UNIVERSITY
GRADUATE SCHOOL
Thesis/Dissertation Acceptance

This is to certify that the thesis/dissertation prepared

By Sina Hamzehlouia

Entitled

MODELING AND CONTROL OF HYDRAULIC WIND ENERGY TRANSFERS

For the degree of Master of Science in Mechanical Engineering

Is approved by the final examining committee:

Dr. Afshin Izadian
Chair

Dr. Sohel Anwar

Dr. Tamer Wasfy

To the best of my knowledge and as understood by the student in the *Research Integrity and Copyright Disclaimer (Graduate School Form 20)*, this thesis/dissertation adheres to the provisions of Purdue University's "Policy on Integrity in Research" and the use of copyrighted material.

Approved by Major Professor(s): Dr. Afshin Izadian

Dr. Sohel Anwar

Approved by: Dr. Sohel Anwar 04/12/2012
Head of the Graduate Program Date

Graduate School Form 20
(Revised 9/10)

PURDUE UNIVERSITY
GRADUATE SCHOOL

Research Integrity and Copyright Disclaimer

Title of Thesis/Dissertation:

MODELING AND CONTROL OF HYDRAULIC WIND ENERGY TRANSFERS

For the degree of Master of Science in Mechanical Engineering

I certify that in the preparation of this thesis, I have observed the provisions of *Purdue University Executive Memorandum No. C-22,* September 6, 1991, *Policy on Integrity in Research.**

Further, I certify that this work is free of plagiarism and all materials appearing in this thesis/dissertation have been properly quoted and attributed.

I certify that all copyrighted material incorporated into this thesis/dissertation is in compliance with the United States' copyright law and that I have received written permission from the copyright owners for my use of their work, which is beyond the scope of the law. I agree to indemnify and save harmless Purdue University from any and all claims that may be asserted or that may arise from any copyright violation.

Sina Hamzehlouia

Printed Name and Signature of Candidate

04/12/2012

Date (month/day/year)

*Located at http://www.purdue.edu/policies/pages/teach_res_outreach/c_22.html

MODELING AND CONTROL OF HYDRAULIC WIND ENERGY TRANSFERS

A Thesis
Submitted to the Faculty
of
Purdue University
by
Sina Hamzehlouia

In Partial Fulfillment of the
Requirements for the Degree
of
Master of Science in Mechanical Engineering

May 2012
Purdue University
Indianapolis, Indiana

To my father who has never failed to provide me financial and moral support, and for being a great source of motivation and inspiration.

To my mother who offered me unconditional love and support throughout the development of my academic skills.

To my brother who has always been by my side since the beginning of my studies.

ACKNOWLEDGEMENTS

I would like to thank Dr. Afshin Izadian for his endless academic and financial support during my research and study, and provisions above the academic contexts. I would like to thank Dr. Sohel Anwar for all his scientific and financial support during my studies. I would like to thank Ms. Ginger Lauderback, Ms. Valerie Lim Diemer, and Ms. Amanda Herrera for their continuous assistance with academic and administrative procedures. I would like to thank my committee members for their assistance and supervision in preparation of this thesis. Finally, I reserve special thanks for my family, for their boundless mental, emotional, and financial support during my hard work.

TABLE OF CONTENTS

Page

Page

LIST OF TABLES

LIST OF FIGURES

Figure Page

Figure Page

Figure Page

Figure Page

Figure Page

Figure Page

Figure Page

Appendix Figure Page

ABSTRACT

Hamzehlouia, Sina. M.S.M.E., Purdue University, May 2012. Modeling and Control of Hydraulic Wind Energy Transfers. Major Professors: Afshin Izadian and Sohel Anwar.

The harvested energy of wind can be transferred to the generators either through a gearbox or through an intermediate medium such as hydraulic fluids. In this method, high-pressure hydraulic fluids are utilized to collect the energy of single or multiple wind turbines and transfer it to a central generation unit. In this unit, the mechanical energy of the hydraulic fluid is transformed into electric energy. The prime mover of hydraulic energy transfer unit, the wind turbine, experiences the intermittent characteristics of wind. This energy variation imposes fluctuations on generator outputs and drifts their angular velocity from desired frequencies. Nonlinearities exist in hydraulic wind power transfer and are originated from discrete elements such as check valves, proportional and directional valves, and leakage factors of hydraulic pumps and motors. A thorough understanding of hydraulic wind energy transfer system requires mathematical expression of the system. This can also be used to analyze, design, and predict the behavior of large-scale hydraulic-interconnected wind power plants.

This thesis introduces the mathematical modeling and controls of the hydraulic wind energy transfer system. The obtained models of hydraulic energy transfer system are experimentally validated with the results from a prototype.

This research is classified into three categories. 1) A complete mathematical model of the hydraulic energy transfer system is illustrated in both ordinary differential equations and state-space representation. 2) An experimental prototype of the energy transfer system is built and used to study the behavior of the system in different operating configurations, and 3) Controllers are designed to address the problems associated with the wind speed fluctuation and reference angular velocity tracking.

The mathematical models of hydraulic energy transfer system are also validated with the simulation results from a SimHydraulics Toolbox of MATLAB/Simulink®. The models are also compared with the experimental data from the system prototype. The models provided in this thesis do consider the improved assessment of the hydraulic system operation and efficiency analysis for industrial level wind power application.

1. INTRODUCTION

1.1 Problem Statement

The utilization of renewable energies as an alternative for fossil fuels is emerging considerably due to the exhaustion and the environmental concerns of hydrocarbons [1], [2]. Potential sources of renewable energy available around the world, if harvested, can provide the entire power demand and eliminate the negative effects of fossil fuels [3]. Wind is considered a compelling source of renewable energy attributed to prevalent accessibility and infinitude of resources. Recent advancements in wind turbine manufacturing reduced production costs such that wind turbines can now become a major source of power for the world's demands [4] experiencing an expansion of 30% in wind energy application [5, 6]. However, the renewable energy harvesting technology has kept its traditional topology. The horizontal axis wind turbines (HAWT) consist of a rotor to convert the wind energy into rotating shaft [7]. This rotor is connected to a drivetrain, gearbox, and electric generator, which are integrated in a nacelle located at the top of towers. These components, specifically the variable speed gearbox, are expensive, bulky, and require regular maintenance, which keeps wind energy production expensive. Moreover, because the gearbox and generator are located at high height, high maintenance expenses are incurred. Furthermore, since gearboxes accommodate a considerable number of moving parts, more recurrent and pricey maintenance is expected

for worn out part replacement and lubricant degradation compensation. Moreover, while the typical expected lifetime of a utility wind turbine is 20 years, gearboxes require an overhaul within 5 to 7 years of operation, and their replacements could cost approximately 10% of the turbine cost [8].

In order to reduce the operating and maintenance costs of wind energy transfer, a gearless hydraulic wind energy harvesting systems is proposed, which provides several advantages over their geared counterparts. As an alternative solution, collecting the energy of multiple wind turbines in one central location will remove the weight from the tower, increase the capacity factor of the plant, and make energy harvesting less costly by reducing capital costs, operation costs, and maintenance costs. Figure 1.1 depicts the hydraulic energy transfer system for a standalone wind turbine. Figure 1.2 displays the collection of the energy of multiple wind turbines into one central generation unit.

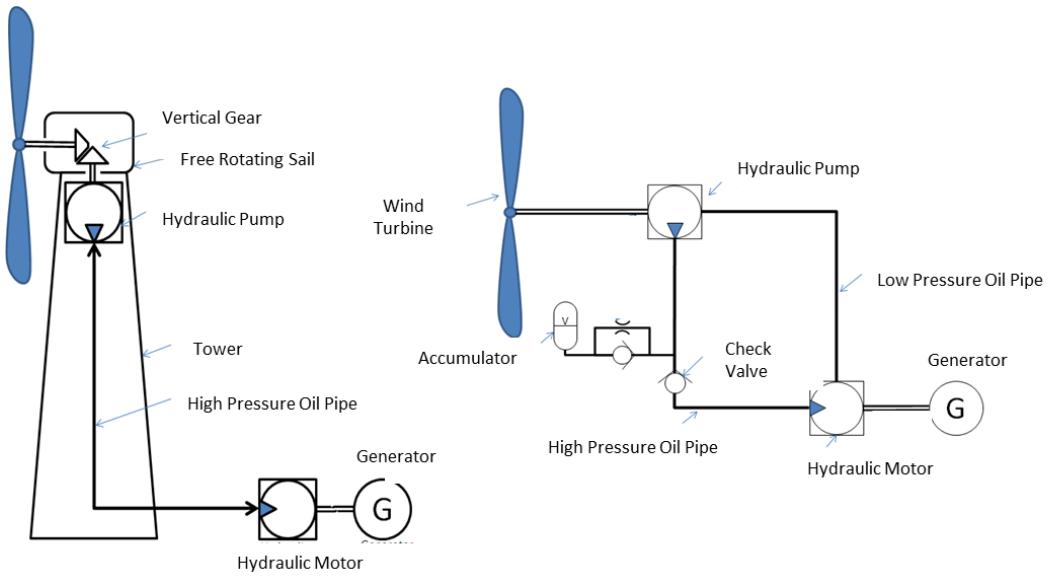

Figure 1.1 Hydraulic energy transfer of a standalone wind turbine

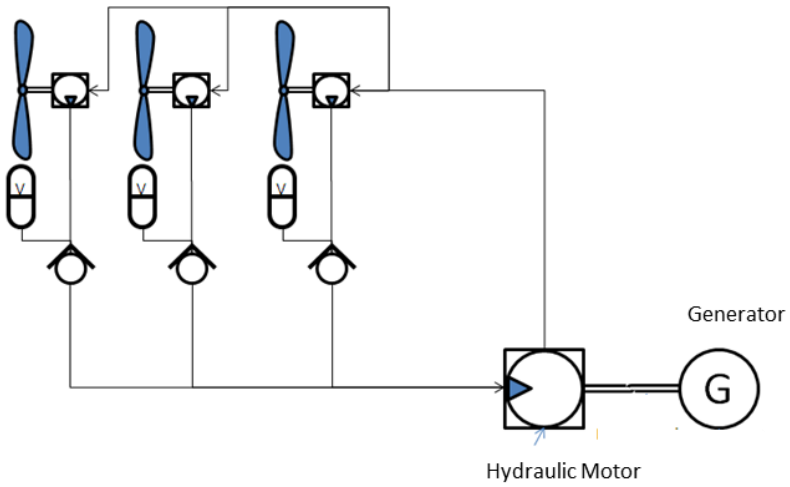

Figure 1.2 System integration for multiple wind turbines

The new wind energy harvesting technique incorporates all the disseminated power generation equipment on individual wind towers in a larger central power generation unit. With the introduction of this new approach, the wind tower only accommodates a hydraulic pump to flow the hydraulic fluid through high-pressure pipes. The gearbox is eliminated and the generator can be located at ground level. This will result in enhanced reliability, increased life span, and reduced maintenance cost of the wind turbine towers. Other benefits of this technique include high-energy transfer rate and reduction of the size of the power electronics. To understand the dynamic behavior of the hydraulic wind energy, a mathematical model of the system is required.

1.2 Previous Work

A Hydraulic Transmission System (HTS) is identified as an exceptional means of power transmission in applications with variable input or output velocities such as

manufacturing, automation, and heavy duty vehicles [9]. It offers fast response time, maintains precise velocity under variable input and load, and is capable of producing high forces at high speeds [11]. HTS also offers a decoupled dynamic, allowing for multiple-input, single-output drivetrain energy transfer configurations [12]. Earlier research has shown the possibility of using this type of power transfer technology in a wind power plant, even though it is not permitted in its electrical counterpart [20]-[24].

Hydraulic systems have been used in several applications including tire rollers, for example [13], Earth moving equipment and machinery [30], oil industry [10], hydrostatic transmission systems [31], servo applications [32], and other actuation purposes [12, 34]. Simulation tools, such as MATLAB/Simulink®, have been developed [14] and used for modeling and control of turbines [15] and hydraulic transmission [16]. Closed loop hydraulic transmission lines have also been modeled by the use of governing equations [17, 18], and by modeling fluid compressibility [19]. However, no verified mathematical model is available for hydraulic transmission of wind power. Therefore, mathematical models of HTS wind turbine power plants are required for understanding the dynamic behavior of the energy transfer system, to investigate the performance of the plant, and to improve their design and controls.

The prime mover of this hydraulic energy transfer unit, the wind turbine, experiences the intermittent characteristics of wind which impose fluctuation on generators and drift their angular velocity and consequently the generated power. Consequently, a control strategy is required to maintain the generator’s angular velocity. To mitigate the effect of the output power fluctuations, different control techniques are

applied to regulate the generated power [25-27]. Optimal speed control of hydraulic systems [28, 29] has been introduced and is used for displacement control of hydraulic cylinders. This thesis introduces flow regulation velocity control techniques to maintain the primary hydraulic motor output in proximity of the reference value.

1.3 Objectives

This thesis introduces the modeling and controls of the hydraulic wind energy transfer system. A computational model of the energy transfer system is combined with experimental prototype to study the characteristics of the system under intermittent/rapidly changing operating conditions.

This objective is accomplished by incorporating the governing equations of hydraulic circuit components that include wind-driven pumps, generator-coupled hydraulic motors, hydraulic safety components, and proportional flow control elements and connecting these modules to create a complete mathematical model of the hydraulic wind energy transfer. This mathematical model is demonstrated in both ordinary differential equation (ODE), and linear and nonlinear state-space representation. The mathematical model is verified with simulation results from a SimHydraulics Toolbox of MATLAB/Simulink® in different operating conditions.

An experimental prototype of the hydraulic energy transfer system is created and linked with dSPACE 1104 fast prototyping hardware, to precisely acquire system operating conditions such as angular velocities, flows, and pressures when the hydraulic

system configuration changes. The results from the experimental setup are utilized to validate the accuracy of the obtained mathematical models.

A control system is designed to maintain the reference angular velocity of the primary motor. The success of the control strategies are first assessed in simulations and further implemented to maintain angular velocity of the generator in prototype.

The intermittent nature of wind speed imposes random output generator frequency fluctuation. When the wind speed is high enough to generate enough flow in the system to maintain the reference primary motor angular velocity, the angular velocity control techniques technique regulates the position of the flow control valve to divert the surplus flow into an auxiliary motor path. The auxiliary motor captures the energy of the excess flow. This condition is known as high wind operation. Conversely, when the wind speed drops below a certain limit, the hydraulic pump would be incapable of generating sufficient flow to maintain the reference primary motor angular velocity. This thesis introduces an energy storage technique which stores the energy captured by the auxiliary motor at high wind in a battery and releases the energy back into the system at low wind to maintain the reference velocity.

1.4 About This Thesis

This thesis is organized as follows: Chapter 2 explains the overall hydraulic power transfer system and its system components. Chapter 3 presents the modeling of the hydraulic transmission system. The system model is demonstrated in ODE and state-space representations. A linear model of the system is demonstrated to address the system

operation in natural flow split. In this configuration, the flow generated by the hydraulic pump is distributed between the motors based on the properties such as inertia, damping coefficient and displacement. A nonlinear model of the system is obtained to address the system nonlinearities in gearless hydraulic wind power transfer, which are originated by operation of discrete elements such as check valves, proportional and directional valves, and leakage factor of hydraulic pumps and motors. To obtain accurate models, the system energy and pressure losses will be modeled and incorporated in the system.

Chapter 4 studies the stability of the mathematical model of the hydraulic wind energy transfer system for both the linear and nonlinear models.

Chapter 5 includes the description of the design and operation of the experimental prototype of the hydraulic system. The hydraulic circuitry of the setup is introduced and the data acquisition system is discussed.

Chapter 6 includes the validation of proposed mathematical models by simulations and experimental results. Firstly, the mathematical model is verified with simulation results from a model created with SimHydraulics toolbox of MATLAB/Simulink® for different operating. Subsequently, experimental data is incorporated to assess the accuracy and efficiency of the simulation model for different system configurations.

Chapter 7 represents the design and application of the control techniques to maintain the reference primary motor angular velocity. Three types of controllers are introduced namely, a PI controller, a model reference adaptive controller (MRAC), and a

rate limit (RL) controller. The success of the control strategies are first assessed in simulations and further implemented to maintain reference tracking of the system prototype.

Chapter 8 investigates further applications of the proposed hydraulic system. An energy storage technique is introduced for gearless wind energy transfers. The system captures the energy of the surplus hydraulic flow in the system and stores the energy in an electrical storage unit in high wind. The energy is released back to the system to compensate for the flow shortcomings in low wind. A hybrid-hydraulic electric vehicle powertrain system is introduced to capture the power of a range extender and store it in a battery. The range extender is supplementary source of power to the vehicle. . The stored energy can be released back to the wheels when the vehicle runs in the full electric configuration.

2. HYDRAULIC SYSTEM DESCRIPTION

2.1 Introduction to the Hydraulic Circuit

The hydraulic wind power transfer system consists of a fixed displacement pump driven by the prime mover (wind turbine) and one or more fixed displacement hydraulic motors. The hydraulic transmission uses the hydraulic pump to convert the mechanical input energy into pressurized fluid. Hydraulic hoses and steel pipes are used to transfer the harvested energy to the hydraulic motors [16].

A schematic diagram of a wind energy hydraulic transmission system is illustrated in Figure 2.1. As the figure demonstrates, a fixed displacement pump is mechanically coupled with the wind turbine and supplies pressurized hydraulic fluid to two fixed displacement hydraulic motors. The hydraulic motors are coupled with electric generators to produce electric power in a central power generation unit. Since the wind turbines generate a large amount of torque at a relatively low angular velocity, a high displacement hydraulic pump is required to flow high-pressure hydraulics to transfer the power to the generators. The pump might also be equipped with a fixed internal speed-up mechanism. Flexible high-pressure pipes/hoses connect the pump to the piping toward the central generation unit.

The hydraulic circuit uses check valves to insure the unidirectional flow of the hydraulic flows. A pressure relief valve protects the system components from the destructive impact of localized high-pressure fluids. The hydraulic circuit contains a specific volume of hydraulic fluid, which is distributed between hydraulic motors using a proportional valve.

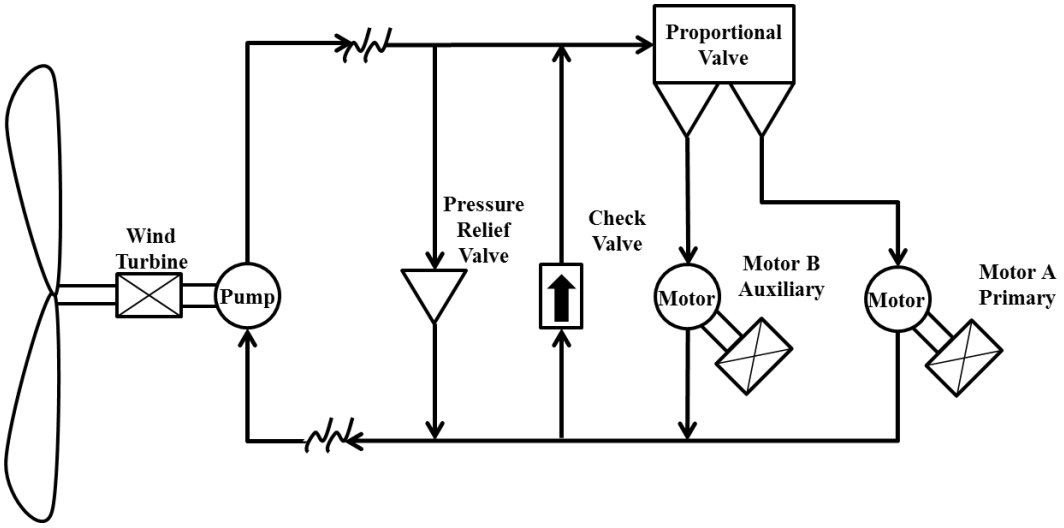

Figure 2.1 Schematic of the high-pressure hydraulic power transfer system. The hydraulic pump is in a distance from the central generation unit [22]

The next section discusses the operation of the hydraulic system components.

2.2 Operation of the Hydraulic Components

This section describes the operation of the components of the hydraulic circuitry. The main components of the system are hydraulic pumps, hydraulic motors, safety valves, proportional valves, check valves, and flexible hoses.

2.2.1 Fixed Displacement Hydraulic Pump/Motor

A fixed displacement hydraulic pump is a pump for which the amount of hydraulic fluid which is moved in every pump cycle is not adjustable. This type of pump creates hydraulic flow by trapping a fixed volume of fluid and forcing it into the discharge section. Gear pumps are the most common type of fixed displacement pumps which are classified as rotary type positive displacement pumps. Gear pumps comprise of two gears and meshing gears to displace fluid by rotation. In general, gear pumps are cost efficient and are available in compact sizes. The mechanical force to rotate the fixed gears in obtained from the shaft of the machine. Figure 2.2 displays a hydraulic fixed displacement gear pump.

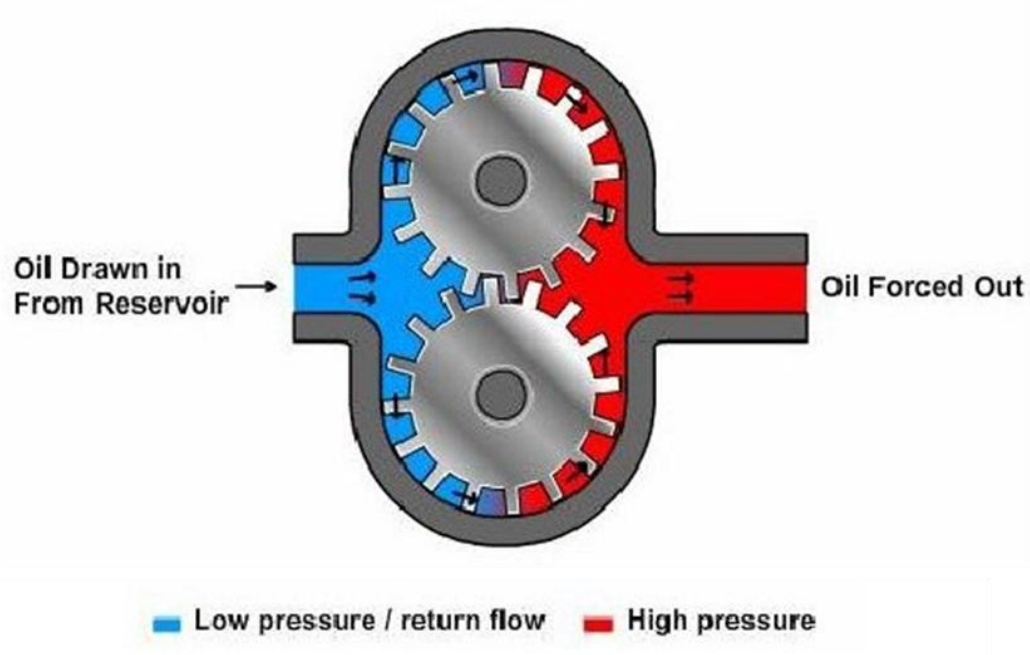

Figure 2.2 Fixed displacement hydraulic gear pump

2.2.2 Fixed Displacement Hydraulic Motor

The hydraulic motor converts the energy of hydraulic pressure and flow into mechanical torque and angular velocity. Hydraulic motors perform inverse operation of hydraulic pumps, meaning most hydraulic pumps could be utilized as hydraulic motors if they are equipped with back-driving capabilities. Similarly, geared motors are the most common type of fixed displacement hydraulic motors. These pumps are equipped with two gears, namely the driven gear and the idle gear. The hydraulic fluid enters the motor and fills the space between the gears and the motor housing and flows to the motor outlet. The energy of the hydraulic fluid which is supplied to the motor rotates the gears and runs the component. Figure 2.3 displays a fixed displacement hydraulic gear motor.

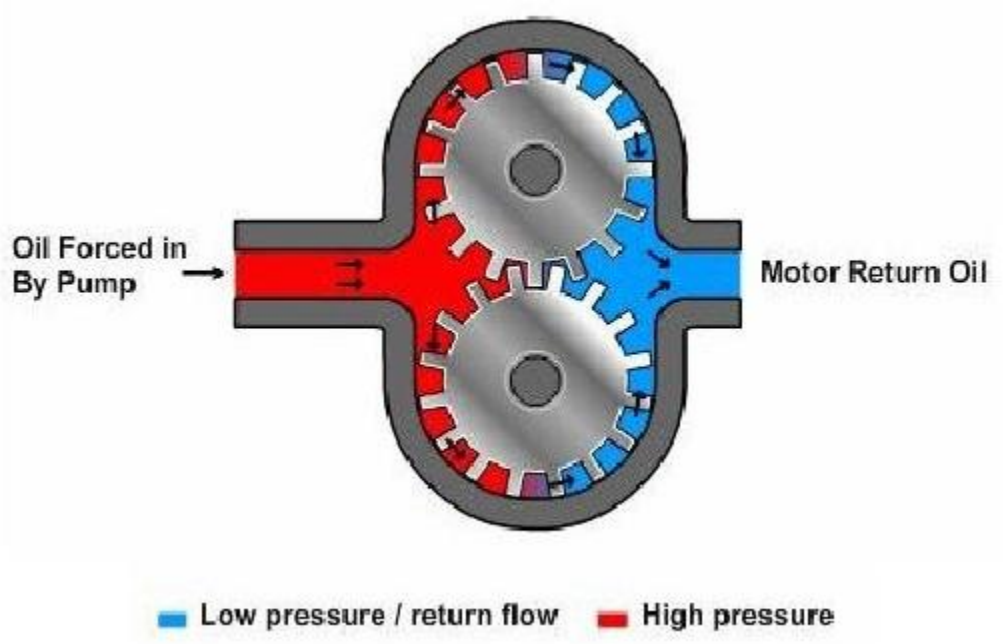

Figure 2.3 Fixed displacement hydraulic gear motor

2.2.3 Check Valve

Check valve (CV) is a safety hydraulic component which ensures unidirectional flow in the system. It is also installed into the system to prevent backflows after system shutdown. The valve has a port for fluid entrance and another port to discharge the fluid. Cracking pressure is an important property of a check valve and is defined as the minimal upstream hydraulic pressure at which the valve operates. A common type of check valves are ball check valves. In this type of check valve, a spherical ball is the membrane which blocks the flow. The ball is loaded with a spring which prevents the flow from passing through. Ball check valves are considered inexpensive and simple components for hydraulic system protection. Figure 2.4 illustrates a ball/spring check valve.

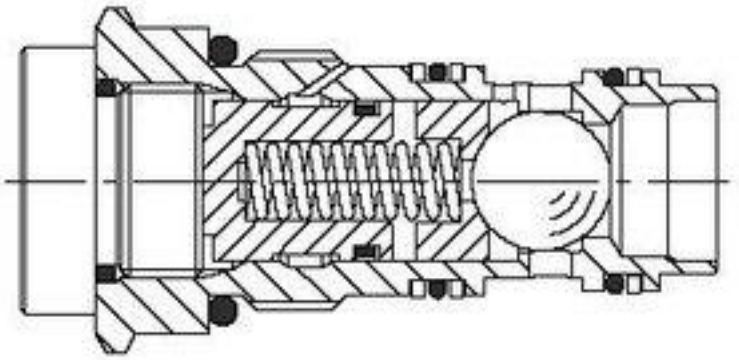

Figure 2.4 Ball spring check valve

2.2.4 Pressure Relief Valve

The pressure relief valve (PRV) is a safety component which limits the amount of pressure in the hydraulic system. The PRV opens when the system pressure exceeds the valve opening pressure and dissipates the excess pressure in the system. Typical PRVs

consist of a metal spherical member which is loaded with a spring. The spherical member blocks the valve opening when the pressure is below the valve opening pressure. When system pressure exceeds the valve opening pressure, the hydraulic fluid pushes the spring open, and the excess pressure is dissipated by directing the flow to the bypass. Pressure relief valves are installed in several locations in a hydraulic circuit, including the return circuit, and next to hydraulic actuators to prevent destructive pressure build up. Figure 2.5 shows a ball spring pressure relief valve.

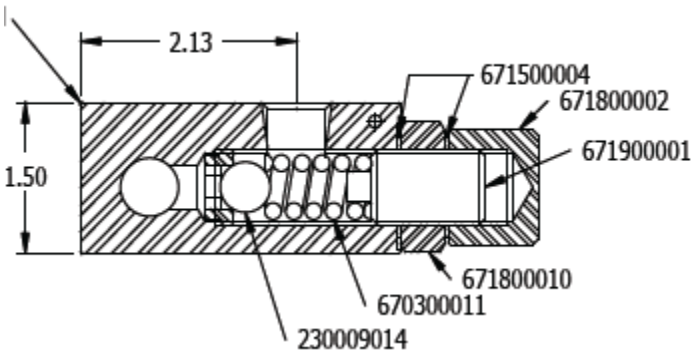

Figure 2.5 Ball spring pressure relief valve

2.2.5 Flow Control Valve

The control valve regulates the flow distribution between the hydraulic motor. A three way proportional valve (PV) is installed in the proposed hydraulic circuit. The position of the pulse driven valve is adjusted by regulating the width of the pulse which is sent to the proportional valve. Proportional valves are generally of electromagnetic type. The valve consists of a solenoid which is controlled by an electric current through the solenoid and a valve. The solenoid converts the electric energy to mechanical energy which displaces the valve opening.

2.2.6 Flexible Hoses

Flexible hoses transport the pressurized hydraulic fluid through the system. The flexibility of the hoses is a property with benefits the packaging of the system. Since the hoses are flexible, fewer fittings are required.

2.2.7 Hydraulic Fluid

Hydraulic fluid is the medium which transfers the energy of the hydraulic pump to the hydraulic motors. The hydraulic fluid must have low compressibility (high bulk modulus) to enhance the system efficiency. The fluid is pressurized according to the resistant in the system and transfers the pressure to the next layer of fluid. The fluid is distributed through the flexible hoses and controlled through the flow control valves.

2.3 Hydraulic System Operation

This section describes the overall operation of the hydraulic wind energy transfers. In operation, the energy of wind generates a torque which forces the turbine blade to rotate. The mechanical coupling between the turbine shaft and the hydraulic pump, transfers the rotational motion to the hydraulic pump. The pump pressurizes the fluid in the system and flows it through the pipes. The energy is transferred in the system through the segments of the hydraulic fluid. The fluid is distributed between auxiliary motor and auxiliary motor based on the position of the proportional flow control valve. The pressurized fluid provides the necessary force to rotate the hydraulic motors. The hydraulic motors are mechanically coupled with electric generators and transfer the rotary motion to the generators. The generators convert the supplied mechanical energy

into electrical energy in form of electrical current. Subsequently, the pressure of the hydraulic fluid drops by performing mechanical work. The low pressure fluid is returned to the hydraulic pump to be re-pressurized. A check valve is positioned in the forward fluid path to prevent the pump high pressurized flow from flowing back into the pump. This reverse could occur in conditions at which the system is idle or the energy is insufficient to run the pump.

A pressure relief valve connects the forward path to the return path. The valve opens if the flow in the return path exceeds the pre-set threshold and diverts the flow to prevent transient high pressure build up and damage to the system components.

A check valve is similarly connected between the forward and return flow paths. The valve only opens if the pressure in the return path exceeds the fluid pressure in the forward path which might happen in case of the mechanical failure of the system components. In case of multiple wind turbines, the check valve only blocks the path into the failed wind turbine system while ensures the other wind turbines continue energy generation.

The proportional vale distributes the flow between the primary motor and the auxiliary motor. The position of the valve is regulated to control the angular velocity of the motors. A controller is coupled with the proportional valve to regulate the valve position to maintain a reference primary motor angular velocity. The controllers receives the angular velocity data from the primary motor and sends a corrective signal to the

valve to mitigate the deviation from the reference velocity. The speed control of the primary motor insures delivery of the generated electric energy in a specific frequency.

3. HYDRAULIC SYSTEM MODELING

3.1 Mathematical Model (ODE)

The dynamic model of the hydraulic system is obtained by using governing equations of the hydraulic components in an integrated configuration. The governing equations of hydraulic motors, pumps, and transmission lines are obtained to calculate flows and torques [20-24], [34-36] and to express the closed loop hydraulic system behavior.

3.1.1 Fixed Displacement Pump

Hydraulic pumps deliver a constant flow determined by

$$Q_p = D_p \omega_p - k_{L,p} P_p \tag{3.1}$$

where Q_p is the pump flow delivery, D_p is the pump displacement, $k_{L,p}$ is the pump leakage coefficient, and P_p is the differential pressure across the pump defined as

$$P_p = P_t - P_q \tag{3.2}$$

where P_t and P_q are gauge pressures at the pump terminals. The pump leakage coefficient is a numerical expression of the hydraulic component probability to leak and is expressed as follows

$$k_{L,p} = K_{HP,p} / \rho\nu \tag{3.3}$$

where ρ is the hydraulic fluid density and v is the fluid kinematic viscosity. $K_{HP,p}$ is the pump Hagen-Poiseuille coefficient and is defined as

$$K_{HP,p} = \frac{D_p \omega_{nom,p}(1-\eta_{vol,p})\nu_{nom}\rho}{P_{nom,p}} \tag{3.4}$$

where $\omega_{\text{nom,p}}$ is the pump's nominal angular velocity, v_{nom} is the nominal fluid kinematic viscosity, $P_{nom,p}$ is the pump's nominal pressure, and $\eta_{\text{vol,p}}$ is the pump's volumetric efficiency. Finally, torque at the pump driving shaft is obtained by

$$T_p = D_p P_p / \eta_{mech,p} \tag{3.5}$$

where $\eta_{\text{mech,p}}$ is the pump's mechanical efficiency and is expressed as

$$\eta_{mech,p} = \eta_{total,p} / \eta_{vol,p} \tag{3.6}$$

3.1.2 Fixed Displacement Motor

The flow and torque equations are derived for the hydraulic motor using the motor governing equations. The hydraulic flow supplied to the hydraulic motor can be obtained by

$$Q_m = D_m \omega_m + k_{L,m} P_m \tag{3.7}$$

where Q_p is the motor flow delivery, D_p is the motor displacement, $k_{L,m}$ is the motor leakage coefficient, and P_m is the differential pressure across the motor

$$P_m = P_a - P_b \tag{3.8}$$

where P_a and P_b are gauge pressures at the motor terminals. The motor leakage coefficient is a numerical expression of the hydraulic component possibility to leak, and is expressed as follows

$$k_{L,m} = K_{HP,m} / \rho\nu \tag{3.9}$$

where ρ is the hydraulic fluid density and v is the fluid kinematic viscosity. $K_{HP,m}$ is the motor Hagen-Poiseuille coefficient and is defined as

$$K_{HP,m} = \frac{D_m \omega_{nom,m}(1-\eta_{vol,m})\nu_{nom}\rho}{P_{nom,m}} \tag{3.10}$$

where $\omega_{\text{nom,m}}$ is the motor's nominal angular velocity, v_{nom} is the nominal fluid kinematic viscosity, $P_{nom,m}$ is the motor's nominal pressure, and $\eta_{\text{vol,m}}$ is the motor's volumetric efficiency. Finally, torque at the motor driving shaft is obtained by

$$T_m = D_m P_m \eta_{mech,m} \tag{3.11}$$

where $\eta_{\text{mech,m}}$ is the motor's mechanical efficiency and is expressed as

$$\eta_{mech,p} = \eta_{total,p} / \eta_{vol,p} \tag{3.12}$$

The total torque produced in the hydraulic motor is expressed as the sum of the torques from the motor loads and is given as

$$T_m = T_I + T_B + T_L \tag{3.13}$$

where T_m is total torque in the motor and T_I,T_B, and T_L represent inertial torque, damping friction torque, and load torque, respectively. This equation can be rearranged as

$$T_m - T_L = I_m(d\omega_m / dt) + B_m\omega_m \tag{3.14}$$

where I_m is the motor inertia, ω_m is the motor angular velocity, and B_m is the motor damping coefficient.

3.1.3 Hose Dynamics

The fluid compressibility model for a constant fluid bulk modulus is expressed in [19]. The compressibility equation represents the dynamics of the hydraulic hose and the hydraulic fluid. Based on the principles of mass conservation and the definition of bulk modulus, the fluid compressibility within the system boundaries can be written as

$$Q_c = (V/\beta)(dP/dt) \tag{3.15}$$

where V is the fluid volume subjected to pressure effect, β is the fixed fluid bulk modulus, P is the system pressure, and Q_c is the flow rate of fluid compressibility, which is expressed as

$$Q_c = Q_p - Q_m \tag{3.16}$$

hence, the pressure variation can be expressed as

$$(dP/dt) = (Q_p - Q_m)(\beta/V) \tag{3.17}$$

3.1.4 Pressure Relief Valve Dynamics

Pressure relief valves are used for limiting the maximum pressure in hydraulic power transmission. A dynamic model for a pressure relief valve is presented in [37]. A simplified model to determine the flow rate passing through the pressure relief valve in opening and closing states [19] is obtained by

$$Q_{PRV} = \begin{cases} k_v(P - P_v), P > P_v \\ 0 \quad\quad , P \le P_v \end{cases} \tag{3.18}$$

where k_v is the slope coefficient of valve static characteristics, P is system pressure, and P_v is valve opening pressure.

3.1.5 Check Valve Dynamics

The purpose of the check valve is to permit flow in one direction and to prevent back flows. Unsatisfactory functionality of check valves may result in high system vibrations and high-pressure peaks [38]. For a check valve with a spring preload [39], the flow rate passing through the check valve can be obtained by

$$Q_{CV} = \begin{cases} Cl_b \dfrac{(P - P_v)A_{disc}}{k_s}, P > P_v \\ 0 \qquad\qquad , P \le P_v \end{cases} \tag{3.19}$$

where Q_{cv} is the flow rate through the check valve, C is the flow coefficient, l_b is the hydraulic perimeter of the valve disc, P is the system pressure, P_v is the valve opening pressure, A_{disc} is the area in which fluid acts on the valve disc, and k_s is the stiffness of the spring.

3.1.6 Proportional Valve Dynamics

Directional valves are mainly employed to distribute flow between rotary hydraulic components. The dynamic model of a directional valve is categorized into two divisions, namely the control device and the power stage. The control device adjusts the position of the valve's moving membrane, while the power stage controls the hydraulic fluid flow rate.

A directional valve model is represented in [40] by specifying the valve orifice maximum area and opening. The hydraulic flow through the orifice Q_{PV} is calculated as

$$Q_{PV} = C_d A \sqrt{\frac{2}{\rho} |P|} \operatorname{sgn}(P) \tag{3.20}$$

where C_d represents the flow discharge coefficient, ρ is the hydraulic fluid density, P indicates the differential pressure across the orifice, A and is the orifice area and is expressed as

$$A = \frac{A_{\max}}{h_{\max}} h_i \tag{3.21}$$

where A_{max} represents the maximum orifice area, h_{max} denotes the maximum orifice opening, and h indicates the orifice opening and is obtained from

$$h_i = h_{i-1} + x_i \tag{3.22}$$

where h_{i-1} is the previous orifice opening, and x_i denotes the variations to the orifice opening which is applied to the proportional valve.

The operation of the hydraulic system, shown in Figure 2.1, could be classified into two categories, namely natural flow split, and forced flow. In the first configuration, the proportional valve is excluded from the hydraulic circuit, and the flow generated by the hydraulic pump is distributed between to motors based on their natural properties, i.e. damping coefficient, inertia, the hydraulic circuitry, and geometric characteristics of the system. In the forced flow configuration, the flow distribution between the motors is enforced by the position of the proportional valve. Block diagrams of the wind energy transfer using MATLAB/Simulink® for both configurations is demonstrated in Figures 3.1 to 3.4. The model incorporates the mathematical governing equations of individual hydraulic circuit components where the pressure is obtained from the bulk modulus.

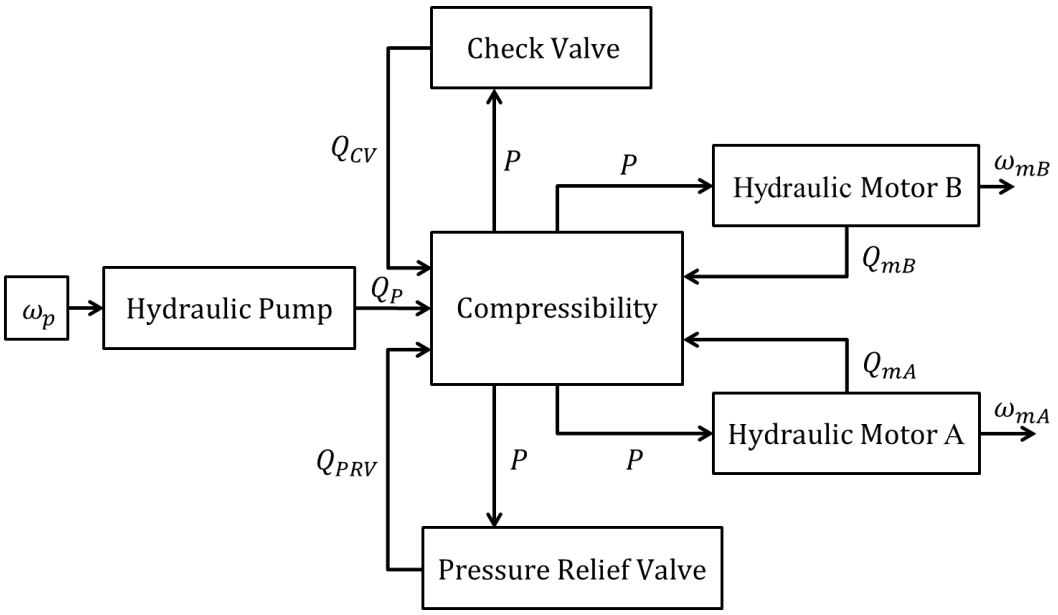

Figure 3.1 Hydraulic wind energy harvesting model schematic diagram for natural flow split

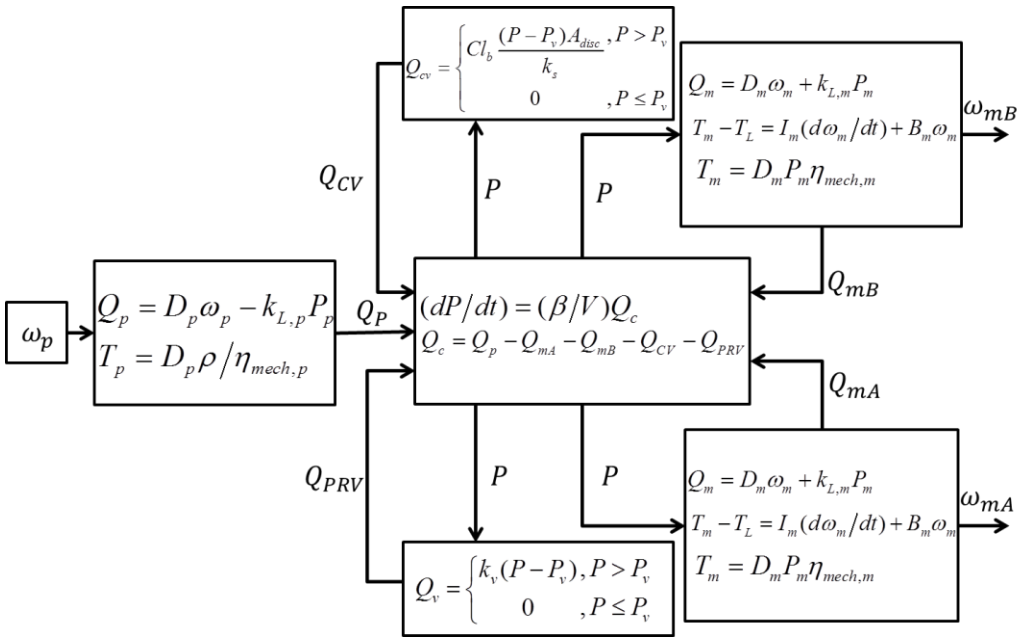

Figure 3.2 Simulink model of hydraulic wind energy harvesting system for natural flow split

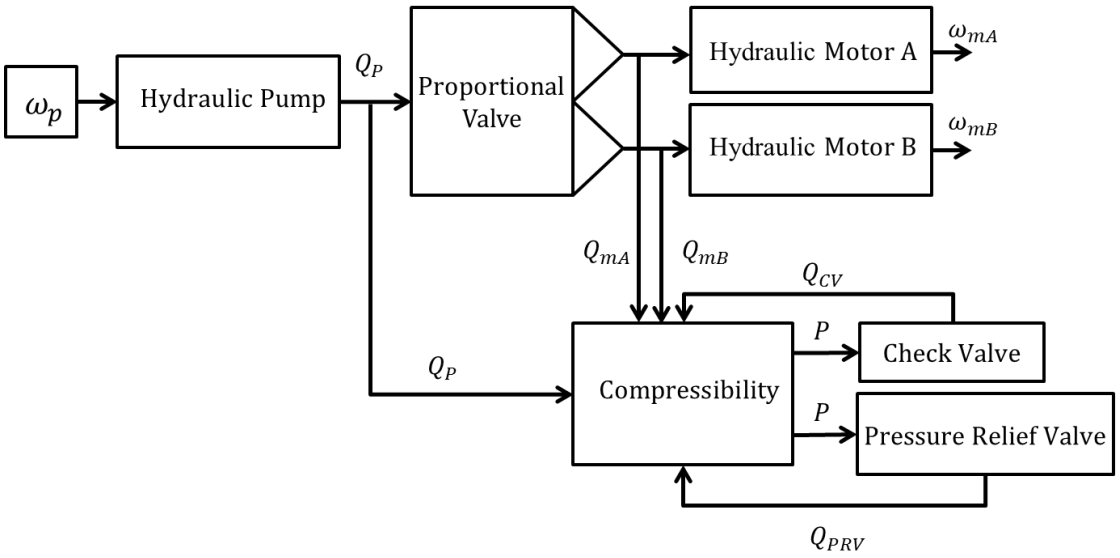

Figure 3.3 Hydraulic wind energy harvesting model schematic diagram for forced flow

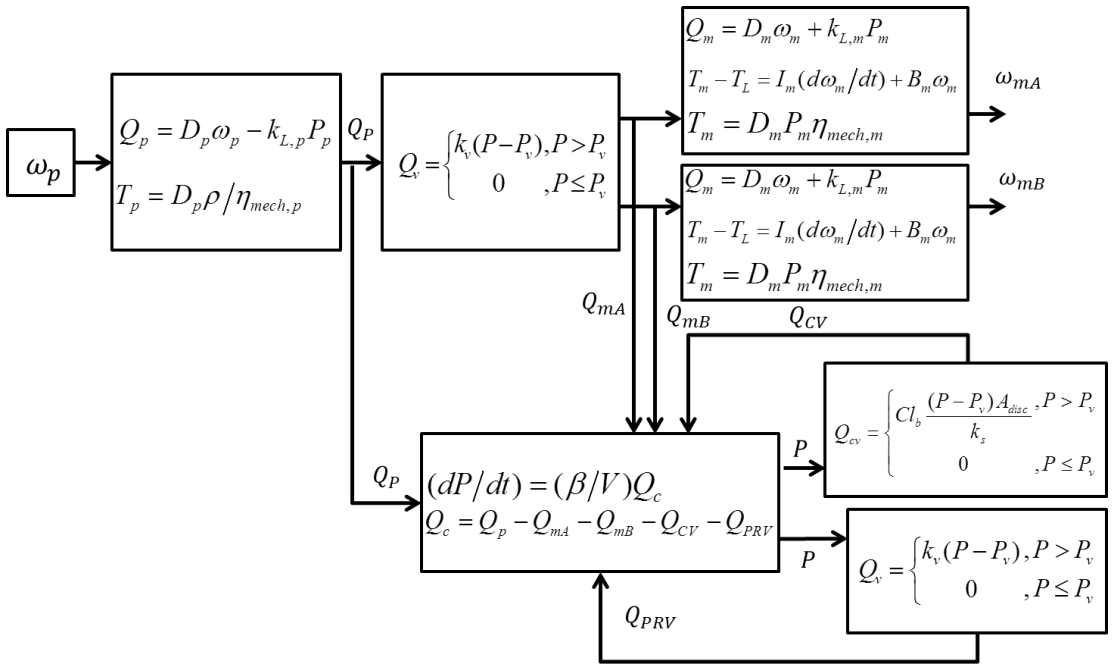

Figure 3.4 Simulink model of hydraulic wind energy harvesting system for forced flow

3.2 State-Space Representation

This section introduces the state-space representation of the hydraulic energy transfer system. The state-space representation is classified into two categories, namely the linear state-space representation, and the nonlinear state space-representation. The linear state-space model represents the natural flow split configuration and is utilized for model validation purposes, while the nonlinear representation illustrates the forced flow configuration and is incorporated for control purposes.

The state space representation of the system is derived from the dynamic equations introduced in the previous section. The main advantages of the state space representation comprise of simplification of the mathematical demonstration of the system, incorporation of initial conditions into solution, simplification of the interrelation of the system equations, suitability for multiple input-multiple output (MIMO) system illustration, and superior computational efficiency for computer implementation [41].

3.2.1 Linear State Space Model

Consider a simplified hydraulic power transfer system where the pump flow is distributed between two hydraulic motors based on the natural characteristics and geometry of the hydraulic circuit, namely the natural flow split. Based on the preceding section, the flow of the rotary hydraulic components are obtained by

$$Q_p = D_p \omega_p - k_{L,p} P_p \tag{3.23}$$

$$Q_{mA} = D_{mA} \omega_{mA} + k_{L,mA} P_{mA} \tag{3.24}$$

$$Q_{mB} = D_{mB} \omega_{mB} + k_{L,mB} P_{mB} \tag{3.25}$$

where the properties associated with the primary motor are represented with the *mA* subscript while the properties affiliated with the auxiliary motor are denoted with the *mB* subscript. According to the compressibility equations and hose dynamics

$$Q_c = Q_p - Q_{mA} - Q_{mB} \tag{3.26}$$

$$Q_p - Q_{mA} - Q_{mB} = (V/\beta)(dP/dt) \tag{3.27}$$

Hence

$$dP/dt = (Q_p - Q_{mA} - Q_{mB})(\beta/V) \tag{3.28}$$

Substituting equations 3.23 to 3.25 into equation 3.28

$$dP/dt = [D_p\omega_p - D_{mA}\omega_{mA} - D_{mB}\omega_{mB} - (k_{L,p}P_p + k_{L,mA}P_{mA} + k_{L,mB}P_{mB})](\beta/V) \tag{3.29}$$

Simplifying the above equation and assuming negligible pressure drop in the system

$$P_p \approx P_{mA} \approx P_{mB} \tag{3.30}$$

Subsequently, the torque equations of the hydraulic motors are derived to introduce the two supplementary first order differential equations.

According to equations 3.11 to 3.14 and assuming a negligible torque load

$$T_m = I_m(d\omega_m/dt) + B_m\omega_m \tag{3.31}$$

By deriving the above equation for both the primary and auxiliary motors

$$D_{mA}P_{mA}\eta_{mech,mA} = I_{mA}(d\omega_{mA}/dt) + B_{mA}\omega_{mA} \tag{3.32}$$

Rephrasing the above equation leads to

$$d\omega_{mA}/dt = (D_{mA}P_{mA}\eta_{mech,mA} - B_{mA}\omega_{mA})/I_{mA} \tag{3.33}$$

Similarly for the auxiliary motor

$$d\omega_{mB}/dt = (D_{mB}P_{mB}\eta_{mech,mB} - B_{mB}\omega_{mB})/I_{mB} \tag{3.34}$$

Consequently, the three interrelated ordinary differential equations are obtained. In general, the state-space model of a system is represented as follows

$$\begin{aligned} \dot{x} &= Ax + BU \\ y &= Cx + DU \end{aligned} \tag{3.35}$$

where x is the state vector, represents the output vector, U is the input vector, A denotes the input matrix, B is the input matrix, C is the output matrix, and D is the feed-forward matrix. The input to the hydraulic system is ω_p, the angular velocity of the hydraulic pump. The state variables are the differential pressure, the primary motor angular velocity, and the auxiliary motor angular velocity. By rearranging the above first order equations, the following state space model is achieved

$$x = \begin{bmatrix} P_p \\ \omega_{mA} \\ \omega_{mB} \end{bmatrix} \tag{3.36}$$

$$A = \begin{bmatrix} -(\beta/V)(k_{L,p} + k_{L,mA} + k_{L,mB}) & -(\beta/V)D_{mA} & -(\beta/V)D_{mB} \\ D_{mA}\eta_{mech,mA} / I_{mA} & -B_{mA} / I_{mA} & 0 \\ D_{mB}\eta_{mech,mB} / I_{mB} & 0 & -B_{mB} / I_{mB} \end{bmatrix} \tag{3.37}$$

$$B = \begin{bmatrix} (\beta/V)D_p \\ 0 \\ 0 \end{bmatrix} \tag{3.38}$$

Matrix C is determined based on the outputs of interest. Assuming the system outputs are the differential pressure and the motors angular velocities, the output matric will become

$$C = \begin{bmatrix} 1 & 0 & 0 \\ 0 & 1 & 0 \\ 0 & 0 & 1 \end{bmatrix} \tag{3.39}$$

and the feed-forward matrix is

$$D = 0 \tag{3.40}$$

This section represented a state space model of the hydraulic wind power transfer system. The dynamic ODE equations of the hydraulic system modules are transformed into a matrix demonstration. The state variables were accordingly selected and the requisite matrices were introduced. Finally, a Simulink model of the hydraulic system was created in Simulink. The next section compares the simulation results of the state space system and a similar system which is created with the SimHydraulics toolbox of MATLAB/Simulink®.

3.2.2 Nonlinear State Space Model

Consider the hydraulic power transfer system shown in Figure 2.1 where the pump flow was distributed between two hydraulic motors based on the position of the proportional valve. According to the preceding section, the flow of the rotary hydraulic components are obtained by

$$Q_p = D_p \omega_p - k_{L,p} P_p \tag{3.41}$$

$$Q_{mA} = C_d \frac{A_{\max}}{h_{\max}} h_i \sqrt{\frac{2}{\rho} |P_p|} \operatorname{sgn}(P_p) \tag{3.42}$$

$$Q_{mB} = C_d \frac{A_{\max}}{h_{\max}} (h_{\max} - h_i) \sqrt{\frac{2}{\rho} |P_p|} \operatorname{sgn}(P_p) \tag{3.43}$$

Similar to the previous section, the properties associated with the primary motor are represented with the *mA* subscript while the properties affiliated with the auxiliary

motor are denoted with the *mB* subscript. According to the compressibility Equations 3.26 and 3.28 and substituting Equations 3.41 to 3.43 into those

$$dP_p/dt = [D_p\omega_p - k_{L,p}P_p - C_d\frac{A_{\max}}{h_{\max}}h_i\sqrt{\frac{2}{\rho}|P_p|}\,\mathrm{sgn}(P_p) - C_d\frac{A_{\max}}{h_{\max}}(h_{\max}-h_i)\sqrt{\frac{2}{\rho}|P_p|}\,\mathrm{sgn}(P_p)](\beta/V) \tag{3.44}$$

Hydraulic motor gauge pressures are calculated from Equation 3.24 and 3.25

$$P_{mA} = (Q_{mA} - D_{mA}\omega_{mA})/k_{L,mA} \tag{3.45}$$

$$P_{mB} = (Q_{mB} - D_{mB}\omega_{mB})/k_{L,mB} \tag{3.46}$$

Substituting Equations 3.42 and 3.43 into the above equations

$$P_{mA} = (C_d\frac{A_{\max}}{h_{\max}}h_i\sqrt{\frac{2}{\rho}|P_p|}\,\mathrm{sgn}(P_p) - D_{mA}\omega_{mA})/k_{L,mA} \tag{3.47}$$

$$P_{mB} = (C_d\frac{A_{\max}}{h_{\max}}(h_{\max}-h_i)\sqrt{\frac{2}{\rho}|P_p|}\,\mathrm{sgn}(P_p) - D_{mB}\omega_{mB})/k_{L,mB} \tag{3.48}$$

According to Equations 3.11 to 3.14 and assuming a negligible torque load

$$D_m P_m \eta_{mech,m} = I_m(d\omega_m/dt) + B_m\omega_m \tag{3.49}$$

By deriving the above equation for both the primary and auxiliary motors

$$D_{mA}P_{mA}\eta_{mech,mA} = I_{mA}(d\omega_{mA}/dt) + B_{mA}\omega_{mA} \tag{3.50}$$

$$D_{mB}P_{mB}\eta_{mech,mB} = I_{mB}(d\omega_{mB}/dt) + B_{mB}\omega_{mB} \tag{3.51}$$

Rephrasing the above equation leads to

$$d\omega_{mA}/dt = (D_{mA}P_{mA}\eta_{mech,mA} - B_{mA}\omega_{mA})/I_{mA} \tag{3.52}$$

Similarly for the auxiliary motor

$$d\omega_{mB}/dt = (D_{mB}P_{mB}\eta_{mech,mB} - B_{mB}\omega_{mB})/I_{mB} \tag{3.53}$$

Substituting Equations 3.47 and 3.48 into Equations 3.52 and 3.53

$$d\omega_{mA}/dt = [D_{mA}((C_d \frac{A_{\max}}{h_{\max}} h_i \sqrt{\frac{2}{\rho}|P_p|}\,\mathrm{sgn}(P_p) - D_{mA}\omega_{mA})/k_{L,mA}) \eta_{mech,mA} - B_{mA}\omega_{mA}]/I_{mA} \tag{3.54}$$

$$d\omega_{mB}/dt = [D_{mB}((C_d \frac{A_{\max}}{h_{\max}} (h_{\max} - h_i) \sqrt{\frac{2}{\rho}|P_p|}\,\mathrm{sgn}(P_p) - D_{mB}\omega_{mB})/k_{L,mB}) \eta_{mech,mB} - B_{mB}\omega_{mB}]/I_{mB}, \tag{3.55}$$

Consequently, Equations 3.44, 3.54, and 3.55 are the governing equations of the nonlinear state space model. In general, the nonlinear state-space model of a system is represented as follows

$$\begin{aligned} \dot{x} &= f(x) + g(x)U \\ y &= h(x) \end{aligned} \tag{3.56}$$

where x is the state vector, y is the output vector, U is the input vector, $f(x)$ denotes an input independent function vector of the states, $g(x)$ is the input dependent function matrix of the state variables, and $h(x)$ is the output function. The inputs to the hydraulic system are ω_p the angular velocity of the hydraulic pump, and h_i the position of the proportional valve. The state variables are the differential pressure, the primary motor angular velocity, and the auxiliary motor angular velocity. By rearranging the above first order equation, the following state space model is achieved

$$x = \begin{bmatrix} P_p \\ \omega_{mA} \\ \omega_{mB} \end{bmatrix} \tag{3.57}$$

$$U = \begin{bmatrix} \omega_p \\ h_i \end{bmatrix} \tag{3.58}$$

$$f(x)=\begin{Bmatrix}\left(-k_{L,p}P_p - C_d A_{\max}\sqrt{\frac{2}{\rho}|P_p|}\,\mathrm{sgn}(P_p)\right)(\beta/V)\\ \left(-{D_{mA}}^2\omega_{mA}\eta_{mech,mA}/k_{L,mA} - B_{mA}\omega_{mA}\right)/I_{mA}\\ \left(D_{mB}C_d A_{\max}\sqrt{\frac{2}{\rho}|P_p|}\,\mathrm{sgn}(P_p)\eta_{mech,mB}/k_{L,mB} - {D_{mB}}^2\omega_{mB}\eta_{mech,mB}/k_{L,mB} - B_{mB}\omega_{mB}\right)/I_{mB}\end{Bmatrix} \quad (3.59)$$

$$g(x)=\begin{bmatrix} D_p(\beta/V) & 0\\ 0 & D_{mA}C_d\frac{A_{\max}}{h_{\max}}\sqrt{\frac{2}{\rho}|P_p|}\,\mathrm{sgn}(P_p)\eta_{mech,mA}/k_{L,mA}I_{mA}\\ 0 & -D_{mB}C_d\frac{A_{\max}}{h_{\max}}\sqrt{\frac{2}{\rho}|P_p|}\,\mathrm{sgn}(P_p)\eta_{mech,mB}/k_{L,mB}I_{mB}\end{bmatrix} \quad (3.60)$$

This section represented a nonlinear state space model of the hydraulic wind power transfer system. The dynamic ODE equations of the hydraulic system modules were transformed into a nonlinear state space demonstration. The state variables were accordingly selected and the requisite state space functions were introduced.

3.3 Pressure Loss Model

The energy in the hydraulic fluid is dissipated due to viscosity and friction. Viscosity, as a measure of the resistance of a fluid to flow, influences system losses as more-viscous fluids require more energy to flow. In addition, energy losses occur in pipes as a result of the pipe friction. The pressure loss and friction loss can be obtained by continuity and energy equations (i.e. Bernoulli's Equation) for individual circuit components such as transmission lines, pumps, and motors [42].

The Reynolds number, which determines the type of fluid in the transmission line (laminar or turbulent), can be used as a design principle for the system component sizing. The Reynolds number is a reference to predict the type of the flow in a pipe and can be obtained by

$$\mathrm{Re} = \frac{\rho v L}{\mu} = \frac{v L}{\nu} \tag{3.61}$$

where ρ is the density of the fluid, L is the length of the pipe, μ is the dynamic viscosity of the fluid, ν is the kinematic viscosity, and v is the average fluid velocity and is expressed as

$$v = \frac{Q}{A_{pipe}} \tag{3.62}$$

where Q is the flow in the pipe and A_{pipe} is the inner area of the pipe. The energy equation is an extension of the Bernoulli's equation by considering frictional losses and the existence of pumps and motors in the system. The energy equation is expressed as

$$Z_1 + \frac{P_1}{\gamma} + \frac{v_1^2}{2g} + H_p - H_m - H_L = Z_2 + \frac{\rho_2}{\gamma} + \frac{v_2^2}{2g} \tag{3.63}$$

where Z is the elevation head, v is the fluid velocity, P is the pressure, g is the acceleration due to gravity, γ is the specific weight, H_p is the pump head pressure, H_m is the motor head pressure and is calculated by the compressibility equation, H_L and is the head loss obtained by

$$H_L = f \frac{L}{D} \frac{v^2}{2g} \tag{3.64}$$

The pipe head loss is calculated by Darcy's Equation, which determines loss in pipes experiencing laminar flows, by

$$f = \frac{64}{\mathrm{Re}} \tag{3.65}$$

The energy equation is utilized along with Darcy's equation and the compressibility equation to calculate the pressure loss at every pipe segment (both horizontal and vertical) and the head of each pump in the system.

4. EXPERIMENTAL PROTOTYPE OF THE HYDRAULIC SYSTEM

The prototype of the hydraulic wind energy transfer system is designed and created to study the system characteristics and performance in different operating conditions. Additionally, the setup is implemented to validate the correctness of the proposed mathematical models of the system. The experimental setup is designed and created according to the schematic diagram of the system which was shown in Figure 2.1. Figure 4.1 depicts an overlay of the experimental setup and hydraulic circuitry. Figure 4.2 displays e schematic diagram of the experimental setup.

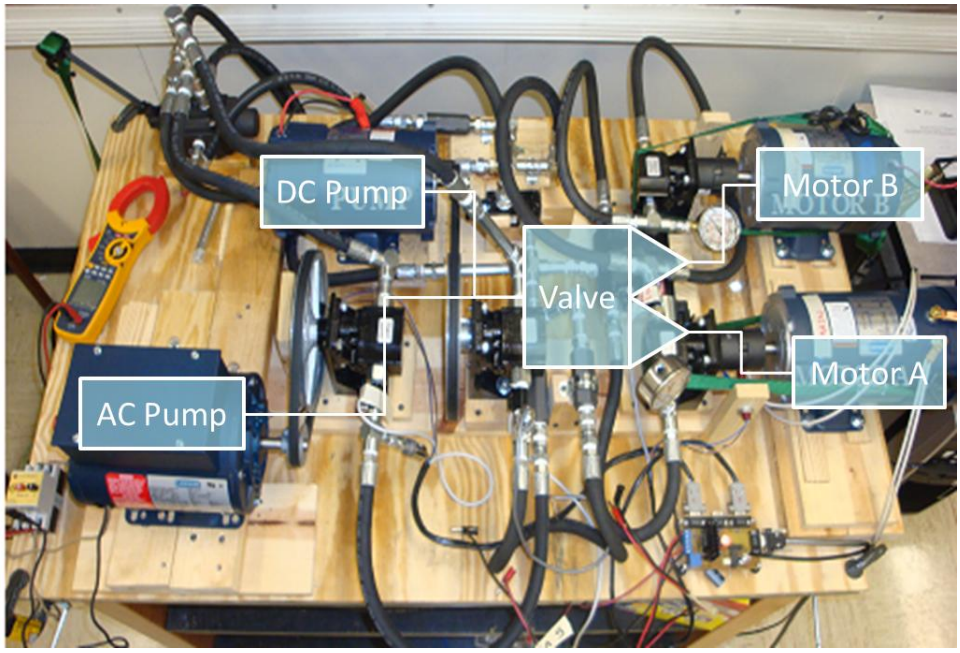

Figure 4.1 Experimental setup of the hydraulic wind power transfer system

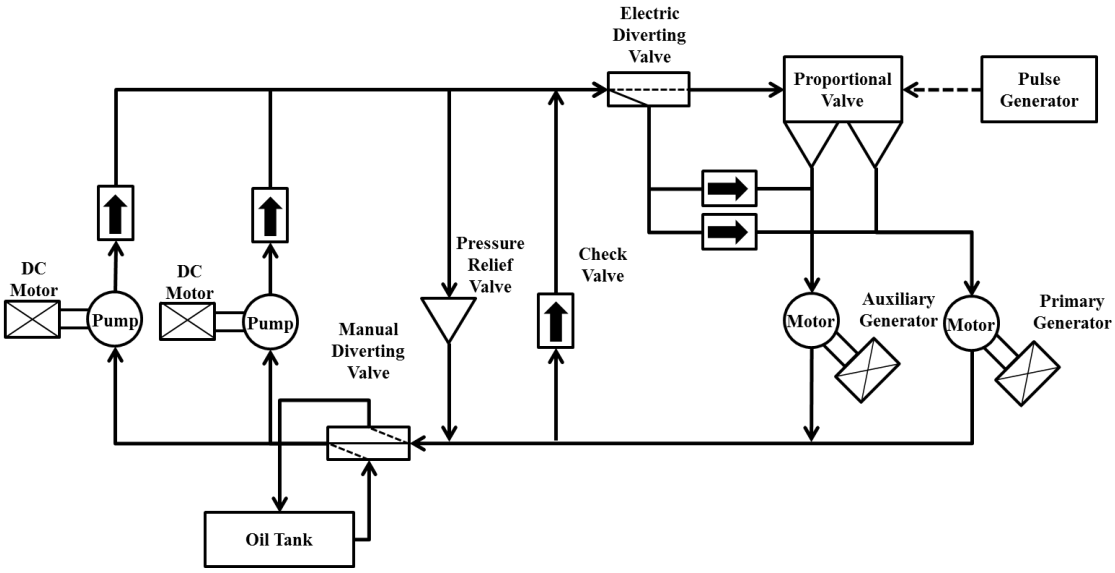

Figure 4.2 Hydraulic circuit schematic of the experimental setup

In this setup, the wind turbines are simulated with DC motors. DC motors possess dynamic characteristics which is similar to wind turbines. Every DC motor is coupled with a hydraulic motor through a speed reduction belt and pulley mechanism. The speed reduction mechanism is used to increase the torque which is transferred to the hydraulic motor sufficiently to run the system. The hydraulic pump generates pressurized fluid which is transferred to the hydraulic motors through flexible hoses. A manual 2-way control valve is used to switch between the closed loop (CL) system configuration, and open loop (OL) system configuration, at which the circuit runs through the hydraulic oil tank and supplementary fluid is forced into the system to eject the trapped air. The flow is distributed between the motors in two configurations, namely natural flow split and forced flow. In natural flow split configuration, a T-fitting distributes the flow generated by the pump based on the geometric characteristics of the hydraulic circuit and properties of the hydraulic pumps and the flow path. In the forced flow configuration, the pump

flow is distributed between the motors through a 3-way proportional valve. The position of the proportional valve is adjusted by supplying a pulse signal to the valve input. An electric flow diverting valve is utilized to switch between these configurations. Figures 4.3 and 4.4 demonstrate the flow distribution configurations.

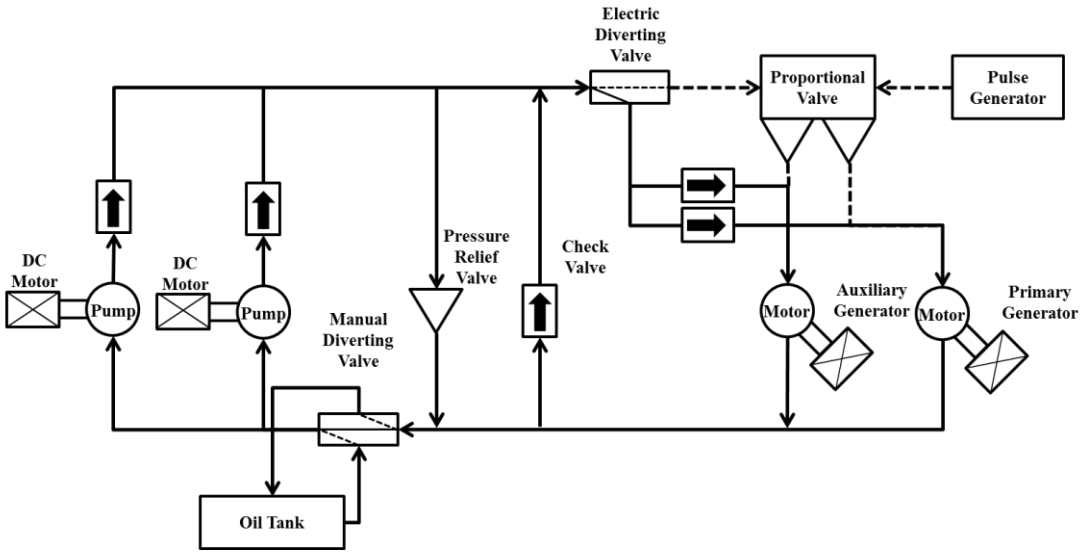

Figure 4.3 Natural flow split configuration of the experimental setup. The proportional valve is excluded from the circuit by switching the solenoid operated directional valve

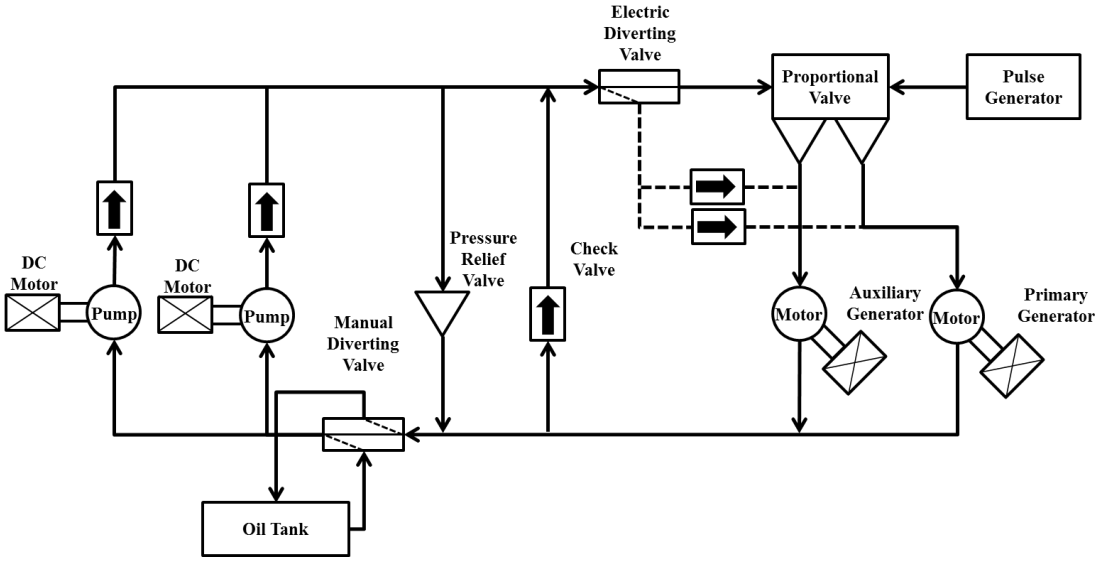

Figure 4.4 Forced flow configuration of the experimental setup

Several sensors are installed to closely monitor the operating conditions such as angular velocity, flow, and pressure. Fast prototyping dSPACE 1104 hardware is used to precisely measure system outputs. Several safety valves protect the system from pressure damage. Figure 4.5 illustrates a schematic diagram of the system operation. According to this figure, the electric dc motor is supplied with a voltage. The motor runs the mechanically coupled hydraulic pump. The pump generates pressurized hydraulic fluid in the system. The flexible hoses transfer the fluid to the 3-way proportional valve. The fluid is distributed between the motors according to the position of the valve. The sensors generate signals based on the system parameter values. The sensor outputs are transferred to dSPACE through the electronic board. The sensor outputs are analyzed by a computer and a corrective valve position pulse signal is generated. dSPACE dictates the position signal to the proportional valve input and regulates the system operation.

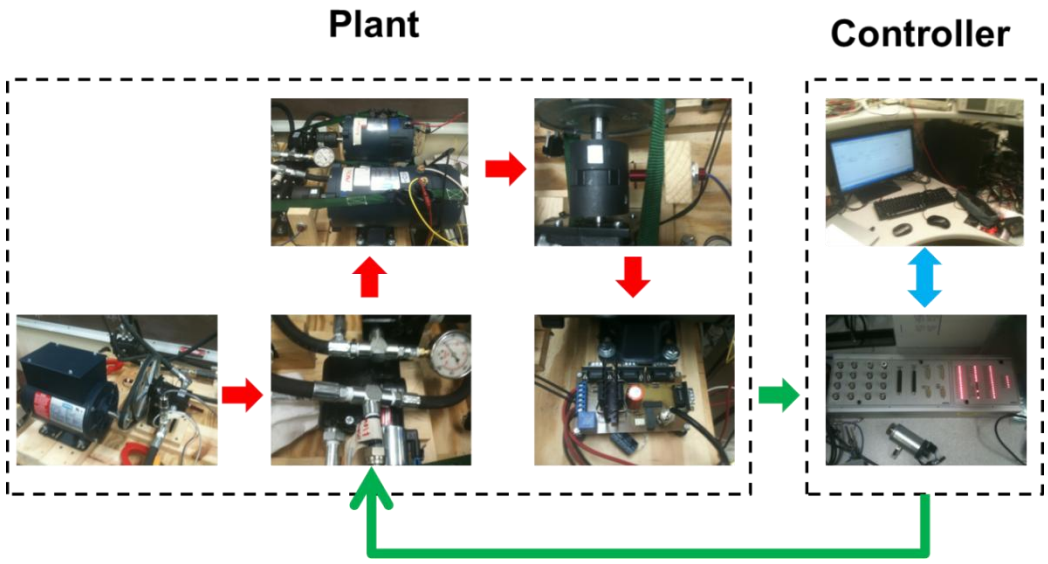

Figure 4.5 Schematic diagram of the experimental setup operation

Subsequently, the operation of the experimental setup components is discussed and the data acquisition procedure from the prototype is introduced.

4.1 System Component Operation

This section describes the operation of the components of the hydraulic system prototype. The characteristics and operation of each individual hydraulic component is discussed individually.

4.1.1 Fixed Displacement Hydraulic Pump

The main hydraulic pump is a fixed displacement gear pump with a displacement of 0.517 in^3/rev. The pump is a product of Haldex model 10567 and designed for bi-directional rotation and is considered highly efficient in operation. The pump consists of an external gear fixed displacement design with durable cast iron housing making it suitable for a wide variety of hydraulic applications. Figure 4.6 shows the hydraulic pump.

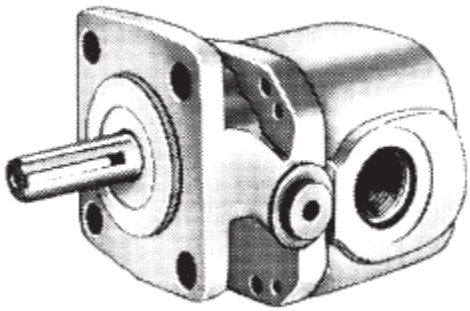

Figure 4.6 Haldex 10567 fixed displacement hydraulic pump

4.1.2 Fixed Displacement Hydraulic Motor

The primary motor and auxiliary motor are both fixed displacement auxiliary motors with a displacement of 0.097 0.517 in^3/rev. The operation of the motors is similar to the hydraulic pump. The motors are manufactured by Haldex model 10563.

4.1.3 Check Valve

The check valves ensure unidirectional flow in the system and prevent backflows. The model of the Figure 4.7 displays the check valve of model CI-T04 which is manufactured by Northman Fluid Power. The cracking pressure of the check valve is 5 psi and the maximum operating pressure is 3000 psi. Check valves are installed at the pump outlets and motor inlets to prevent back flow to the rotary hydraulic components. An additional check valve connects the forward path to the reverse path and only allows flow if reverse path flow pressure exceeds forward path flow pressure.

Figure 4.7 Northman Fluid Power CI-T04 check valve

4.1.4 Pressure Relief Valve

A ball spring type pressure relief valve is installed in the hydraulic circuit which protects the system from pressure damage. Figure 4.8 displays the PRV of model RD-1800a product of Prince Manufacturing Corporation. The valve is fast opening and

suitable for pressure spike protection. The valve opening pressure is adjustable between 1000 psi to 2500 psi. Figure 4.89displays the valve operating chart at different set points. The maximum capacity of the inlet flow of the valve is 20 gpm.

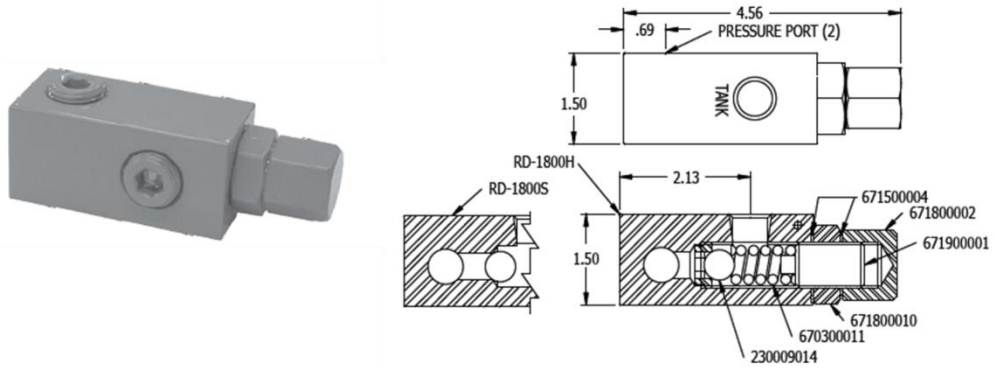

Figure 4.8 Prince Manufacturing Corporations RD-1800 pressure relief valve

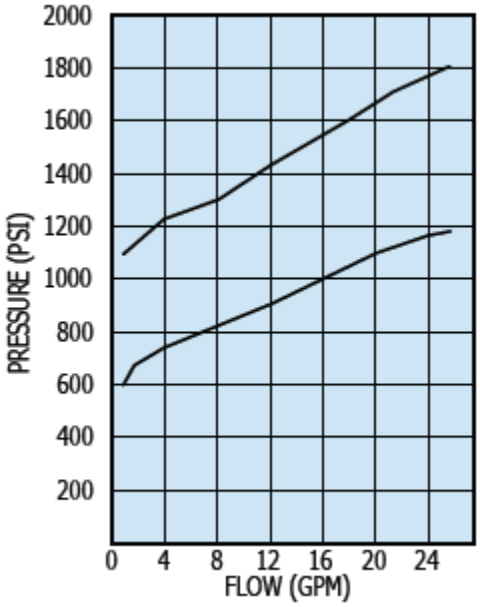

Figure 4.9 Pressure relief valve operation at different set points

4.1.5 Flow Control Valve

Flow control valves control the path and distribution of the flow which is generated by the hydraulic pump.

4.1.5.1 3-Way Proportional Valve

The three way proportional valve distributes the pump flow between the motors. The valve is manufactured by Brand Hydraulics. The valve incoming flow is pressure compensated and proportional to the current received by the coil. The valve flow can vary between fully closed to wide open. The valve has two output ports, namely the control flow (CF) port which directs the flow to the primary motor and the excess flow (EX) port which distributes the flow the auxiliary motor. The flow distribution is adjusted by the supplied current to the solenoid. As the solenoid current increases, the variable orifice moves proportionally. Figure 4.10 illustrates the proportional valve with dimensions.

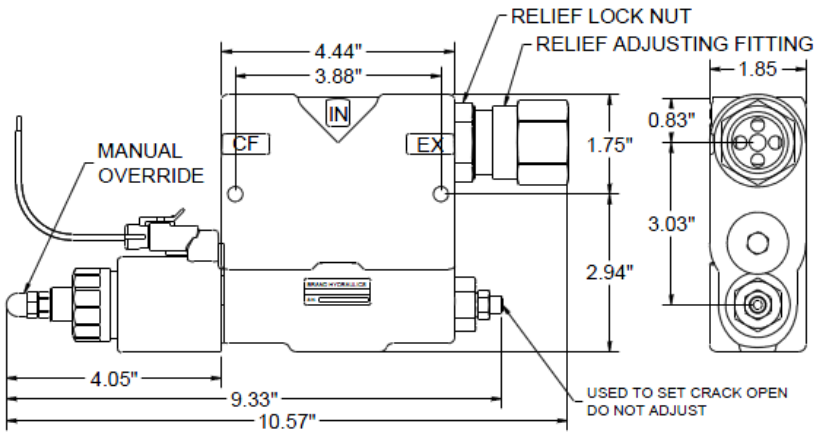

Figure 4.10 Brand Hydraulics 3-way proportional flow control valve

4.1.5.2 Manually Operated Directional Valve

The manual directional flow control valve of model HD-T03 which is a product of Northman Fluid Power is displayed in Figure 4.11. The valve switches the system between the OL and CL configuration. The valve switches to OL by pulling down the lever. In OL configuration the fluid goes through the oil tank and the trapped air in the system is ejected by further adding hydraulic fluid to the hoses. Figure 4.12 displays the operation of the directional valve between open loop and closed loop configurations.

Figure 4.11 Northman Fluid Power HD-T03 Manually Operated Directional Valve

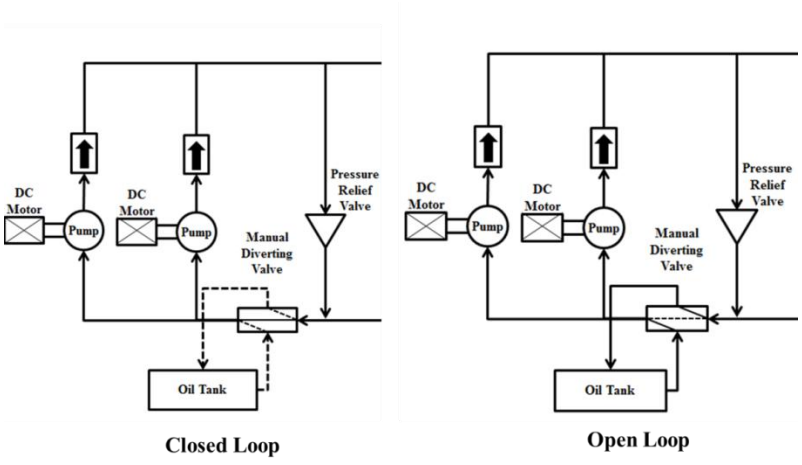

Figure 4.12 Closed loop and open loop configurations of the hydraulic circuit

4.1.5.3 Solenoid Operated Directional Valve

The electric flow diverting valve is a SWH-G02 series of Northman Fluid Power. The valve switches the hydraulic system between the natural flow split and forced flow configuration. When the valve is energized by appropriate current, the system switches to the natural flow split configuration and the 3-way proportional valve is excluded from the circuit. Otherwise, the system runs in forced flow configuration and the fluid is distributed through the proportional valve between the motors. Figure 4.13 shows the model of the valve.

Figure 4.13 Northman Fluid Power SWH-G02 Series solenoid operated directional valve

4.1.6 Flexible Hoses

The flexible hoses direct the flow path. They transfer the flow from the pump to the motors and recirculate the flow back to the pump. The flexible hoses are R2AT model which is manufactured by SAE. The maximum operating pressure of the hoses is 4000 psi.

4.1.7 Hydraulic Fluid

The system is filled with hydraulic fluid which transfers the energy of pump to the motors. The hydraulic fluid which is used in the experimental setup is Mag1 anti-wear R&O ISO 32.

4.1.8 Sensors

Several sensors are used in the system prototype to measure the system operation, namely angular velocity of the rotary components, hydraulic flow and pressure accurately.

4.1.8.1 Angular Velocity Sensor

Gear tooth Hall Effect sensors are used to measure the angular velocity of the rotary components. The application of these sensors is where ferrous edge detection or near zero speed sending is required. The current sinking output of the sensor requires the using a pull up resistor. Figure 4.14 shows the speed sensor with the electric circuit. The sensor exerts a signal when sensing the ferrous edge of the couplings and generate a pulse.

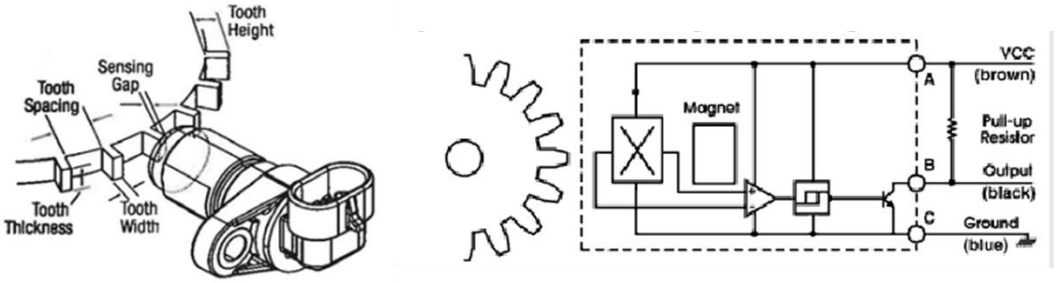

Figure 4.14 Gear tooth hall effect angular velocity sensor

4.1.8.2 Flow Sensor

The FT-110 Series TurboFlow® sensor measures flow rates of 0.1 to 8 GPM. The Hall Effect sensor is low cost and has a repeatability of 0.5%.The sensor output is a pulse rate according to the flow which passes through. Figure 4.15 shows the model of the flow sensor.

Figure 4.15 TurboFlow FT-110 Series flow sensor

4.1.8.3 Pressure Sensor

The MSP 300 series pressure transducer from the Microfocused line of MEAS is a high performance, low cost and high volume pressure sensor for commercial and industrial applications. The transducer pressure cavity is made of stainless steel, and includes a pipe thread allowing leak proof, all metal sealed system. Figure 4.16 shows a model of the pressure sensor.

Figure 4.16 MEAS MSP 300 Series pressure sensor

4.1.9 dSPACE 1104

dSPACE 1104 is a fast prototyping controller board which is used for control system development and data acquisition. The real-time hardware based on PowerPC technology and the associated set of I/O interfaces transform the board into an ideal solution for developing controllers in a variety of industrial and research fields.

4.2 Data Acquisition from the System Prototype

The sensors measure the system parameters by exerting outputs which are either pulses or voltages. An electronic board is designed to transfer the sensor outputs to dSPACE. Simulink blocks are created to convert the sensor output into numerical values. The ControlDesk software of dSPACE is used to numerically display and store the parameter values.

4.2.1 Angular Velocity Sensor

The Hall Effect is production of Hall Voltage across an electric conductor, similar to the electric current and magnetic field in a conductor. The Hall Effect sensor varies output voltage in proximity of a magnetic field. A combination of the Hall Effect sensor with an electric circuit results in a digital on/off sensor which exerts pulses according to the type of the material in the magnetic field. The type of the speed sensor which is installed in the experimental setup detects the ferrous metal edges and exerts a positive pulse when exposed to it. The hydraulic motors and generators are coupled together with a metal coupling and a rubber fitting which fills the space between the metal parts. The angular velocity sensors are installed next to the motor/generator coupling. Consequently, during the rotation of the motor, the sensor is either exposed to the metal part or the rubber material. Every time the sensor is exposed to the metal coupling, it exerts a positive pulse. Figure 4.17 shows the rubber fitting and the exerted pulse.

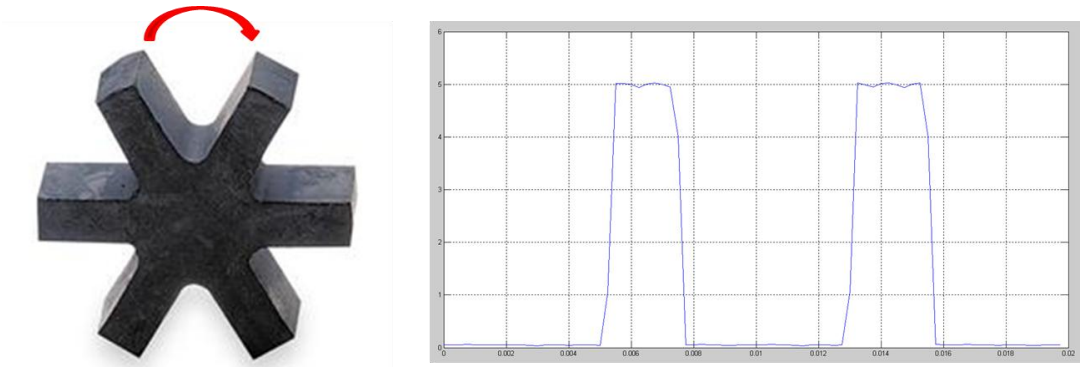

Figure 4.17 Motor/Generator rubber coupling and angular velocity sensor pulses

Since the rubber fitting is made of six teeth, every revolution of the motor is translated into six pulses. A Simulink block is created to measure the time between every two pulses, namely the time between pulses. This time is multiplied by six to find the motor angular velocity. Sample averaging is used to minimize fluctuation of the measurements.

4.2.2 Flow Sensor

The flow sensor exerts pulses as long as hydraulic fluid is passing through the sensor. The flow sensor has a mapping table which relates the number of pulses into fluid volume. Measurement of the number of pulses in a certain time window results in the flow. In another technique, instead of counting the number of pulses which leads to data oscillation, the time between two pulses is computed similar to the angular velocity sensor. Appropriate conversions are used to convert the measured time into flow values. Sample averaging is used to minimize the flow value oscillations. Table 4.1 illustrates the conversion from number of pulses to flow.

Table 4.1 Flow sensor output pulse conversion to flow

Flow Range		**Pulse Per**		**Frequency**
GPM	**Liters**	**Gallon**	**Litter**	**Output**
0.26-4.0	1-15	8300	2200	37550 Hz
0.53-7.9	2-30	3800	1000	33500 Hz

4.2.3 Pressure Sensor

The pressure sensor generates a proportional positive voltage according the fluid pressure. A linear correlation is used to convert the sensor output voltage into pressure in psi. Figure 4.18 illustrates the linear correlation.

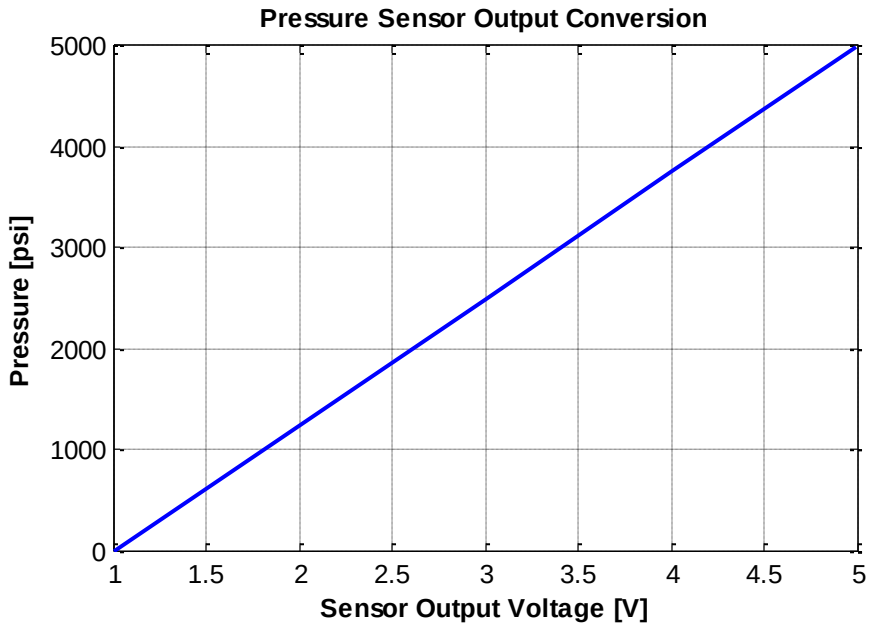

Figure 4.18 Pressure sensor output voltage conversion to psi

5. THE MATHEMATICAL MODEL ANALYSIS

This section studies the stability of the mathematical model of the system. The nonlinearities in the system is a result of the discrete system components, namely proportional valves, variable leakage coefficients, and discrete safety valves. The linear mathematical model describes the hydraulic system in natural flow split configuration. In order to analyze the system stability and locate system resonances, the linear state-space model of the system into transfer function representation, and the stability of the transfer functions from every output to the system input is analyzed with appropriate tools. Additionally, the stability of the non-linear mathematical model is discussed in brief. The nonlinear model represents the forced flow configuration model of the hydraulic system.

5.1 Linear Model Stability Analysis

According to Chapter 3, the state-space representation of a linear dynamic system is represented by

$$\begin{aligned} \dot{x} &= Ax + BU \\ y &= Cx + DU \end{aligned} \tag{5.1}$$

The state space representation of the system could be transformed into transfer function representation by

$$TF = C(sI - A)^{-1}B + D \tag{5.2}$$

where *s* is the Laplace operator, and *I* is an identity matrix with the same dimension as *A*. The state-space representation is transformed to transfer function from every output to the input as following

$$\begin{Bmatrix} P_p(s) \\ \omega_{mA}(s) \\ \omega_{mB}(s) \end{Bmatrix} = \begin{bmatrix} s+(\beta/V)(k_{L,p}+k_{L,mA}+k_{L,mB}) & (\beta/V)D_{mA} & (\beta/V)D_{mB} \\ -D_{mA}\eta_{mech,mA}/I_{mA} & s+B_{mA}/I_{mA} & 0 \\ -D_{mB}\eta_{mech,mB}/I_{mB} & 0 & s+B_{mB}/I_{mB} \end{bmatrix}^{-1} \begin{Bmatrix} (\beta/V)D_p \\ 0 \\ 0 \end{Bmatrix} \omega_p(s) \tag{5.3}$$

The frequency response of the system is achieved by switching from time domain (*s)* to frequency domain ($j\omega$)

$$\begin{Bmatrix} P_p(j\omega) \\ \omega_{mA}(j\omega) \\ \omega_{mB}(j\omega) \end{Bmatrix} = \begin{bmatrix} j\omega+(\beta/V)(k_{L,p}+k_{L,mA}+k_{L,mB}) & (\beta/V)D_{mA} & (\beta/V)D_{mB} \\ -D_{mA}\eta_{mech,mA}/I_{mA} & j\omega+B_{mA}/I_{mA} & 0 \\ -D_{mB}\eta_{mech,mB}/I_{mB} & 0 & j\omega+B_{mB}/I_{mB} \end{bmatrix}^{-1} \begin{Bmatrix} (\beta/V)D_p \\ 0 \\ 0 \end{Bmatrix} \omega_p(j\omega) \tag{5.4}$$

Table 5.1 illustrates the parameter values of the hydraulic system. The parameter values are applied to Equation 5.3 to achieve numerical transfer functions.

$$\frac{P_p(s)}{\omega_p(s)} = \frac{7.475s^2+71.76s+171}{s^3+9.785s^2+106.7s+398.1} \tag{5.5}$$

$$\frac{\omega_{mA}(s)}{\omega_p(s)} = \frac{218.7s+962.1}{s^3+9.785s^2+106.7s+398.1} \tag{5.6}$$

$$\frac{\omega_{mB}(s)}{\omega_p(s)} = \frac{218.7s+1137}{s^3+9.785s^2+106.7s+398.1} \tag{5.7}$$

The repeated expression in the denominator of the three transfer functions is the system characteristic equation which represents system poles in time domain. The system poles are computed by solving the characteristic equation for the Laplace operator *s*

$$s^3+9.785s^2+106.7s+398.1=0 \tag{5.8}$$

$$s_{1,2} = -2.6925 + j8.7040$$
$$s_3 = -4.8090 \tag{5.9}$$

The system is stable since all three poles are on the left half plane.

Table 5.1 Simulation parameters for stability analysis

Symbol	Quantity	Value	Unit
D_p	Pump Displacement	0.517	in^3/rev
D_{mA}	Primary Motor Displacement	0.097	in^3/rev
D_{mB}	Auxiliary Motor Displacement	0.097	in^3/rev
I_{mA}	Primary Motor Inertia	0.0005	$kg.m^2$
I_{mB}	Auxiliary Motor Inertia	0.0005	$kg.m^2$
B_{mA}	Primary Motor Damping	0.0026	N.m/(rad/s)
B_{mB}	Auxiliary motor Damping	0.0022	N.m/(rad/s)
$K_{L,p}$	Pump Leakage Coefficient	0.01	
$K_{L,mA}$	Primary Motor Pump Leakage Coefficient	0.001	
$K_{L,mB}$	Auxiliary Motor Pump Leakage Coefficient	0.001	
η_{total}	Pump/Motor Total Efficiency	0.90	
η_{vol}	Pump/Motor Volumetric Efficiency	0.95	
β	Fluid Bulk Modulus	183695	psi
ρ	Fluid Density	0.0305	lb/in^3
υ	Fluid Viscosity	7.12831	cSt

The transfer function shown in Equation 5.5 represents the system dynamics from the first output, hydraulic pump gauge pressure, to the system input, pump angular velocity. The numerator of this transfer function is solve for *s* to find the system zeros

$$7.475s^2 + 71.76s + 171 = 0 \tag{5.10}$$

$$z_1 = -5.20$$
$$z_2 = -4.40 \tag{5.11}$$

The transfer function shown in Equation 5.6 represents the system dynamics from the second output, primary motor angular velocity, to the system input, pump angular velocity. The numerator of this transfer function is solve for *s* to find the system zeros

$$218.7s + 962.1 = 0 \tag{5.12}$$

$$z = -4.40 \tag{5.13}$$

The transfer function introduced in Equation 5.7 represents the system dynamics from the third output, auxiliary motor angular velocity, to the system input, pump angular velocity. The numerator of this transfer function is solve for *s* to find the system zeros

$$218.7s + 1137 = 0 \tag{5.14}$$

$$z = -5.20 \tag{5.15}$$

Subsequently, the frequency responses of the system are analyzed. The natural frequency and damping ratio of a second order underdamped pole are computed by

$$s_{1,2} = -\omega_n \xi \pm j\omega_n \sqrt{\xi^2 - 1} \tag{5.16}$$

where ω_n is the natural frequency of the system, and ξ is the damping ratio of the system.

For this particular system

$$\begin{cases} \omega_n \xi = 2.6925 \\ \omega_n \sqrt{\xi^2 - 1} = 8.7040 \end{cases} \tag{5.17}$$

$$\begin{cases} \xi = 0.29 \\ \omega_n = 9.11 \end{cases} \tag{5.18}$$

Figure 5.1 to 5.3 depict the bode diagram of the frequency response function between the system outputs and pump angular velocity. According to the figures, the resonance frequency of the system is at 9.11 *rad/sec*.

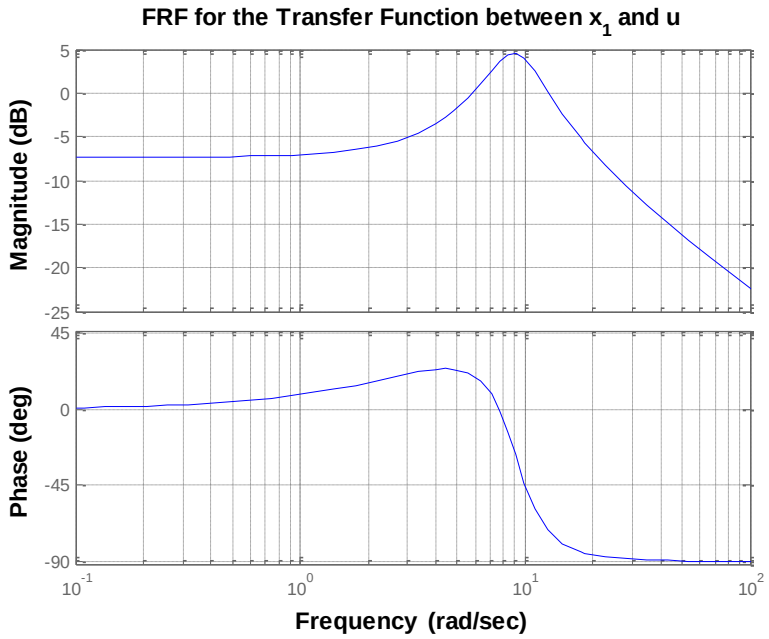

Figure 5.1 Frequency response function (FRF) from pump gauge pressure to pump angular velocity

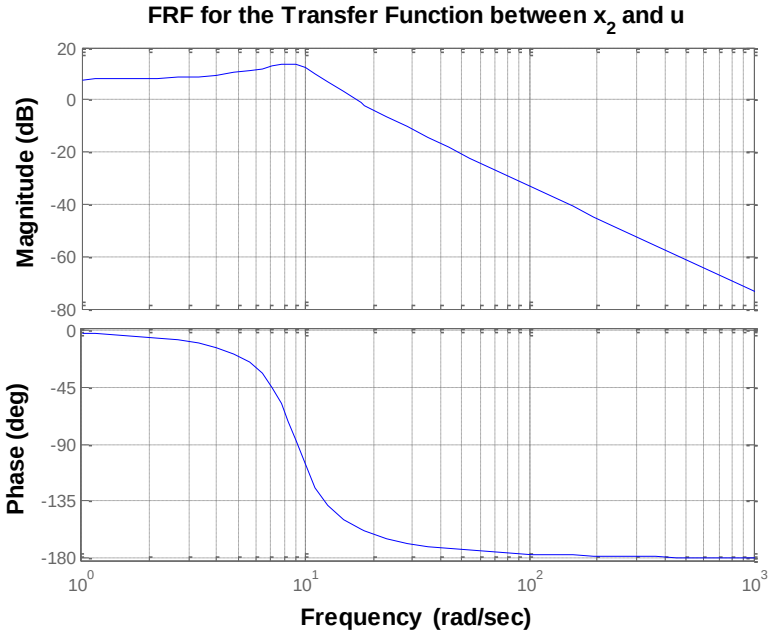

Figure 5.2 Frequency response function (FRF) from primary motor angular velocity to pump angular velocity

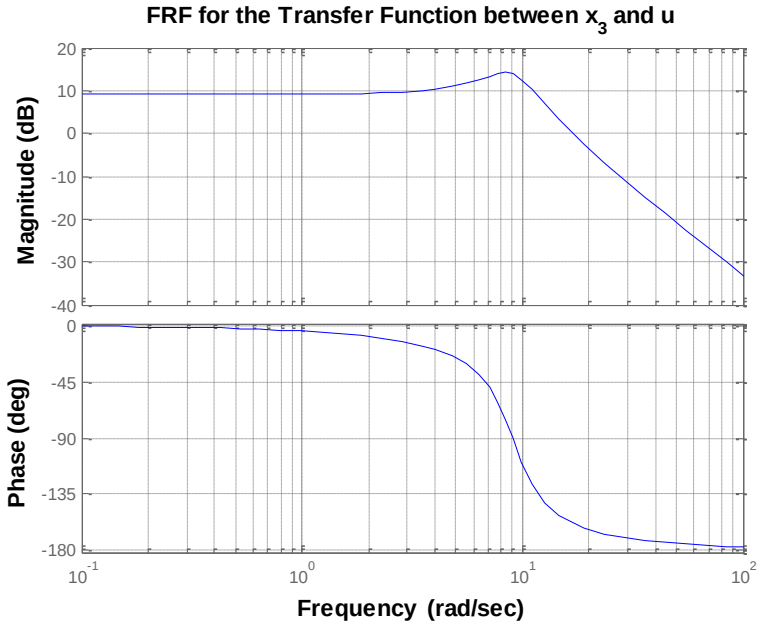

Figure 5.3 Frequency response function (FRF) from auxiliary motor angular velocity to pump angular velocity

This section studied the stability of the linear model of the hydraulic energy transfer system. The results of the simulations confirm the stability of the system dynamics from every output to the system input.

5.2 Linear Model Stability Analysis

The nonlinear state-space representation of a dynamic system is introduced in Equation 3.60

$$\begin{aligned} \dot{x} &= f(x) + g(x)U \\ y &= h(x) \end{aligned} \tag{5.19}$$

In order to study the stability of the nonlinear system, the nonlinear state-space equation is simplified by attenuation of the constant parameters in the equations into a coefficient k_i

$$\begin{Bmatrix} dP/dt \\ d\omega_{mA}/dt \\ d\omega_{mB}/dt \end{Bmatrix} = \begin{Bmatrix} k_1 P_p + k_2\sqrt{|P_p|}\,\mathrm{sgn}(P_p) \\ k_3\omega_{mA} \\ k_4\sqrt{|P_p|}\,\mathrm{sgn}(P_p) + k_5\omega_{mB} \end{Bmatrix} + \begin{bmatrix} k_6 & 0 \\ 0 & k_7\sqrt{|P_p|}\,\mathrm{sgn}(P_p) \\ 0 & k_8\sqrt{|P_p|}\,\mathrm{sgn}(P_p) \end{bmatrix} \begin{Bmatrix} \omega_p \\ h_i \end{Bmatrix} \tag{5.20}$$

where

$$\begin{aligned} &k_1, k_2, k_3, k_5, k_8 < 0 \\ &k_4, k_6, k_7 > 0 \end{aligned} \tag{5.21}$$

The nonlinear state-space equation could be further simplified by substituting the state variables with x_i

$$\begin{Bmatrix} x_1 \\ x_2 \\ x_3 \end{Bmatrix} = \begin{Bmatrix} k_1 x_1 + k_2\sqrt{|x_1|}\,\mathrm{sgn}(x_1) \\ k_3 x_2 \\ k_4\sqrt{|x_1|}\,\mathrm{sgn}(x_1) + k_5 x_3 \end{Bmatrix} + \begin{bmatrix} k_6 & 0 \\ 0 & k_7\sqrt{|x_1|}\,\mathrm{sgn}(x_1) \\ 0 & k_8\sqrt{|x_1|}\,\mathrm{sgn}(x_1) \end{bmatrix} \begin{Bmatrix} \omega_p \\ h_i \end{Bmatrix} \tag{5.20}$$

The equilibrium point of the nonlinear system is computed by solving *f(x)=0*

$$\begin{cases} f_1(x) = 0 \\ f_2(x) = 0 \\ f_3(x) = 0 \end{cases} \tag{5.21}$$

By solving the first equation

$$k_1 x_1 + k_2\sqrt{|x_1|}\,\mathrm{sgn}(x_1) = 0 \tag{5.22}$$

The first solution to the equation is

$$x_1 = 0 \tag{5.23}$$

If $x_1 > 0$

$$k_1 x_1 + k_2\sqrt{x_1} = 0 \tag{5.24}$$

hence,

$$\frac{x_1}{\sqrt{x_1}} = \frac{-k_2}{k_1} \tag{5.25}$$

however, according to the x_i condition

$$\frac{x_1}{\sqrt{x_1}} > 0 \tag{5.26}$$

and according to Equation 5.21

$$\frac{-k_2}{k_1} < 0 \tag{5.27}$$

Consequently the equation does not have a solution.

By solving the second equation

$$k_3 x_2 = 0 \tag{5.28}$$

Hence

$$x_2 = 0 \tag{5.29}$$

Lastly, by solving the final equation

$$k_4 \sqrt{|x_1|}\,\mathrm{sgn}(x_1) + k_5 x_3 = 0 \tag{3.30}$$

According to Equation 5.23 the above equation is simplified to

$$k_3 x_3 = 0 \tag{5.31}$$

Hence

$$x_3 = 0 \tag{5.32}$$

Consequently the equilibrium point of the nonlinear system is computed according to Equations 5.23, 5.29, and 5.32.

$$x_e = \begin{Bmatrix} 0 \\ 0 \\ 0 \end{Bmatrix} \tag{5.33}$$

A limit cycle is an oscillatory behavior of a nonlinear system about the reference value. The existence of limit cycles in the nonlinear system is computed by finding the sign of divergence of vector *f(x)*

$$\nabla f = \frac{df_1}{dx_1} + \frac{df_2}{dx_2} + \frac{df_3}{dx_3} \tag{5.34}$$

A nonlinear system does not have a limit cycle if the divergence of *f(x)* is nonzero

$$\frac{df_1}{dx_1} + \frac{df_2}{dx_2} + \frac{df_3}{dx_3} \neq 0 \tag{3.35}$$

By analyzing the first term of Equation 5.34

$$\frac{df_1}{dx_1} = \frac{d(k_1 x_1 + k_2 \sqrt{|x_1|}\,\mathrm{sgn}(x_1))}{dx_1} \tag{5.36}$$

If $x_1=0$

$$\frac{df_1}{dx_1} = 0 \tag{5.37}$$

If $x_1>0$

$$\frac{df_1}{dx_1} = k_1 + k_2 \frac{1}{2\sqrt{|x_1|}} \tag{5.38}$$

According to Equation 5.21

$$\frac{df_1}{dx_1} < 0 \tag{5.39}$$

Similarly for the other terms of Equation 5.34 and by using Equation 5.21

$$\frac{df_2}{dx_2} = k_3 < 0 \tag{5.40}$$

$$\frac{df_3}{dx_3} = k_5 < 0 \tag{5.41}$$

The existence of a limit cycle for the nonlinear equation is studied by using Equations 5.37 to 5.41

$$\frac{df_1}{dx_1} + \frac{df_2}{dx_2} + \frac{df_3}{dx_3} < 0 \tag{5.42}$$

Consequently, the nonlinear system doesn't have a limit cycle.

6. HYDRAULIC SYSTEM MATHEMATICAL MODEL VERIFICATION

The nonlinearities in gearless hydraulic wind power transfer are originated by operation of discrete elements, such as flow control valves and variable leakage coefficients. These nonlinearities are addressed in the forced flow configuration of the system. In this configuration, a control command is sent to the proportional valve to regulate the valve position. However, different types of valves possess diverged characteristics from one to another, and are modeled distinctively. In order to solely focus on the linear hydraulic characteristics of the hydraulic system, and the similarities between the available models, the mathematical model is validated in natural flow split configuration.

This chapter validates the mathematical model of the hydraulic system, in both ODE and state-space representations, with simulations and experimental data. A detailed hydraulic model is created by the SimHydraulics toolbox of MATLAB/Simulink® and the simulation results are compared with the mathematical model. Subsequently, the experimental data from the system prototype are compared with the mathematical model simulation results.

6.1 Model Verification with SimHydraulics Simulation Package

The SimHydraulics toolbox of MATLAB is a powerful tool to model and implement hydraulic energy transfer for wind power transfer [43]. The toolbox contains hydraulic components which could be connected together as modules and form a complete hydraulic circuit.

The SimHydraulics toolbox was utilized to create a hydraulic system similar to Figure 2.1. The hydraulic pump and motors are governed by identical equations compared to the ones implemented in the proposed hydraulic mathematical model. Moreover, both systems are assumed to contain the same type of hydraulic fluid, which translates into similar fluid density, fluid bulk modulus, and fluid kinematic viscosity respectively denoted by respectively.

The differences between the mathematical model and SimHydraulics are in the details of hose dynamics and centralized compressibility model. The SimHydraulics model implements a complex hose model which considers several geometric characteristics of the pipe such as inner pipe diameter, internal friction, and thickness. However, the mathematical model uses a simple compressibility model which focuses on the properties of the hydraulic fluid. Moreover, application of the SimHydraulics toolbox requires adjustment of the units of the variables, and transformation between unitless signals to physical parameters within the simulation model. The geometric characteristics of the pipes along with the total volume of fluid subjected to pressure effect are assumed similar in both models

In order to validate the proposed hydraulic mathematical model with SimHydraulics, and to analyze the impact of dissimilarities of the hose dynamics on dynamics of the system, a specific pump angular velocity profile is supplied to both the hydraulic system model and the SimHydraulics model. Simulation results are compared under identical operating conditions considering the following assumptions [44]:

1. The hydraulic fluid is assumed incompressible.
2. No loading is considered on pump and motor shafts (i.e. inertia, friction, spring and etc.).
3. Leakage inside the pump and motor are assumed to be linearly proportional to their respective differential pressure [36].

In simulations, a fixed displacement pump with a displacement of 0.517 in^3/rev supplies hydraulic fluid to a primary motor (Motor A) and an auxiliary motor (Motor B) both with fixed displacements of 0.097 in^3/rev. A specific angular velocity profile is supplied to the hydraulic pump to run the simulation model. This velocity profile is supplied to the hydraulic pump as a step input from 300 rpm to 400 rpm, and from 400 rpm back to 300 rpm to accommodate both overshoot and undershoot characteristics of the hydraulic system. Subsequently the mathematical ODE model and linear state space model are compared with the simulation results from the SimHydraulics model.

6.1.1 Mathematical Model (ODE) Verification

This section validates the mathematical ODE model of the hydraulic system with a similar model which is created with the SimHydraulics toolbox of

MATLAB/Simulink®. In simulations, a specific pump angular velocity profile is supplied to both models and the results of the simulations are compared in detail. Figure 6.1 depicts the angular velocity profile which is supplied to the pump. The profile is a step input from 300 rpm to 400 rpm, and back to 300 rpm to address both overshoot and undershoot dynamics of the system.

Table 5.1 shows the simulation parameters for both SimHydraulics and simulation models. The comparison between the simulation response of the SimHydraulics model and the derived mathematical model to the supplied hydraulic pump angular velocity profile are shown in Figures 6.2 to 6.9.

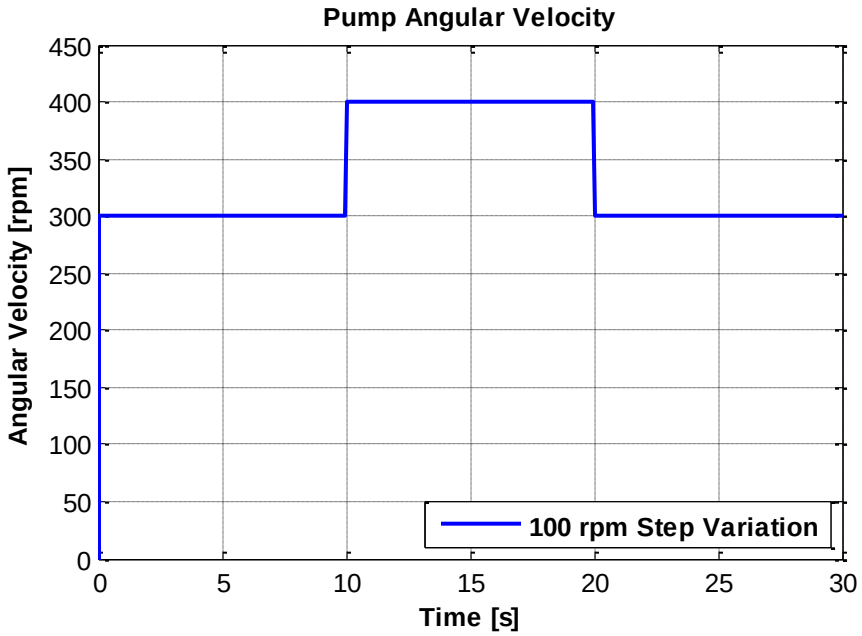

Figure 6.1 Hydraulic pump angular velocity profile

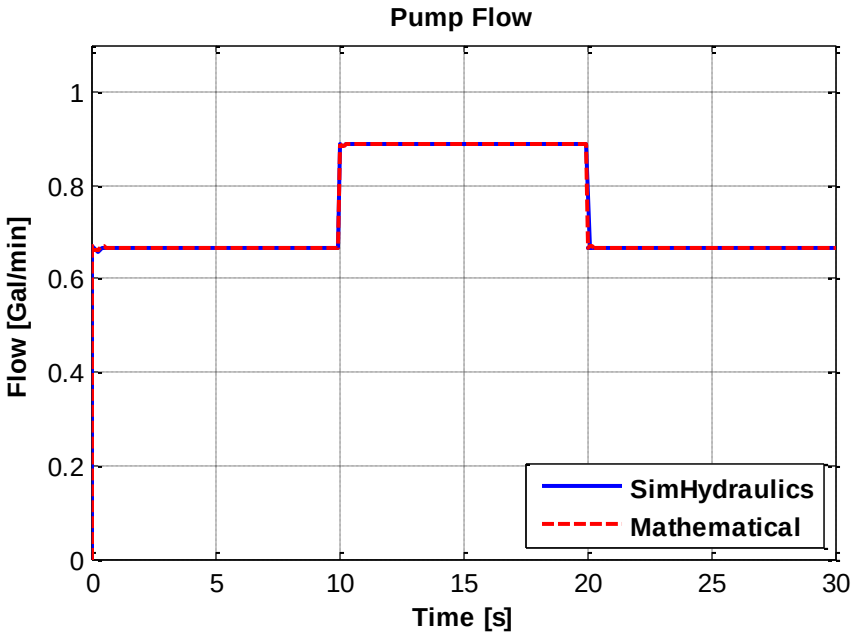

Figure 6.2 Comparison between the hydraulic pump flow of the mathematical model and SimHydraulics model

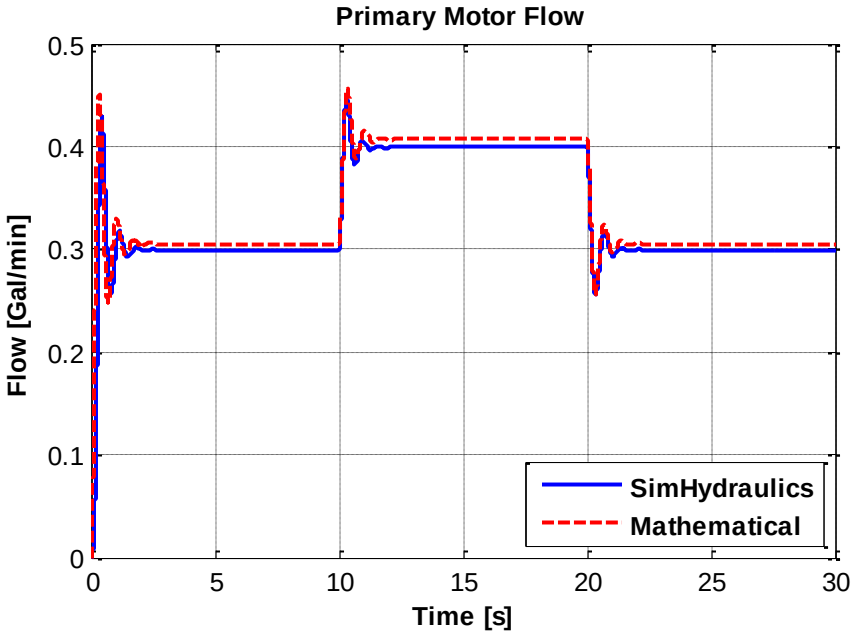

Figure 6.3 Comparison between the primary hydraulic motor flow of the mathematical model and SimHydraulics model

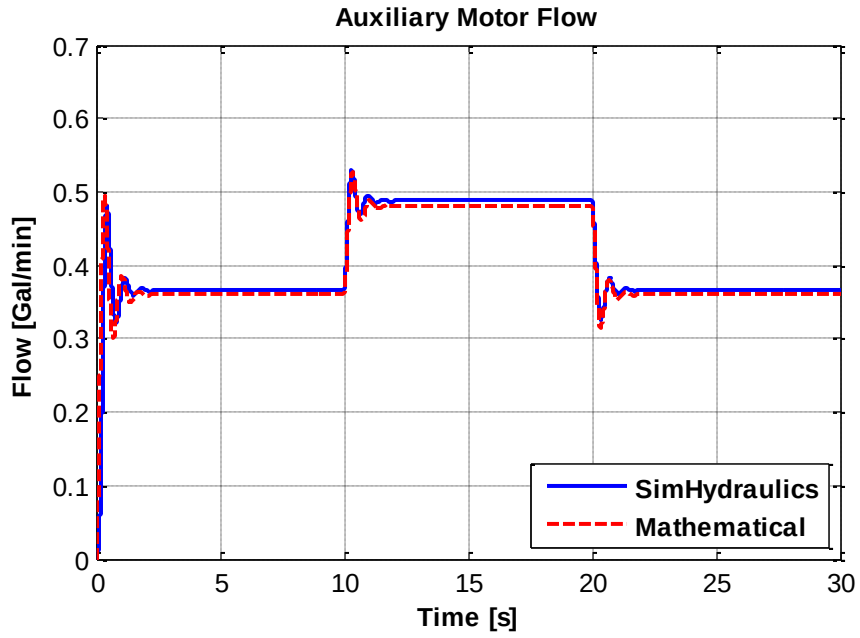

Figure 6.4 Comparison between the auxiliary hydraulic motor flow of the mathematical model and SimHydraulics model

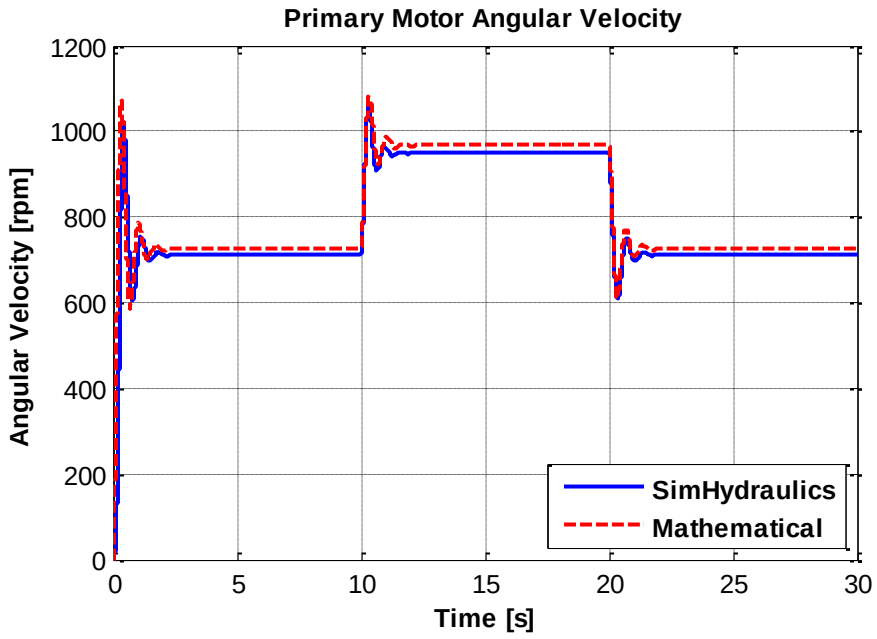

Figure 6.5 Comparison between the primary hydraulic motor angular velocity of the mathematical model and SimHydraulics model

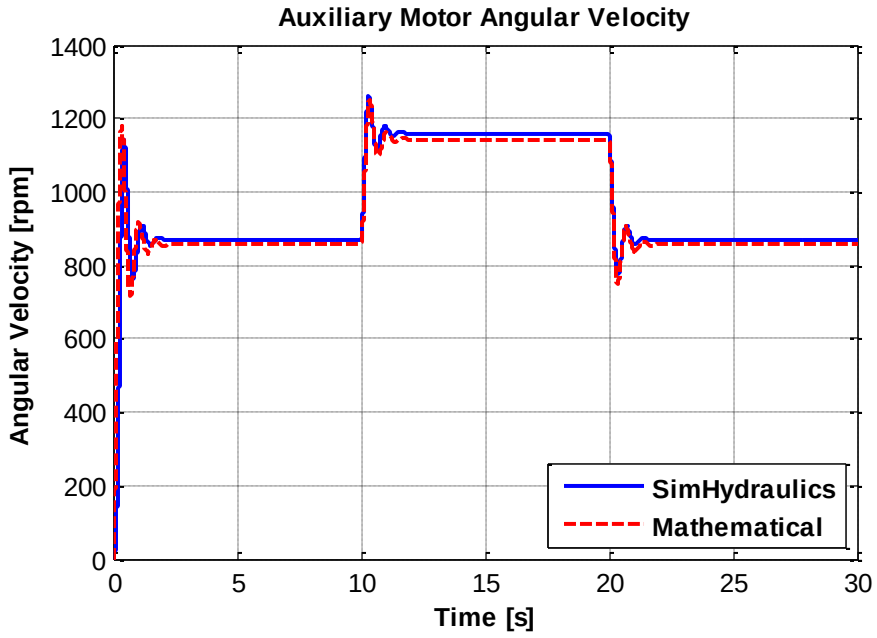

Figure 6.6 Comparison between the auxiliary hydraulic motor angular velocity of the mathematical model and SimHydraulics model

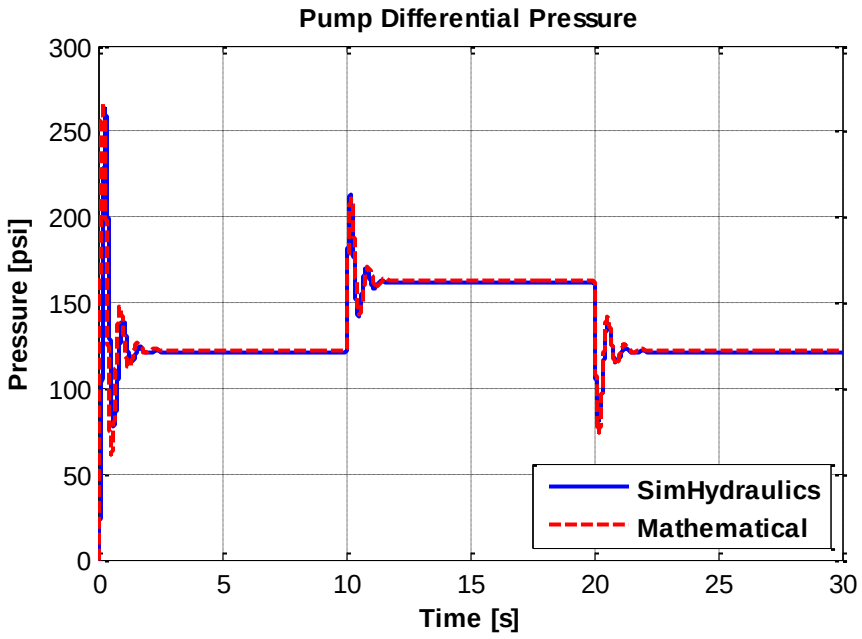

Figure 6.7 Comparison between the hydraulic pump terminal pressure of the mathematical model and SimHydraulics model

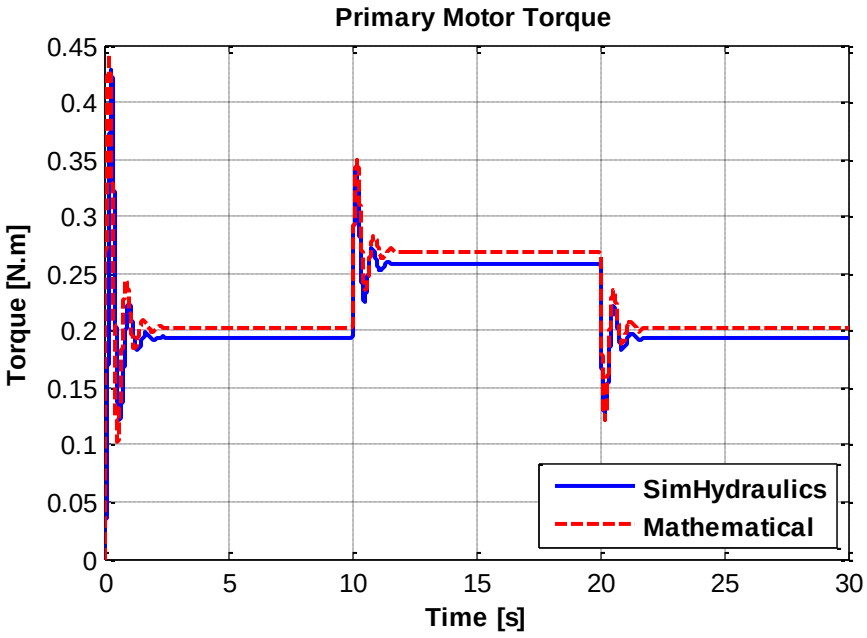

Figure 6.8 Comparison between the primary hydraulic motor output torque of the mathematical model and SimHydraulics model

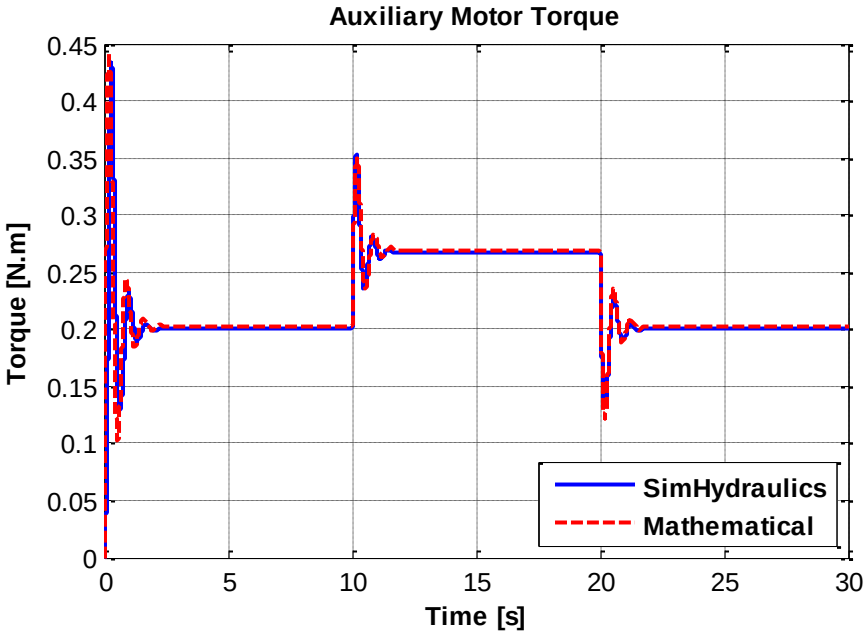

Figure 6.9 Comparison between the auxiliary hydraulic motor output torque of the mathematical model and SimHydraulics model

Figure 6.2 illustrates pump flow in response to the step change in the pump shaft speed. As the figure illustrates the generated pump flow in mathematical model matches that of the SimHydraulics toolbox. The transients of the mathematical model follow the same pattern as the simulation software and reach the same steady state values. This similarity is due to negligible dependency of pump flow to pressure variation. Although pump flow is a function of terminal pressure, small pump leakage coefficient minimizes the effect of pressure variation.

As a result of the step variation in the pump shaft speed, the flows generated and distributed in the hydraulic circuit primary and auxiliary motors are demonstrated in Figures 6.3 and 6.4. The results show that the simulated motor flows are identical.

Figures 6.5 and 6.6 depict the angular velocity associated to primary motor and auxiliary motor. The velocities generated from mathematical models result in similar transient and steady state values. However due to geometric material properties of the hoses which are considered in detail in SimHydraulics model, there is a slight deviation between motor output angular velocities obtained from mathematical model and SimHydraulics model.

Figure 6.7 illustrates hydraulic pump terminal pressure generated from mathematical model and from SimHydraulics. As the figure illustrates, the pressures follow similar pattern, and the mathematical results shows considerable similarity in both transient and steady state response with the SimHydraulics model. The pressure in

mathematical model has been obtained from the compressibility model while the pressure model in SimHydraulics considers complex pipe dynamics.

Figures 6.8 and 6.9 illustrate the shaft torque of primary motor and auxiliary motor. As the figures demonstrate the calculated torque from mathematical model and the one obtained from SimHydraulics follow the same pattern, and result in a close steady state values with accuracy of less than 2% deviation.

This section compared the simulation response of the dynamic model to a detailed model built with the SimHydraulics toolbox of MATLAB. Two distinct angular velocity profiles were supplied to the hydraulic pump in both model and the simulation results were compared. The pump speed, system pressure, and motor speeds, flows and torques obtained from mathematical models were in good agreement with the results obtained from software simulation. Some deviations were also observed in the simulation results which are due to simplified model of compressibility and dynamics of transmission lines. The main benefits of the mathematical model, besides a close dynamic simulation, is the compactness of the governing equations and achievement of a high-speed simulations compared to other software packages.

6.1.2 Linear State-Space Model Verification

In order to validate the proposed hydraulic state space model with SimHydraulics, and to analyze the impact of dissimilarities of the hose dynamics on dynamics of the system, a pump angular velocity profile was supplied to both models, and simulation

results were compared under identical operating conditions. Table 5.1 shows the simulation parameters for both SimHydraulics and simulation models.

In simulations, a fixed displacement pump with a displacement of 0.517 in^3/rev supplies hydraulic fluid to a primary motor (Motor A) and an auxiliary motor (Motor B) both with fixed displacements of 0.097 in^3/rev. Figure 6.10 displays the angular velocity profile which is supplied to the hydraulic pump as a step input from 300 rpm to 400 rpm, and from 400 rpm back to 300 rpm. Figures 6.11 to 6.16 illustrate the comparison between the simulation response of the SimHydraulics model and the derived state space model to a similar hydraulic pump angular velocity profile.

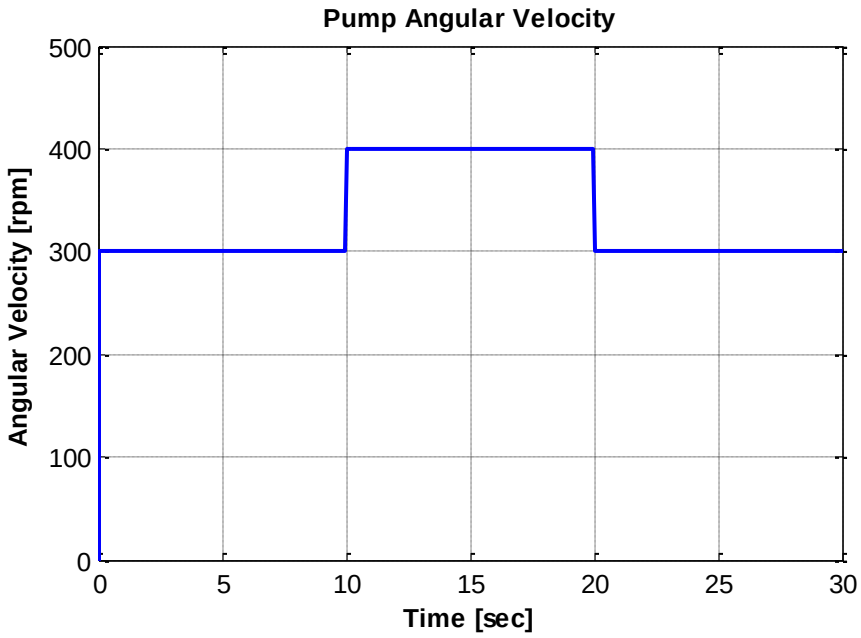

Figure 6.10 Hydraulic pump angular velocity profile

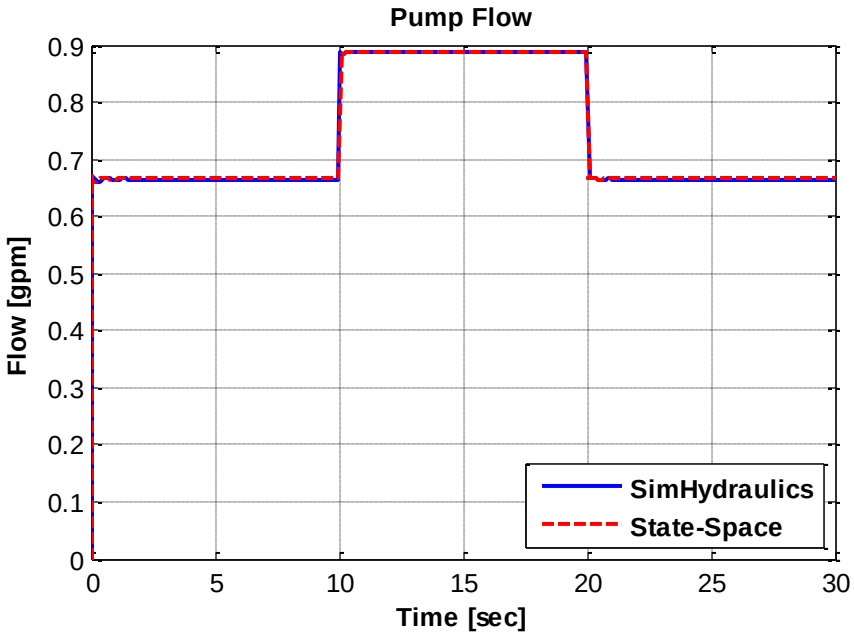

Figure 6.11 Comparison between the hydraulic pump flow of the state-space model and SimHydraulics model

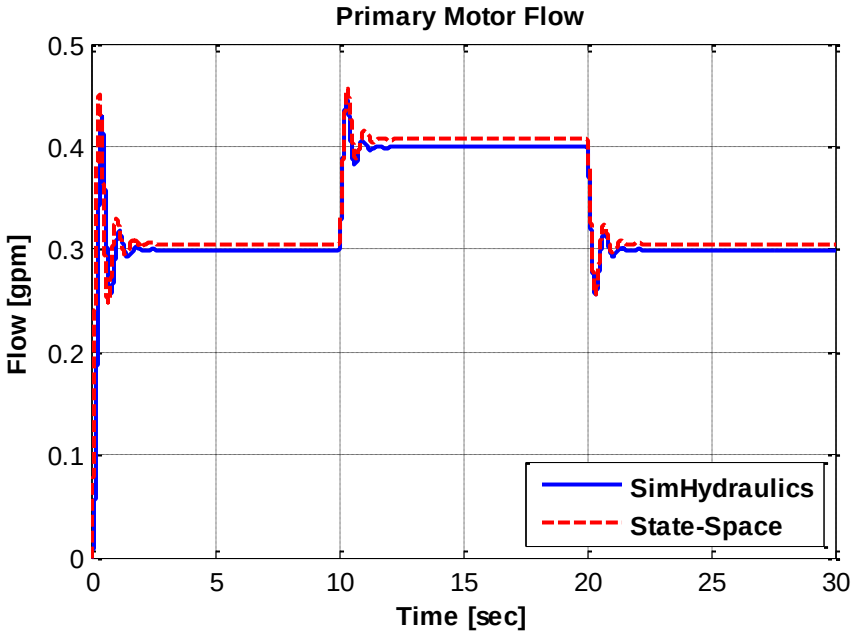

Figure 6.12 Comparison between the primary hydraulic motor flow of the state-space model and SimHydraulics model

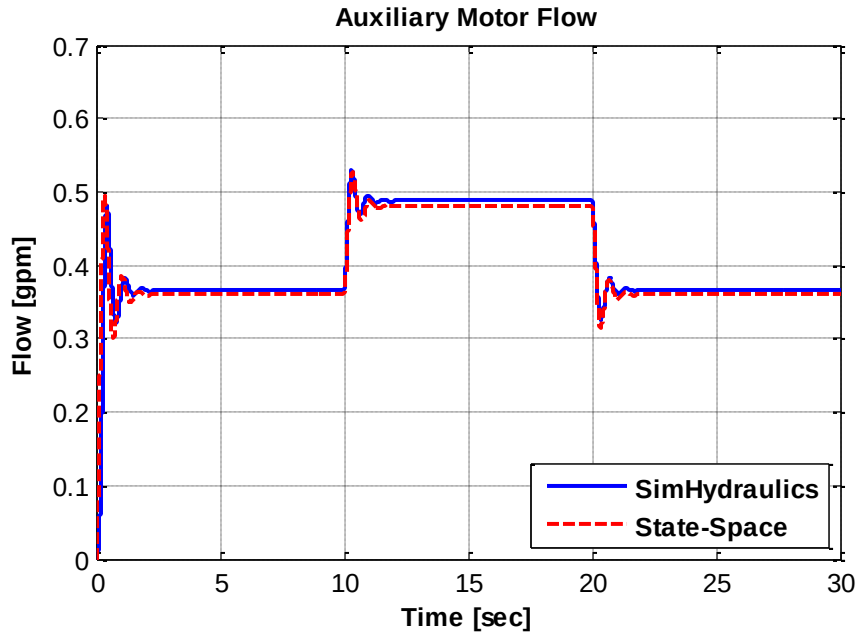

Figure 6.13 Comparison between the auxiliary hydraulic motor flow of the state-space model and SimHydraulics model

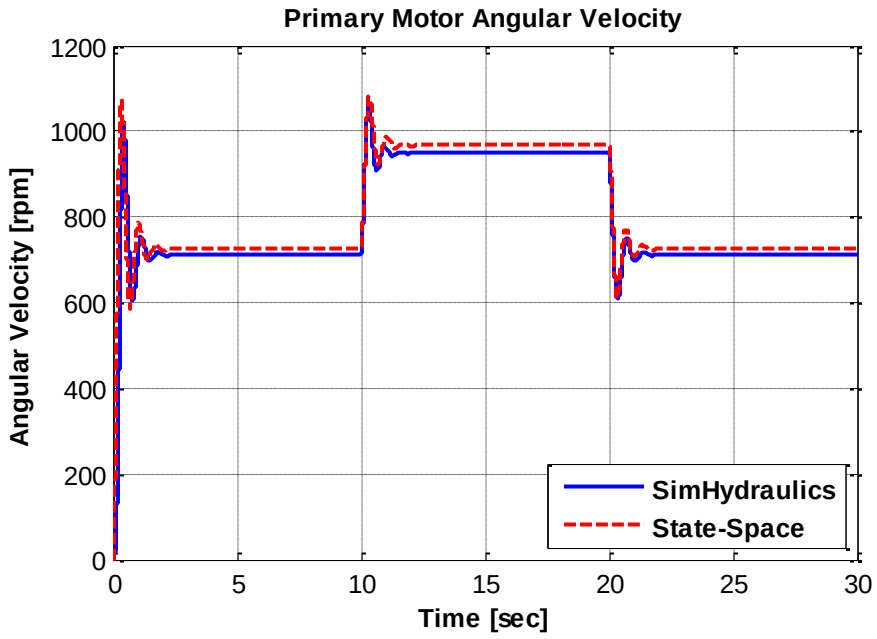

Figure 6.14 Comparison between the primary hydraulic motor angular velocity of the state-space model and SimHydraulics model

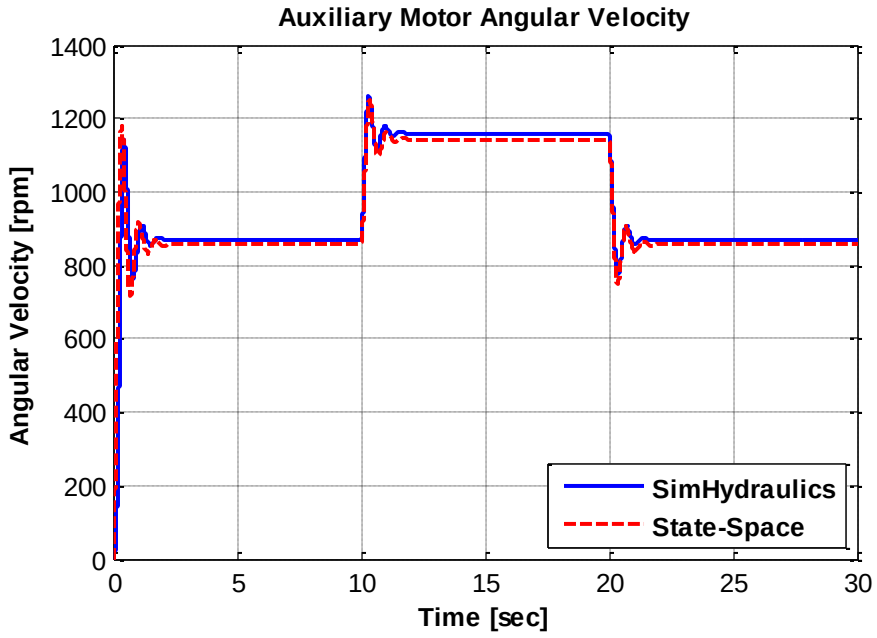

Figure 6.15 Comparison between the auxiliary hydraulic motor angular velocity of the state-space model and SimHydraulics model

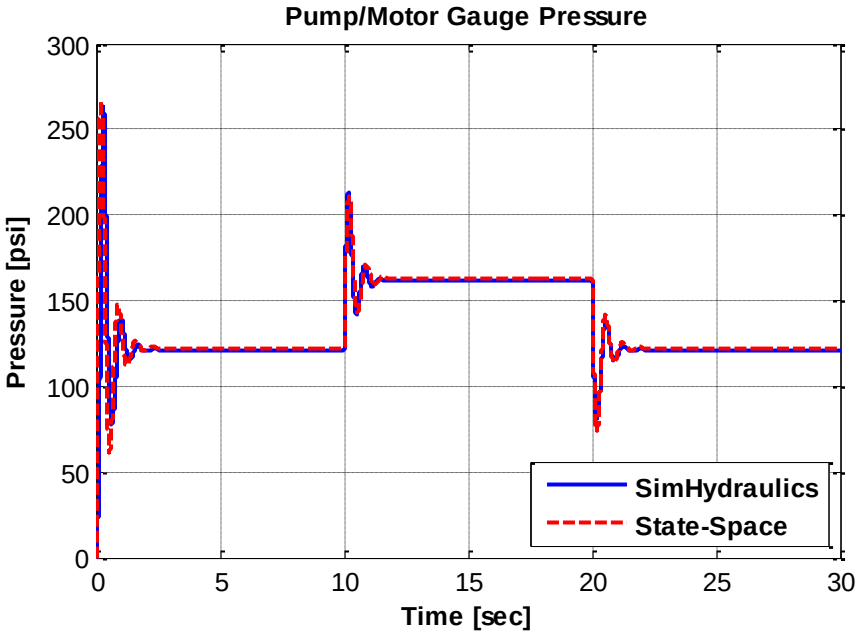

Figure 6.16 Comparison between the hydraulic pump terminal pressure of the state-space model and SimHydraulics model

Figure 6.11 depicts the variation of the pump flow with respect to the input angular velocity profile. Based on the figure, the flow generated by the pump in the state space model is similar to the result obtained from the SimHydraulics toolbox. The transients of the state space model response also matches with the SimHydraulics results, while the two responses approach the identical state space values after step inputs. The similarity is rationalized by the minor dependency of the pump flow to the pressure variations, since the small pump leakage coefficient, minimizes the effect of those variations.

Figures 6.12 and 6.13 demonstrate the flows generated and distributed in the hydraulic circuit between the primary and auxiliary motors. The results illustrate the similarity between the simulation responses for motor flows. Figures 6.14 and 6.15 depict the angular velocity associated with primary motor and auxiliary motor. The velocities generated from the state space model result in similar transient and steady state values.

The hydraulic pump terminal pressure generated from the state space model and from SimHydraulics is illustrated in Figure 6.16. As the figure demonstrates, the pressures track similar pattern, and the state space model results depict considerable resemblance equally in transient and steady state response with the SimHydraulics model. The results are quite notable since pressure in state space model is obtained from a less complicated compressibility model while the pressure model in SimHydraulics considers complex pipe dynamics.

The comparison of the results of the simulation response of the state space model of the hydraulic system to a detailed model which was created with the SimHydraulics toolbox of MATLAB/Simulink® was represented in this section. A designated angular velocity profile was supplied to the hydraulic pump in both models and the simulation results were compared. The pump speed, system pressure, motor speeds, and flows obtained from the state space model were in close agreement with the results acquired from software simulation. The main benefits of the state space model, besides a close dynamic simulation, are the simplicity of the governing equations and accomplishment of a superior high-speed simulation compared to other software packages.

6.2 Model Verification with Experimental Data

This section verifies the mathematical models of the hydraulic system by comparing the simulation results with the experimental data from the prototype.

6.2.1 Mathematical Model (ODE) Verification

In this section, the mathematical model behavior is compared with the experimental results obtained from a prototype. The prototype parameters and system values are listed in Table 6.3. Figure 6.17 demonstrates an overlay of the experimental setup and hydraulic circuitry. In order to maintain sufficient torque at the hydraulic pump, a speed reduction belt and pulley mechanism was installed in the prototype. This system increased the torque transferred from the DC motor to the hydraulic pump. The system operating conditions such as angular velocity, flows, and pressures were precisely measured by fast prototyping dSPACE 1104 hardware.

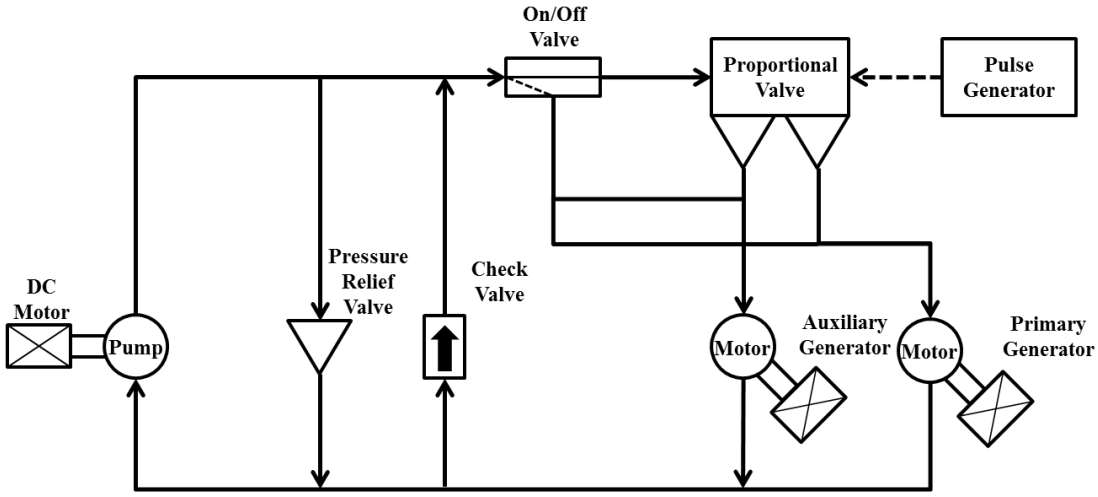

Figure 6.17 Schematic diagram of the overall hydraulic circuit of the experimental setup

To demonstrate the accuracy of the mathematical model of hydraulic wind energy transfer prototype, two distinct test configurations were considered as 1) forced flow distribution and 2) natural flow distribution between the hydraulic motors. These configurations were used to analyze the dynamic system behavior and to evaluate the mathematical model performance. In the first configuration, the valve was completely open to direct the flow towards the auxiliary motor (Motor B). Hence, the primary motor (Motor A) was excluded from the hydraulic circuit. In the second configuration, which was also known as the natural flow split, a directional valve was used to distribute the flow generated by the DC pump between both hydraulic motors, based on the hydraulic circuitry and geometric characteristics of the prototype

Table 6.1 Simulation parameters for mathematical model verification with experimental data

Symbol	Quantity	Value	Unit
D_p	Pump Displacement	0.517	in^3/rev
D_{mA}	Primary Motor Displacement	0.097	in^3/rev
D_{mB}	Auxiliary Motor Displacement	0.066	in^3/rev
I_{mA}	Primary Motor Inertia	0.0014	$kg.m^2$
I_{mB}	Auxiliary Motor Inertia	0.0014	$kg.m^2$
B_{mA}	Primary Motor Damping	0.0016	N.m/(rad/s)
B_{mB}	Auxiliary motor Damping	0.0032	N.m/(rad/s)
$K_{L,p}$	Pump Leakage Coefficient	0.46-0.68	
$K_{L,mA}$	Primary Motor Pump Leakage Coefficient	0.06	
$K_{L,mB}$	Auxiliary Motor Pump Leakage Coefficient	0	
η_{total}	Pump/Motor Total Efficiency	0.90	
η_{vol}	Pump/Motor Volumetric Efficiency	0.95	
β	Fluid Bulk Modulus	183695	psi
ρ	Fluid Density	0.0305	lb/in^3
υ	Fluid Viscosity	7.12831	cSt

6.2.1.1 Verification for the One Motor and One Pump Configuration

Figure 6.18 shows the schematic diagram of the hydraulic circuit configuration for the forced flow distribution towards the auxiliary motor to exclude the primary motor from the hydraulic circuit. A PWM signal of 100 Hz with 10% duty cycle was used to control the proportional valve to direct the flow toward the auxiliary motor. The speed step response of the system was generated by applying a step voltage to the DC motor to accelerate the hydraulic pump from zero to 300 rpms. After reaching the steady state, a second step voltage was applied to speed up the system from 300 to 400 rpms, followed by a step down back to 300 rpms to analyze the undershoots. Figures 6.19 to 6.22 display the results of the comparison between experimental and simulation data.

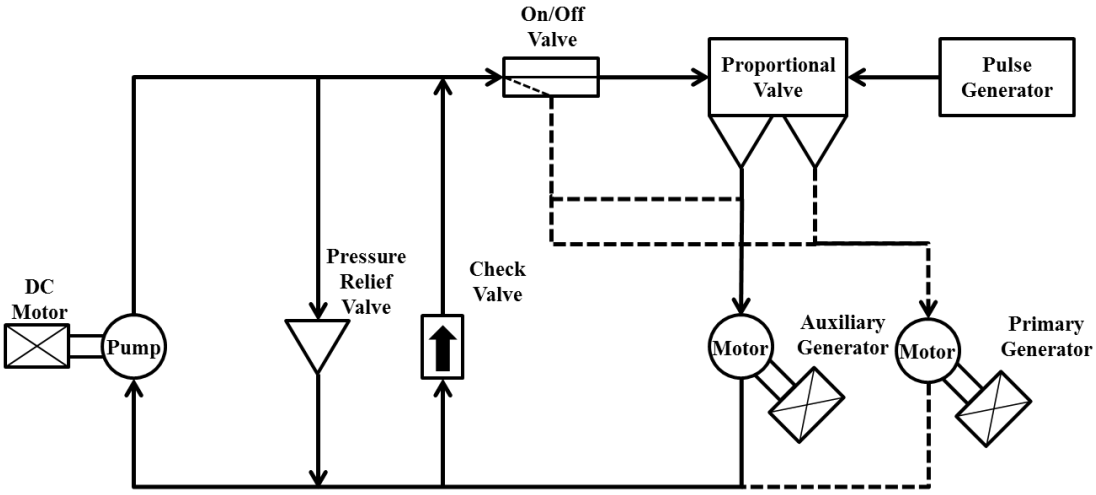

Figure 6.18 Schematic diagram of the experimental setup for the one motor configuration

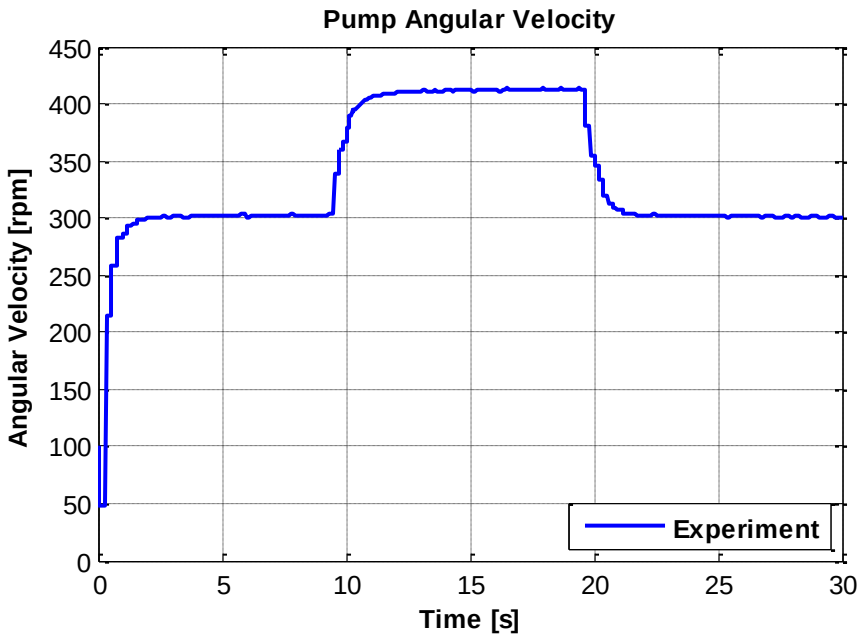

Figure 6.19 Hydraulic pump angular velocity profile

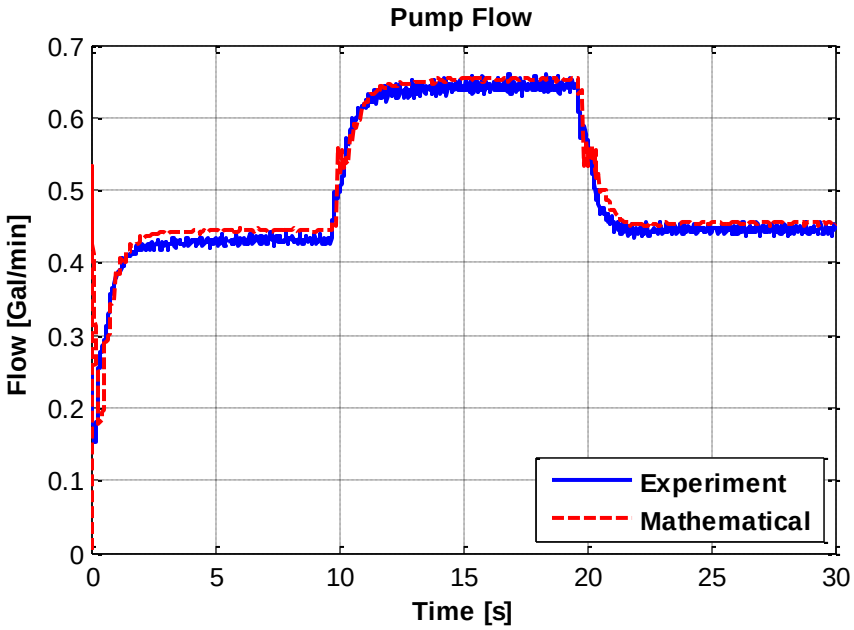

Figure 6.20 Comparison between the hydraulic pump flow of the mathematical model and the experimental results

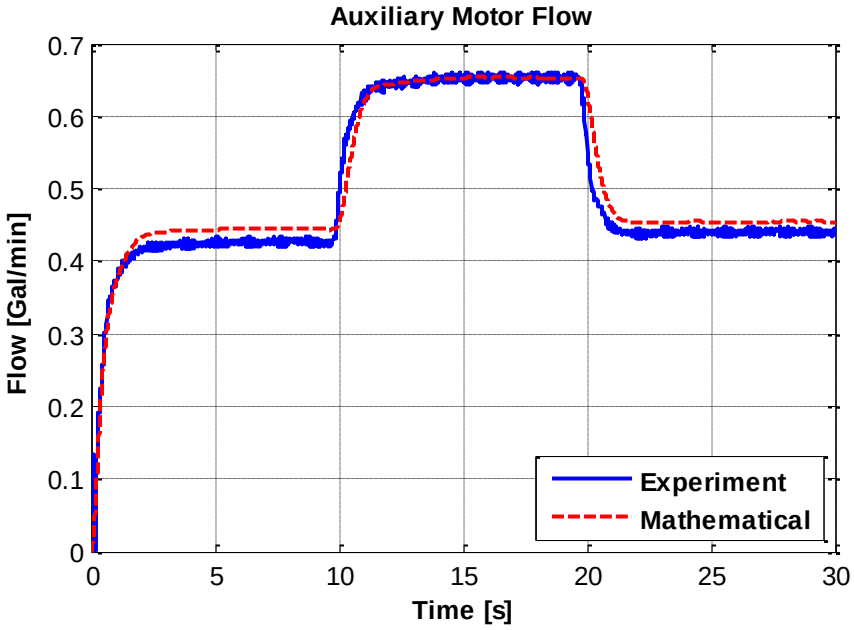

Figure 6.21 Comparison between the auxiliary hydraulic motor flow of the mathematical model and the experimental results

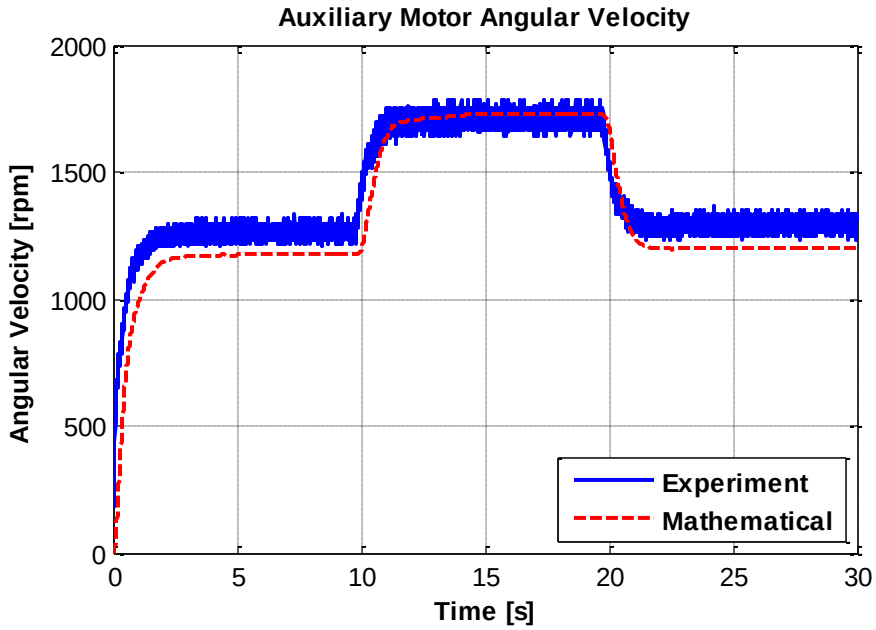

Figure 6.22 Comparison between the auxiliary hydraulic motor angular velocity of the mathematical model and the experimental results

Figure 6.19 illustrates the angular velocity profile applied to both the prototype and the mathematical model. Figure 6.20 shows the flows of the hydraulic pump obtained from the mathematical model and measured from the prototype. The figure demonstrates close transient profile and steady state values obtained from the model and the experiment.

Figure 6.21 illustrates the auxiliary motor flows obtained from the mathematical model and the experimental setup. The figure demonstrates a close agreement in the auxiliary motor velocity as a result of step-up and step-down pump velocities, and proves the accuracy of the mathematical model. Figure 6.22 shows the angular velocity of the auxiliary motor obtained from the mathematical model and the experimental setup. As the figure shows, the velocities are close. The mechanical system imperfections and

dependency on operating pressure resulted in a slight deviation at lower angular velocities. A slight difference between the measured and calculated values was the result of geometry differences in the prototype and the mathematical model. The experimental results demonstrate the accuracy and performance of the mathematical model of the hydraulic wind energy transfer system when the auxiliary motor is in the circuit.

6.2.1.2 Verification for the Two Motors and One Pump Configuration

In the second configuration, the natural flow split, a directional valve distributed the flow generated by the DC pump (wind turbine) between both hydraulic motors. The flow was naturally distributed between the hydraulic motors through the hydraulic circuitry considering the geometry characteristics of the prototype, the displacement of the motors, and the position of the flow-control valves, such as check valves and the pressure relief valves. Figure 6.23 displays the schematic diagram of the second hydraulic circuit configuration.

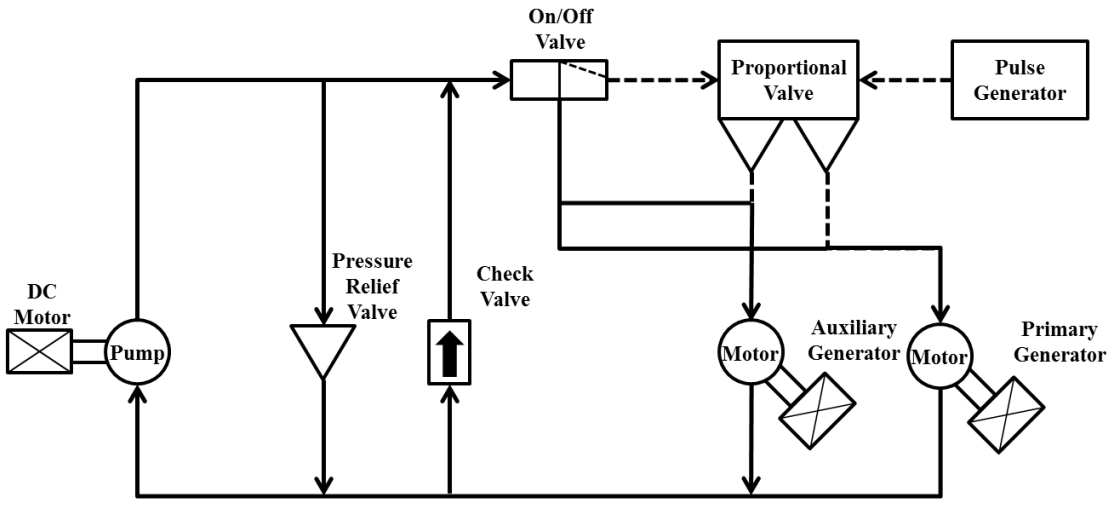

Figure 6.23 Schematic diagram of the experimental setup natural flow split configuration

In this configuration, a step input voltage is applied to the DC motor to emulate a speed-step input to the hydraulic pump from 0 to 300 rpm. As the system reached steady state condition, in about 10 seconds, another step function was applied to increase the speed from 300 to 400 rpm. A speed step down was also scheduled from 400 to 300 rpm to investigate the accuracy of the mathematical model in determining undershoots. Figure 6.24 illustrates the supplied pump angular velocity profile. This speed was applied to the mathematical model to investigate the modeling performance. Figures 6.24 to 6.29 display the results of the comparisons.

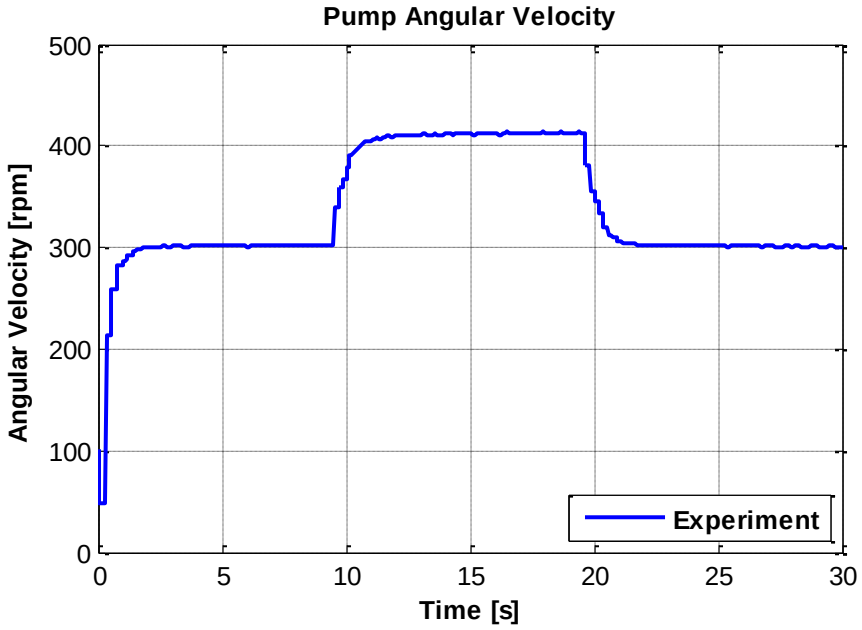

Figure 6.24 Hydraulic pump angular velocity profile

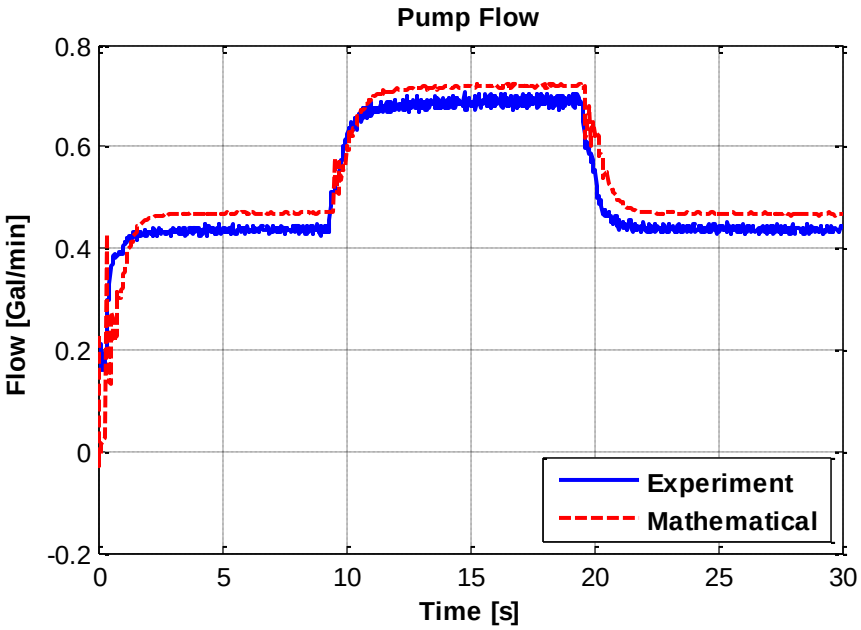

Figure 6.25 Comparison between the hydraulic pump flow of the mathematical model and the experimental results

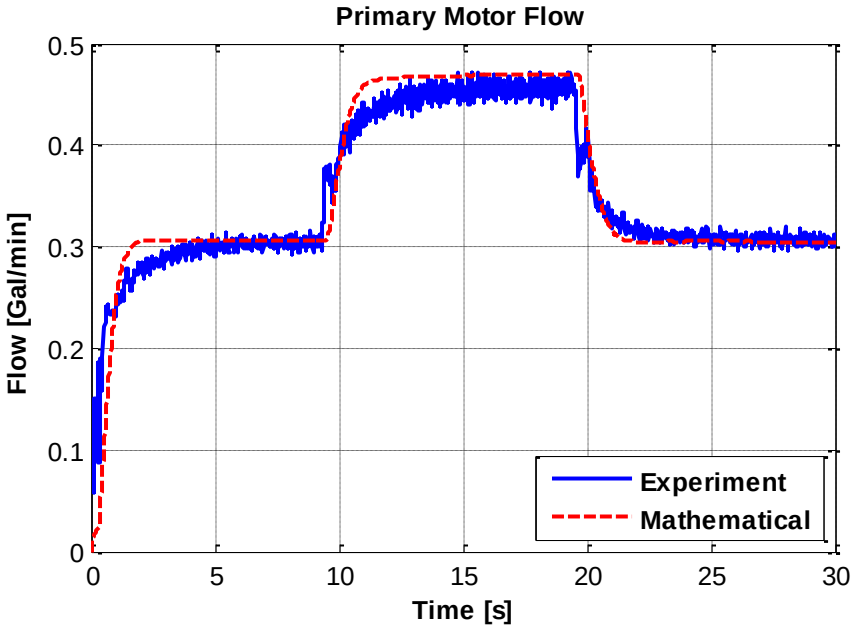

Figure 6.26 Comparison between the primary hydraulic motor flow of the mathematical model and the experimental results

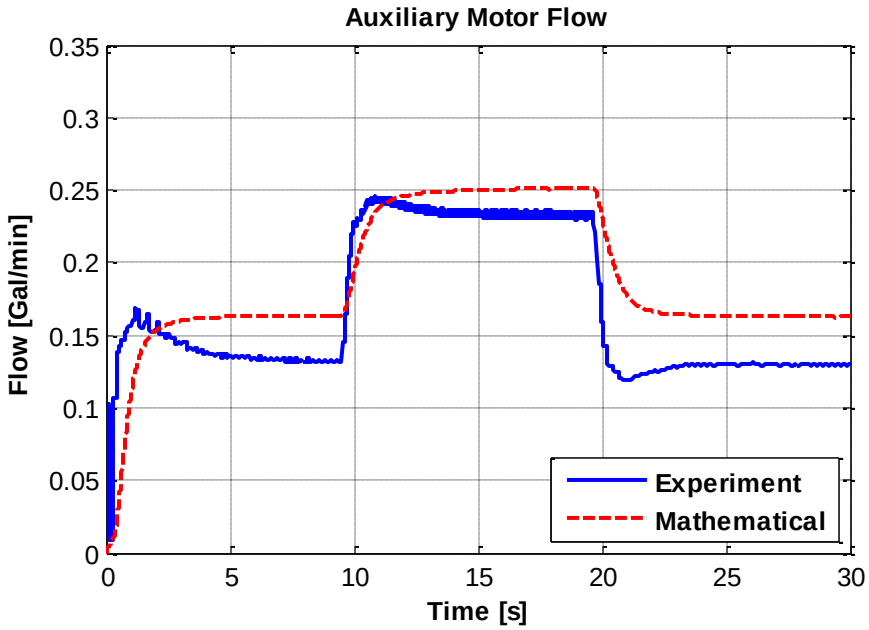

Figure 6.27 Comparison between the auxiliary hydraulic motor flow of the mathematical model and the experimental results

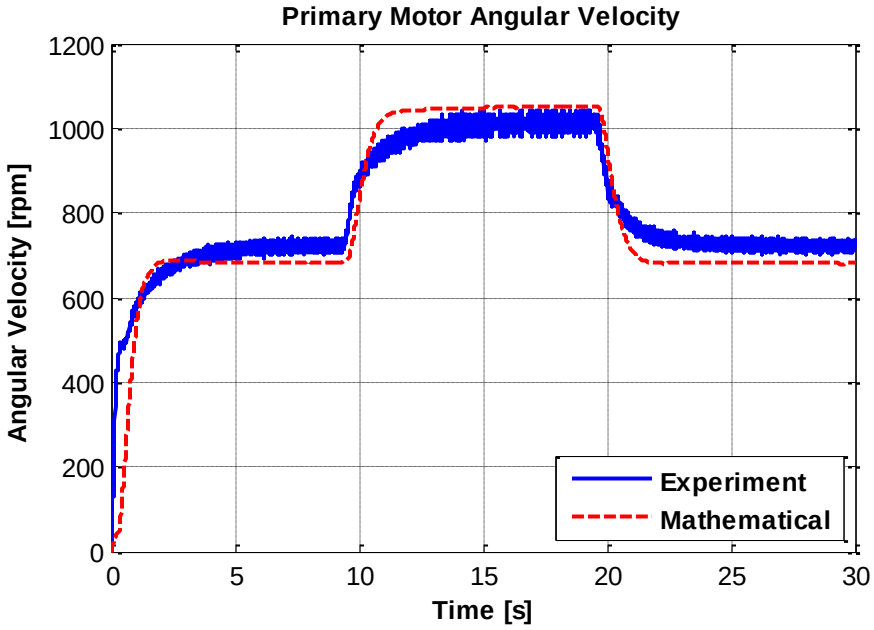

Figure 6.28 Comparison between the primary hydraulic motor angular velocity of the mathematical model and the experimental results

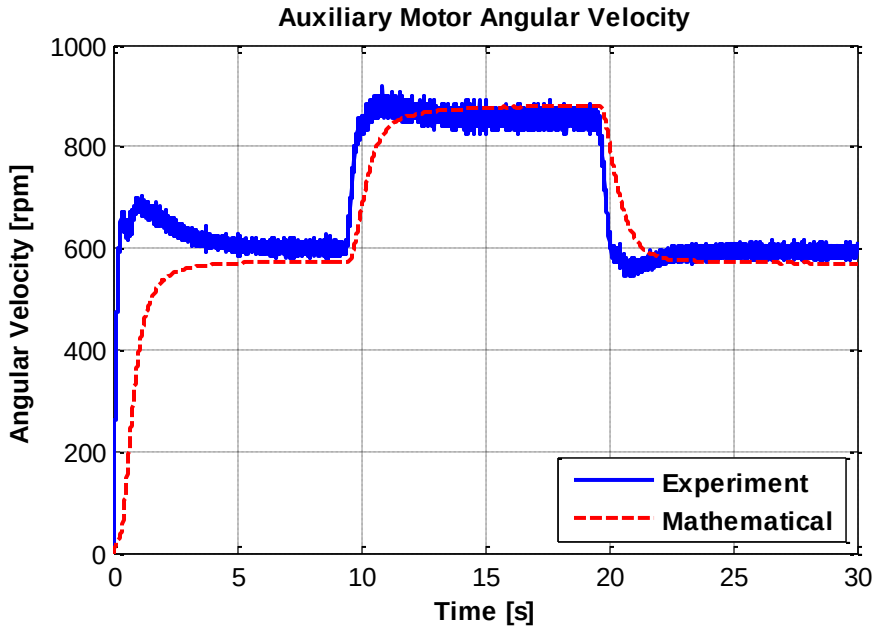

Figure 6.29 Comparison between the auxiliary hydraulic motor angular velocity of the mathematical model and the experimental results

Figure 6.25 illustrates both the pump flow measured from the prototype and that of the mathematical model. The figure demonstrates close flow profiles generated from the mathematical model and the experimental set up both in transient and steady state conditions.

Figure 6.26 illustrates accurate calculation of the primary motor flow from the mathematical model, which was in good agreement with the prototype. Due to asymmetries in the hydraulic circuit and un-modeled dynamics of transmission lines, the flow recorded from the auxiliary motor showed a slight shift from what the mathematical model calculated, at 300 rpm. Some of the contributing factors to this dissimilarity are, namely, the effect of the hydraulic circuit, the effect of directional valve dynamics, asymmetries in the hydraulic circuit, and the slight displacement and leakage factor

variation in the experimental setup. The flow profile of the auxiliary motor is shown in Figure 6.27.

Figures 6.28 and 6.29 illustrate the angular velocity profiles of the primary and the auxiliary motors obtained from the mathematical model and from the experimental setup. As the figures demonstrate, the speed profiles of the mathematical model and the experimental setup are in close agreement both in transients and in steady state values. A slight deviation was observed at the starting point transients of the auxiliary motor, which was due to the effects described for flow calculations (Figure 6.26). The speed of the auxiliary motor was also influenced by motor inertia and the damping factor.

The experimental results prove the accuracy and performance of the mathematical model of the hydraulic wind energy transfer system. The transient dynamics of the system and steady state values were in good agreement with what was obtained from the prototype.

6.2.2 Linear State-Space Model Verification

This section compares the simulation results from the state space model to the experimental data from a prototype of the hydraulic system in natural flow split configuration. Figure 6.30 displays a simplified diagram of the hydraulic circuit. In this configuration, namely the natural flow split, the proportional valve is excluded from the system. A directional valve distributed the flow generated by the DC pump (wind turbine) between both hydraulic motors. The flow is naturally distributed between the hydraulic motors through the hydraulic circuitry considering the geometry characteristics of the

prototype, the displacement of the motors, and the position of the flow-control valves, such as check valves and the pressure relief valves.

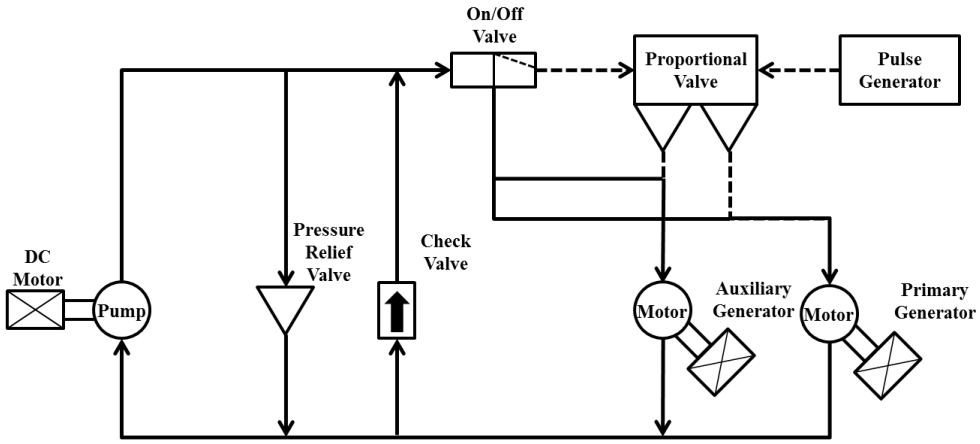

Figure 6.30 Schematic diagram of the experimental setup in natural flow split configuration

Similar to the preceding section, a step input voltage is applied to the DC motor to emulate a speed-step input to the hydraulic pump from 0 to 300 rpm. As the system reached steady state condition, in about 10 seconds, another step function was applied to increase the speed from 300 to 400 rpm. A speed step down was also scheduled from 400 to 300 rpm to investigate the accuracy of the mathematical model in determining undershoots. Figure 6.31 depicts the angular velocity profile which is supplied to the pump. This speed profile was supplied to the state space model which was created in Simulink® to investigate the modeling performance. Table 6.4 displays the simulation parameters. The hydraulic motors displacements, leakage coefficients, and damping coefficients are calculated by using a least square approximation. Figures 6.32 to 6.36 depict the result of the comparison.

Table 6.2 Simulation parameters for linear state-space model verification with experimental data

Symbol	Quantity	Value	Unit
D_p	Pump Displacement	0.3793	in^3/rev
D_{mA}	Primary Motor Displacement	0.1036	in^3/rev
D_{mB}	Auxiliary Motor Displacement	0.0750	in^3/rev
I_{mA}	Primary Motor Inertia	0.0005	$kg.m^2$
I_{mB}	Auxiliary Motor Inertia	0.0005	$kg.m^2$
B_{mA}	Primary Motor Damping	0.0026	N.m/(rad/s)
B_{mB}	Auxiliary motor Damping	0.0022	N.m/(rad/s)
$K_{L,p}$	Pump Leakage Coefficient	0.0255	
$K_{L,mA}$	Primary Motor Pump Leakage Coefficient	0.0085	
$K_{L,mB}$	Auxiliary Motor Pump Leakage Coefficient	0.0460	
β	Fluid Bulk Modulus	183695	psi
ρ	Fluid Density	0.0305	lb/in^3
υ	Fluid Viscosity	7.12831	cSt

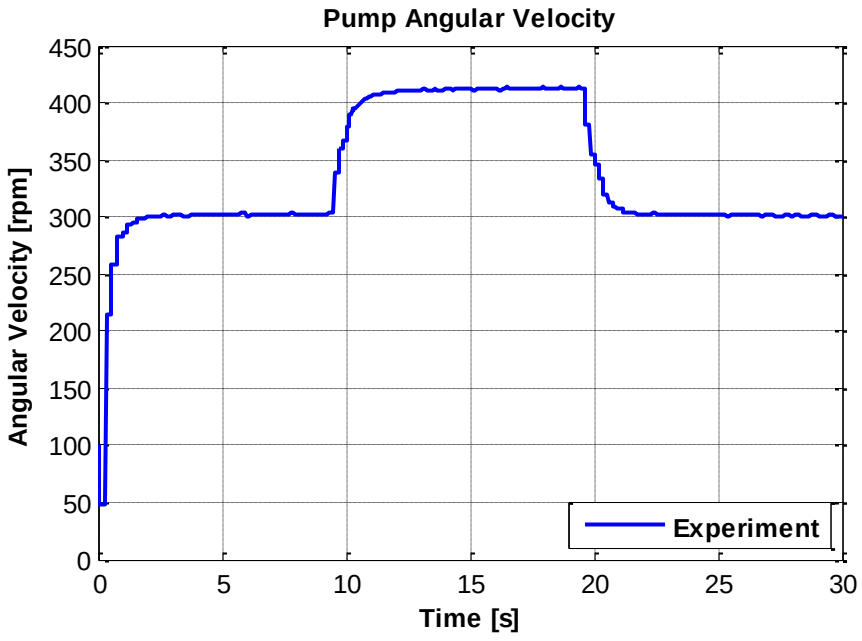

Figure 6.31 Hydraulic pump angular velocity profile

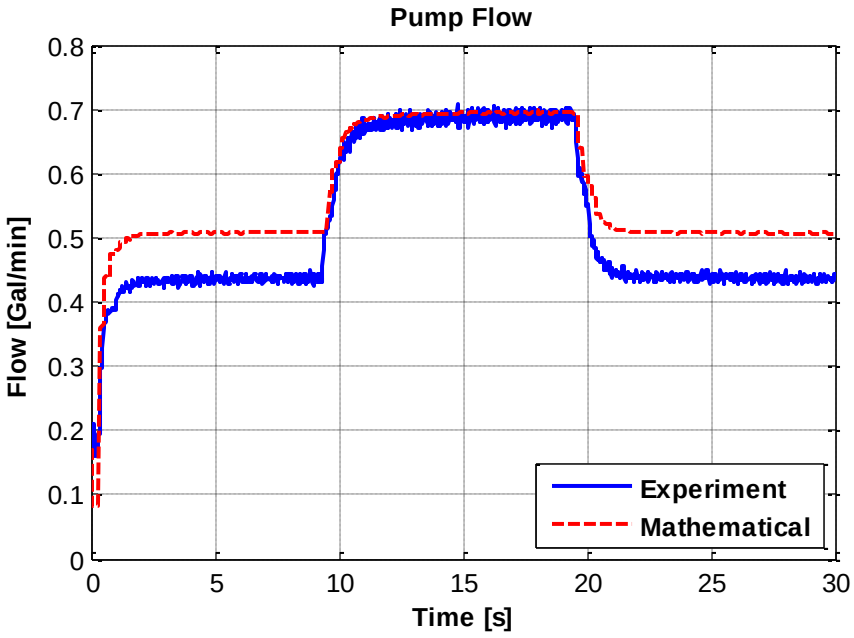

Figure 6.32 Comparison between the pump flow of the state-space model and experimental results

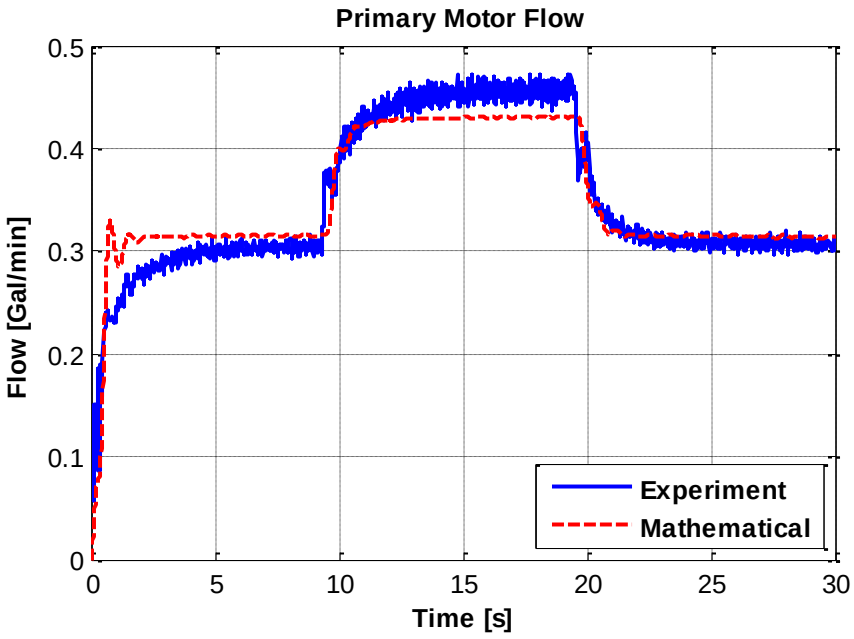

Figure 6.33 Comparison between the primary hydraulic motor flow of the state-space model and experimental results

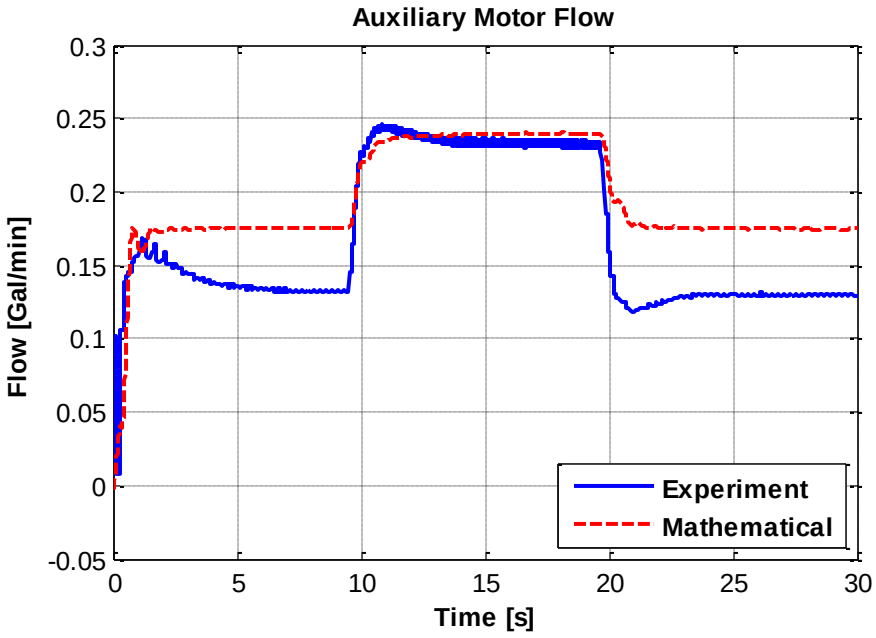

Figure 6.34 Comparison between the auxiliary hydraulic motor flow of the state-space model and experimental results

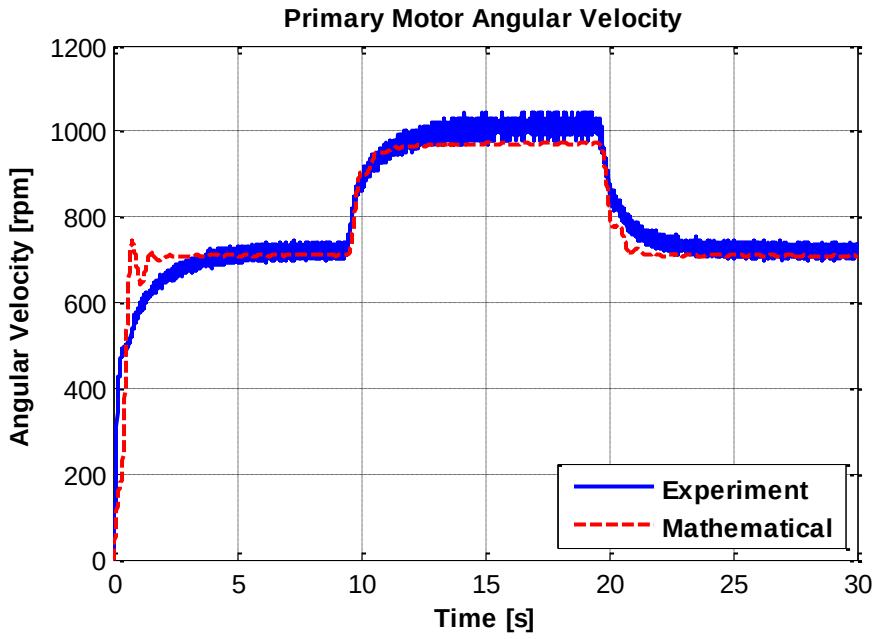

Figure 6.35 Comparison between the primary hydraulic motor angular velocity of the state-space model and experimental results

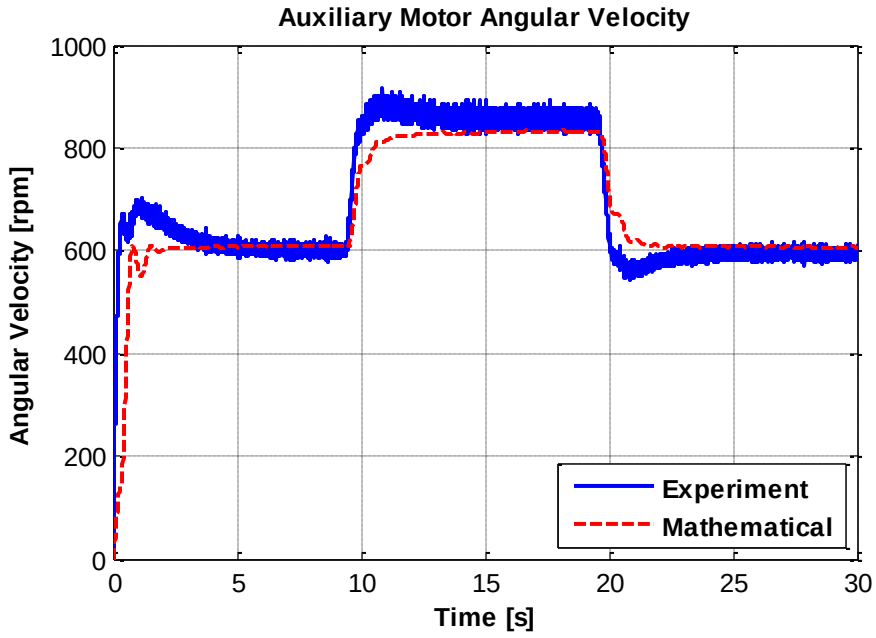

Figure 6.36 Comparison between the auxiliary hydraulic motor angular velocity of state-space model and experimental results

Figure 6.32 displays the pump flow which was measured from the prototype compared with the pump flow which was generated through the simulations. The figure demonstrates a close agreement between the transient and steady state flow profiles generated from the state space model and the experimental setup.

Figure 6.33 illustrates the comparison between the experimental values of the primary motor and the calculation of the primary motor flow from the simulation. The transient and steady state flow values are generally similar and follow a close profile. The dissimilarities of the flow values are because asymmetries in the hydraulic circuit and un-modeled dynamics of transmission lines. Some of the contributing factors to this divergence are, namely, the effect of the hydraulic circuit, the effect of directional valve

dynamics, and the slight displacement and leakage factor variation in the experimental setup. The flow profile of the auxiliary motor is shown in Figure 6.34.

Figures 6.35 and 6.36 depict the angular velocity profiles of the primary and the auxiliary motors obtained from the mathematical model and from the experimental setup. As the figures demonstrate, the speed profiles of the state space model and the experimental setup are in close agreement both in transients and in steady state values. A slight deviation of the angular velocities at the 400 rpm input pump angular velocity was observed for both the auxiliary and primary motors, which was due to the effects described for flow calculations. The speed of the motors was additionally influenced by motor inertia and the damping factor.

The experimental results show a close agreement with the simulation results obtained from the state space model.

6.3 System Efficiency Analysis

This section analyzes the efficiency of the hydraulic wind energy transfer system. The pressure loss equations which were introduced in Chapter 4 are incorporated in the mathematical model to compute the pressure losses of the system. These losses are considered along with the hydraulic pump and hydraulic motor mechanical and volumetric efficiencies to account for overall system losses. The input power of the pump and the output power of the motors are calculated as following

$$P = T\omega \tag{6.1}$$

where P is the power, T is the torque, and ω is the angular velocity.

$$\eta_{total} = \frac{P_{mA} + P_{mB}}{P_p}$$

where η_{total} is the system power transfer efficiency, P_{mA} is the output primary motor angular velocity, P_{mB} is the output auxiliary motor angular velocity, and P_p is the input pump power. Figure 6.37 shows the system efficiency for the system with parameters tabulated in Table 5.1. The pump angular velocity, which is depicted in Figure 6.1, is applied to the model to analyze the quality of power generation. According to Figure 6.37 the steady state efficiency of the power transfer system is 78%.

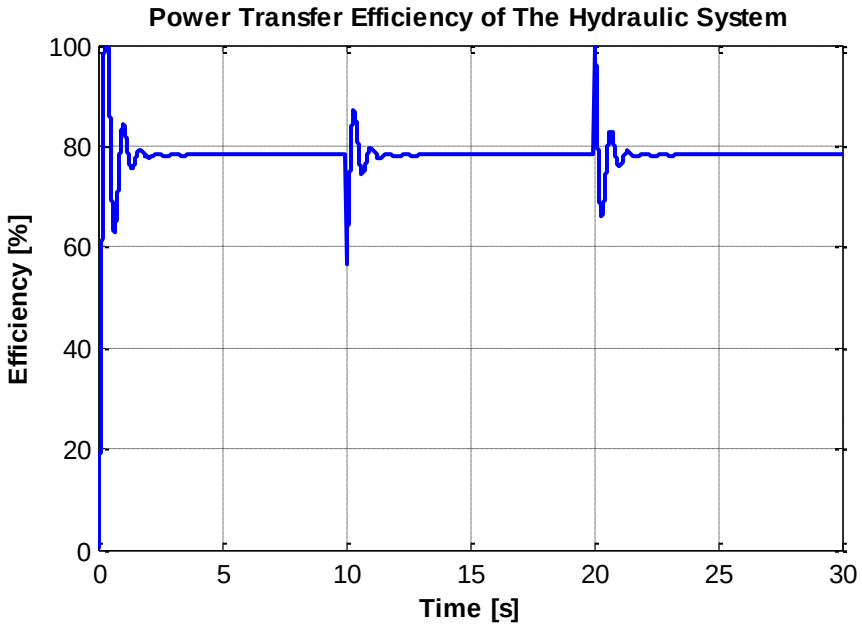

Figure 6.37 Efficiency analysis of hydraulic wind power transfer

7. CONTROLS OF HYDRAULIC WIND POWER TRANSFERS

The prime mover of this hydraulic energy transfer unit, the wind turbine, also experiences the intermittent nature of wind. This imposes fluctuation on generators and drifts their angular velocity and consequently the generated power. To mitigate the effect of the output power fluctuations, different control techniques are applied to regulate the generated power.

This chapter represents the design and incorporation of the controllers for the hydraulic energy transfer system. The controllers are first designed and their effectiveness is verified with simulation models. Subsequently, the approved control strategies are implemented in the experimental prototype to regulate the proportion valve position according to the selected reference angular velocity.

7.1 Controller Design for the Simulation Model

This section introduces design of the angular velocity controllers for the simulation models of the hydraulic system. The purpose of the controller is to regulate the position of the proportional valve model to maintain tracking of a reference primary motor angular velocity. The controller designs for the ODE mathematical model and nonlinear-state space model are presented.

7.1.1 Controller Design for the Mathematical ODE Model

The complete ODE mathematical model of the hydraulic system is introduced in Chapter 3. The model runs in two configurations namely, natural flow split and forced flow configuration. In the former configuration the only system input is the pump angular velocity profile. The model of the 3-way proportional valve is added to create the later configuration model, which adds a supplementary input to the system, namely the valve displacement. The displacement of the valve is regulated in the forced flow configuration to vary the flow distribution of the hydraulic motors. The valve input could be regulated by a controller to maintain a specific primary motor angular velocity.

Subsequently, two control techniques are introduced to maintain a reference primary motor angular velocity. The first technique controls angular velocity to the primary motor by regulating the pressure of the distributed flow. Successively, a model reference adaptive controller (MRAC) is introduced to regulate the hydraulic plant to maintain output tracking of an ideal hydraulic model.

7.1.1.1 PI angular velocity Controller Pressure Regulation Design with Gain Scheduling

This section represents a model based pressure control technique to maintain a constant frequency at the wind turbine generator for a hydraulic energy distribution system with one pump and one motor. Figure 7.1 shows a schematic diagram of the hydraulic system. The system has a fixed displacement hydraulic pump coupled to the wind turbine. Since the wind turbine generates a large amount of torque at a relatively low angular velocity, a high displacement hydraulic pump is required to flow high-

pressure hydraulics to transfer the power to the generators. High-pressure pipes connect the pump to the path toward the central generation unit. A flow control unit is implemented before the hydraulic motor to provide a bypass for the flow, which is excess to the speed requirements of the motor. The purpose of control unit is to regulate the frequency of the hydraulic motor by controlling the flow of the hydraulic fluid.

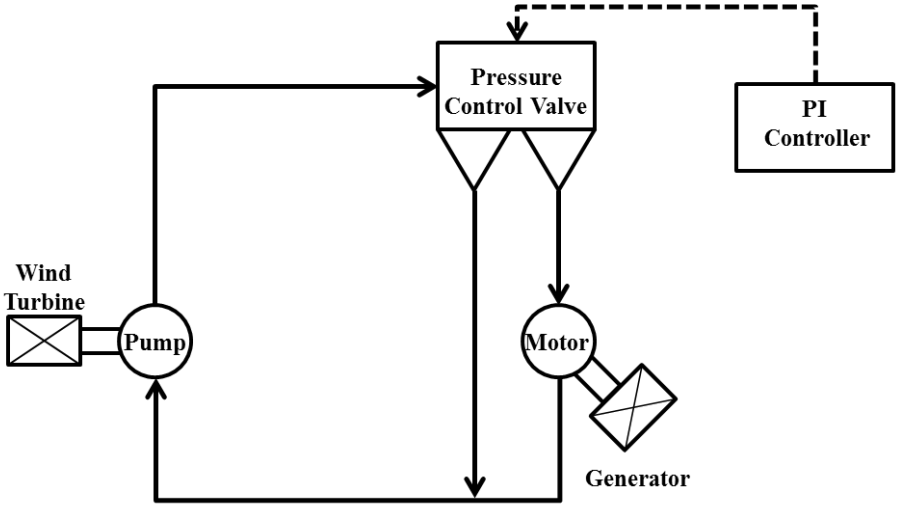

Figure 7.1 Schematic diagram of the hydraulic system model

A model based control system is designed to compensate for the speed fluctuation of the hydraulic motor-generator under load or input flow variation. These fluctuations may be resulted from intermittent wind speeds or load demands. In order to regulate the speed and consequently the generated power from the generator, a controlled proportional flow valve is required to distribute the hydraulic fluid delivery of the pump to the main hydraulic motor and the excess bypass flow to the hydraulic pump. The objective of the flow control is to compute the angular velocity deviation from the reference and apply a corrective control signal to the valve to adjust the valve opening that allows the flow

controls. Optimal speed control of hydraulic systems is represented in [28], [29]. These control techniques are mainly used for displacement control of hydraulic cylinders. This section uses a PI control technique for frequency control of the generator.

The control law to regulate the frequency of the hydraulic motor is given as

$$C(s) = k_p + \frac{k_i}{s} \tag{7.1}$$

where k_p is the proportional gain and k_i is the integrator gain that can be adjusted to achieve a fast and accurate speed regulation. Figure 7.2 shows the control system configuration with a PI controller and a plant (mathematical model). After adjustments, the control parameters can be determined to achieve the required performance.

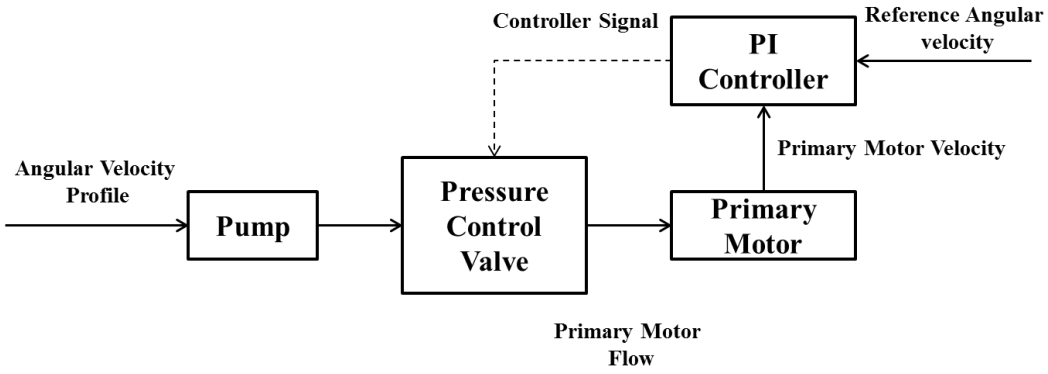

Figure 7.2 Block diagram of the close loop control system

A gain-scheduling technique [45] was used to improve the performance of control at different operating points of the system. To achieve a fast dynamic response, high proportional and low integration gains are required. To reduce settling time and undershoot and to decrease the steady state tracking error low proportional and high

integration gains are applied at a proper time to achieve high profile regulation performance. The gains applied in this system are shown in Table 7.1. Figures 7.2 to 7.7 show the results of the simulation.

Table 7.1 Controller Parameters

Control Gain	**Quantity**
t<0.25 s	
K_p	0.1
K_i	0.001
t≥0.25 s	
K_p	0.0015
K_i	0.06

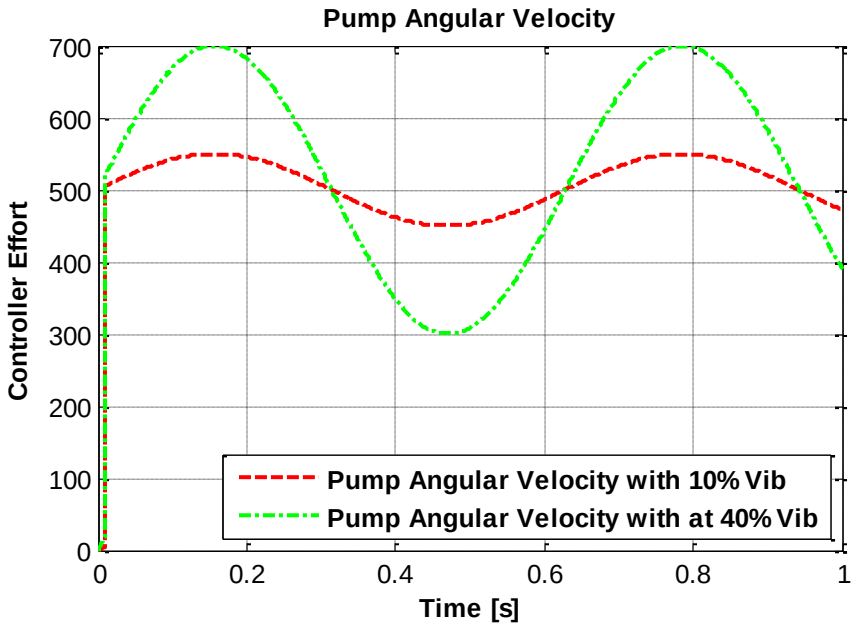

Figure 7.3 Hydraulic pump angular velocity profile for 10% and 40% wind speed variation

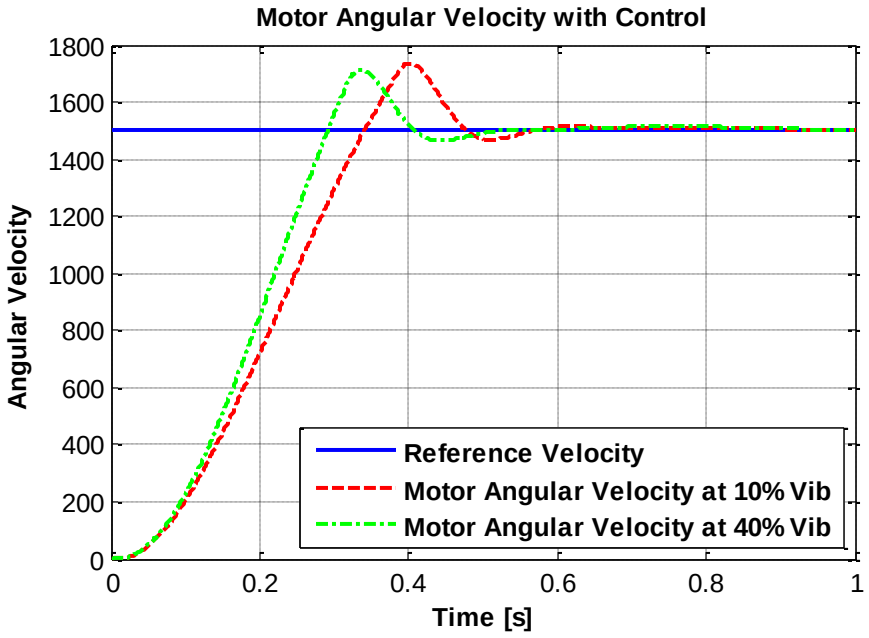

Figure 7.4 Hydraulic motor angular velocity for a reference speed of 1500 rpm and wind speed variation of 10% and 40%

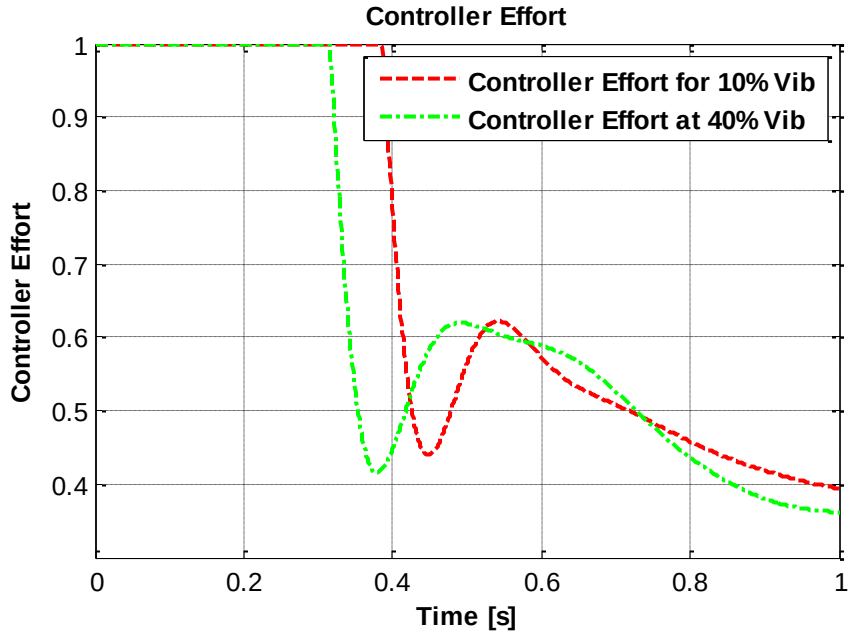

Figure 7.5 Controller effort to mitigate steady state tracking error

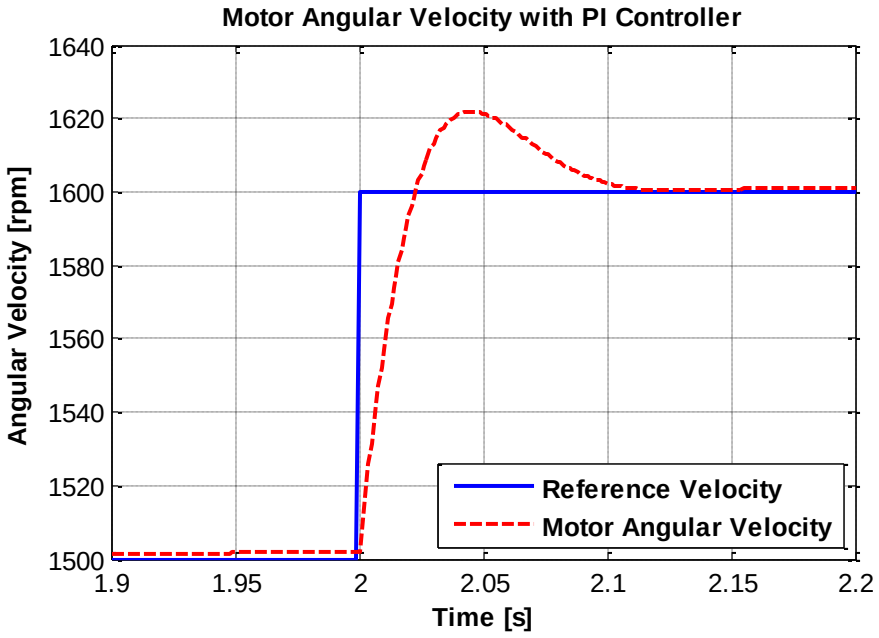

Figure 7.6 Hydraulic motor angular velocity at 10% wind speed variation for alteration of reference angular velocity from 1500 rpm to 1600 rpm

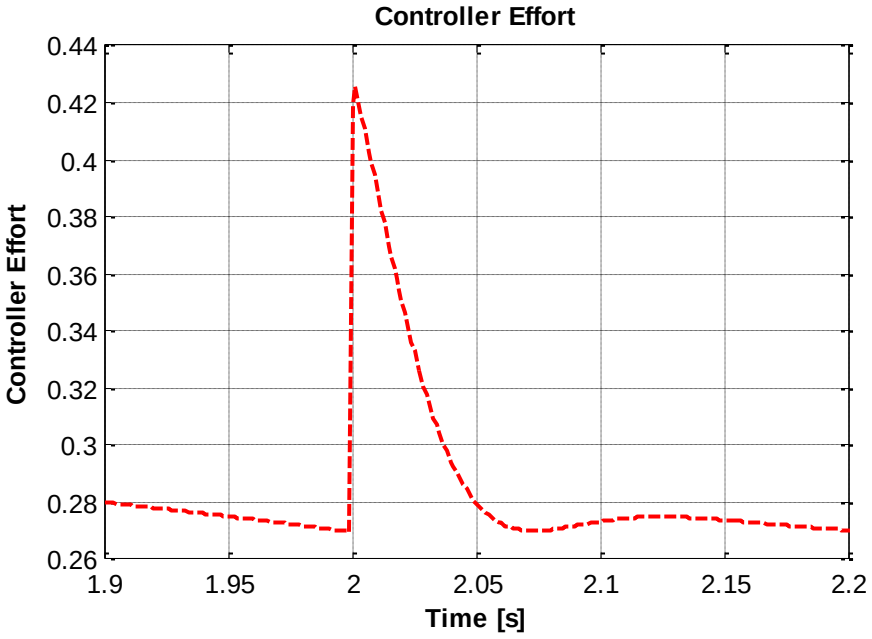

Figure 7.7 Controller effort at 10% wind speed variation for alteration of reference angular velocity from 1500 rpm to 1600 rpm

As the load of the generator increases, the frequency of the power generation will decrease. To compensate for this drop, a droop controller is used to set the new speed reference. In the control scheme of this section, the control command is applied to a valve to enforce a flow distribution to the main and excess flow outlets. This technique will be used to control the flow and therefore the speed of the generator. To analyze the performance of the speed control, a 10% and 40% variation in velocity as sine waveform was applied to the hydraulic pump input shaft to model the wind intermittency. Table 2 displays the controller parameters in a gain-scheduling scheme.

Figure 7.3 shows the angular velocity profiles which are supplied to the hydraulic pump with 10% and 40% velocity vibration respectively.

Figure 7.4 shows the hydraulic system dynamic response to a 1500 rpm reference angular velocity at 10% and 40% wind speed variation. The controller was proven very effective on controlling the high-pressure hydraulic motor. The steady state error despite a constant variation of the input shaft speed reached zero. The overshoot was resulted from a high gain controls in the beginning.

Figure 7.5 shows the controller effort at 10% and 40% wind speed variation, which is defined as the signal generated by the PI controller to regulate the flow distribution with the purpose of steady state tracking error mitigation. It is noted that, as the vibration amplifies to higher values and the flow distribution of diverted flow increases. As the control command demonstrates, the valve was fully open during this period to compensate for the delay in the rise-time observed in mathematical modeling.

The plot shows 14.3% overshoot and 0.5 sec settling time at 10% wind speed fluctuation and 11.35% overshoot and 0.47 sec settling time at 40% wind speed fluctuation which both are within the satisfactory range.

Figure 7.6 shows motor angular velocity profile for changing the reference speed from 1500 rpm to 1600 rpm at the motor shaft at 10% wind speed fluctuation. The figure shows the effectiveness of the control system to maintain the reference speed at the motor output and eliminate the steady state error for both reference speeds. Figure 7.7 shows the controller effort to regulate for the reference angular velocity alteration. It is noted that, as the reference angular velocity amplifies to higher values, the flow distribution of motor increases, hence resulting in a high profile control performance in hydraulic wind energy transfer.

7.1.1.2 Model Reference Adaptive Controller Design for Plant Output Synchronization

Despite the benefits that a hydraulic wind power transfer demonstrates, non-idealities imposed by pressure drop along with the connecting hoses, dependency of leakage coefficients of hydraulic machinery on pressure variation, and other unknown system parameters such as motor/generator coupling, and damping coefficient degrade the performance of the primary generator and reduce the output velocity compared to an ideal system. To compensate for system uncertainties, a model reference adaptive controller is developed in this section. The controller is used to regulate the frequency of AC synchronous wind generators. The mathematical modeling of a gearless hydraulic wind power transfer which is presented in Chapter 3 is used to generate an accurate

model of the hydraulic plant. The control performance is verified with simulation results, which demonstrates a close tracking profile.

Figure 3.1 displays a block diagram of the proposed ideal model for the hydraulic energy transfer system. MATLAB/ Simulink ® is used to create an ideal model of the system. The model incorporates the governing mathematical equations of every individual hydraulic circuit component in block diagrams. Figure 3.2 shows the governing equations of the hydraulic wind energy harvesting system.

The ideal system model neglects the effect of pressure drop in the hydraulic system which is mainly due to inner hose friction, hose geometry, temperature variation, fluid viscosity, couplings and adapters, and flow rate [46]. Moreover, the practical leakage coefficient of the rotary machinery is a function of operating pressure. The non-ideal model of the system incorporates these imperfections.

Figures 3.3 and 3.4 illustrate a schematic diagram of a gearless wind energy transfer system. The prototype of the hydraulic system is used to derive the correlation between pump gauge pressure and pump leakage coefficient. In this model, unlike the ideal model where the hydraulic motors are supplied with the differential pressure across their terminals, a proportional valve distributes the flow between motors. The main purpose of this valve is to maintain the required angular velocity profile in the main hydraulic motor.

7.1.1.3 Adaptive Controller Design

This section introduces a model reference adaptive control approach to regulate the flow of hydraulic liquid to the main hydraulic motor. The flow regulation should maintain a specified frequency of generated voltage in standalone applications, and control the amount of generated power in grid connected applications. The control law and gain adaptation technique are represented for hydraulic wind power transfers [47-49]. The control law is expressed as

$$f_y = k_r r + k_e (y_p - y_m) + k_p y_p \tag{7.2}$$

where y_p and y_m are the reference model and plant output signals, r denotes the reference input and k_r , k_e , and k_p are controller gains that are adjusted simultaneously according to a gain adaptation law to mitigate the tracking error. Considering the estimated values of the control gains, the equivalent control $\hat{C}$ command is defined as

$$\hat{C} = \hat{k}_r r + \hat{k}_e e + \hat{k}_p y_p \tag{7.3}$$

where $\hat{k}_r$, $\hat{k}_e$, $\hat{k}_p$ and are the estimations of the control gain and are computed according to the gain adaptation technique as

$$\dot{\hat{k}}_r = -P_0 \operatorname{sgn}(s) r \tag{7.4}$$

$$\dot{\hat{k}}_p = -P_0 \operatorname{sgn}(s) y_p \tag{7.5}$$

$$\dot{\hat{k}}_e = -P_0 \operatorname{sgn}(s) e \tag{7.6}$$

where P_0 is the adaptation gain and s denotes the sliding surface is defined such that it satisfies the switching equation

$$s = Ge = 0 \tag{7.7}$$

where G represents the gain switching matrix and e is the tracking error which is expressed as

$$e = y_p - y_m \tag{7.8}$$

The stability proof of this controller is provided in [50-51].

Consider the following Lyapunov function with positive gain $P_0>0$ as

$$V = \frac{1}{2}e^2 + \frac{|s|}{2P_0}(\tilde{k}_e^2 + \tilde{k}_r^2 + \tilde{k}_p^2) \tag{7.9}$$

satisfying

$$i) V > 0 \tag{7.10}$$

$$ii) V(\bar{0}, t) = 0 \tag{7.11}$$

where (~) sign denotes the estimation error of each component. Consider the system in sliding mode and note that the sliding surface exists even at zero-tracking error condition. The time derivative of the Lyapunov function can be computed at different sliding directions in two cases as

a)If $sign(s)>0$ then

$$\begin{aligned} \dot{V} &= e\dot{e} + \frac{s}{2P_0}(2\dot{\hat{k}}_e\hat{k}_e - 2\dot{\hat{k}}_e k_e + 2\dot{\hat{k}}_r\hat{k}_r - 2\dot{\hat{k}}_r k_r + 2\dot{\hat{k}}_p\hat{k}_p - 2\dot{\hat{k}}_p k_p) \\ &+ \frac{\dot{s}}{2P_0}(\tilde{k}_e^2 + \tilde{k}_r^2 + \tilde{k}_p^2) \end{aligned} \tag{7.12}$$

replacing with the gain adaptation yields

$$\dot{V} = e(\tilde{k}_e e + \tilde{k}_r r + \tilde{k}_p y_p) - \frac{s}{2P_0}(\tilde{k}_e e + \tilde{k}_r r + \tilde{k}_p y_p) \tag{7.13}$$

b) If $sign(s)<0$ then

$$\dot{V} = e\dot{e} - \frac{-s}{2P_0}(2\dot{\hat{k}}_e\hat{k}_e - 2\dot{\hat{k}}_e k_e + 2\dot{\hat{k}}_r\hat{k}_r - 2\dot{\hat{k}}_r k_r + 2\dot{\hat{k}}_p\hat{k}_p - 2\dot{\hat{k}}_p k_p) - \frac{\dot{s}}{P_0}(\tilde{k}_e^2 + \tilde{k}_r^2 + \tilde{k}_p^2) \tag{7.14}$$

replacing with the gain adaptation yields

$$\dot{V} = e(\tilde{k}_e e + \tilde{k}_r r + \tilde{k}_p y_p) - \frac{s}{2P_0}(\tilde{k}_e e + \tilde{k}_r r + \tilde{k}_p y_p) \tag{7.15}$$

Considering Equations 7.13 and 7.15 the following expression is implied

$$\dot{V} = [\tilde{k}_e e^2 - \tilde{k}_e se] + [\tilde{k}_r er - \tilde{k}_r sr] + [\tilde{k}_p ey_p - \tilde{k}_p sy_p] \tag{7.16}$$

replacing the sliding surface condition results in the following equation

$$\dot{V} = [1-G]e[\tilde{k}_e e + \tilde{k}_r r + \tilde{k}_p y_p] \tag{7.17}$$

Considering a constant identity value for gain-switching matrix (i.e. $G=I$) in Equation 7.17, results in $\dot{V} = 0$, which satisfies the La Salle's global invariant set theorem [49]; therefore, the control law with gain adaptation results in an asymptotically stable system.

Figure 7.8 illustrates the control system configuration with two hydraulic power transfers comprised of an ideal hydraulic system (model) and an imperfect system with unknown parameters (plant). The controller synchronizes the angular velocity of the plant with that of the model and compensates for the non-idealities to reduce the effect of pressure drop, leakage coefficient variation and unknown load damping coefficient of the plant.

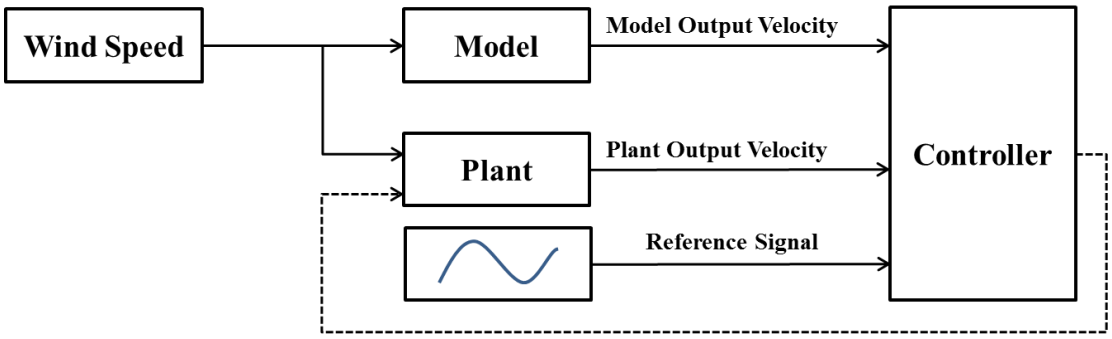

Figure 7.8 Controller configuration, the output motor frequency synchronization

The system non-idealities degrade the open loop performance of the power generation and deviated from the specified velocities. Closed loop control of the output velocity, and therefore the generated voltage frequency, requires compensation of time varying parameter variations with adaptive controllers. The control command is a PWM signal that is generated to open a proportional valve and control the flow of hydraulic liquid. Table 7.2 illustrates the simulation parameter values and their units.

Figure 7.9 shows the pump leakage coefficient variation with changes in pump terminal pressure. This leakage coefficient variation pattern is integrated to the plant model to account for a plant parameter uncertainties. Since lower or higher relative damping coefficients impose diverge dynamics on the system response, the damping coefficients of the motor/generator in the plant were considered ±10% of the damping coefficient of the ideal model for the primary motor and auxiliary motors respectively. The results of the simulation are depicted in Figures 7.10 to 7.15.

Table 7.2 Simulation parameters for the mathematical model with MRAC

Symbol	Quantity	Value	Unit
D_p	Pump Displacement	0.517	in^3/rev
D_{mA}	Primary Motor Displacement	0.097	in^3/rev
D_{mB}	Auxiliary Motor Displacement	0.097	in^3/rev
I_{mA}	Primary Motor Inertia	0.0014	$kg.m^2$
I_{mB}	Auxiliary Motor Inertia	0.0014	$kg.m^2$
B_{mA}	Primary Motor Damping	0.0026	N.m/(rad/s)
B_{mB}	Auxiliary motor Damping	0.0022	N.m/(rad/s)
$K_{L,p}$	Pump Leakage Coefficient	0.17	
$K_{L,mA}$	Primary Motor Pump Leakage Coefficient	0.1	
$K_{L,mB}$	Auxiliary Motor Pump Leakage Coefficient	0.001	
η_{total}	Pump/Motor Total Efficiency	0.90	
η_{vol}	Pump/Motor Volumetric Efficiency	0.95	
β	Fluid Bulk Modulus	183695	psi
ρ	Fluid Density	0.0305	lb/in^3
υ	Fluid Viscosity	7.12831	cSt
P_0	Adaptation Gain	10	

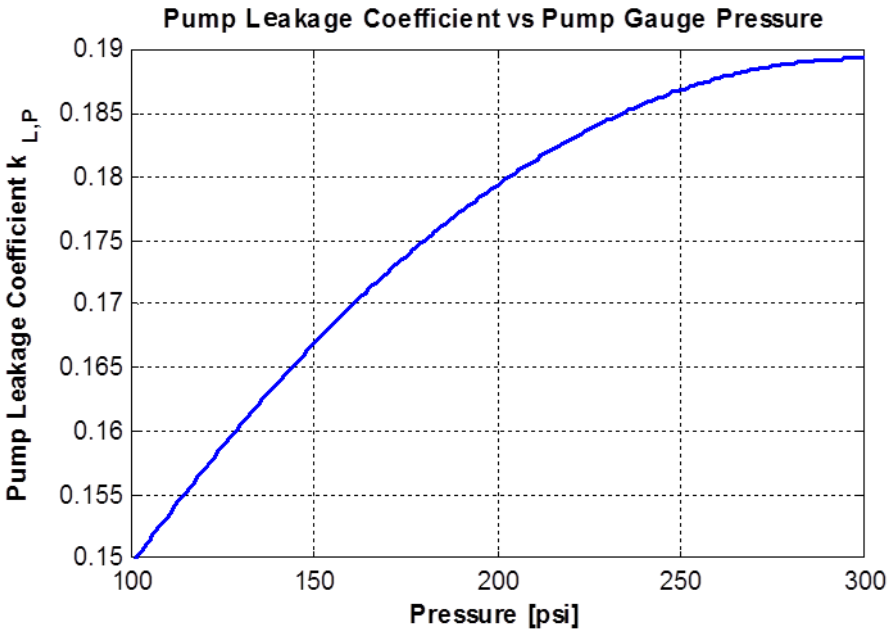

Figure 7.9 Hydraulic pump leakage coefficient variation with pressure change

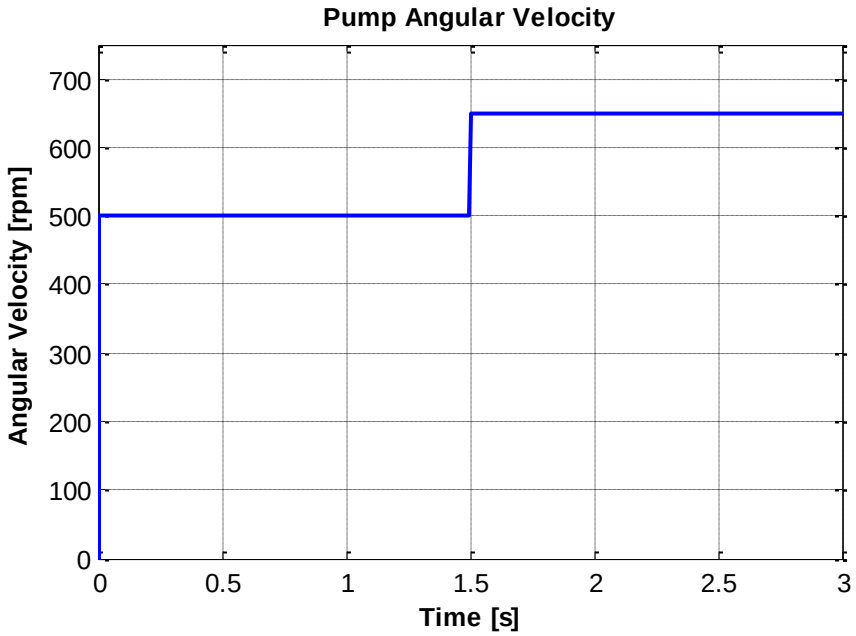

Figure 7.10 Hydraulic pump angular velocity profile

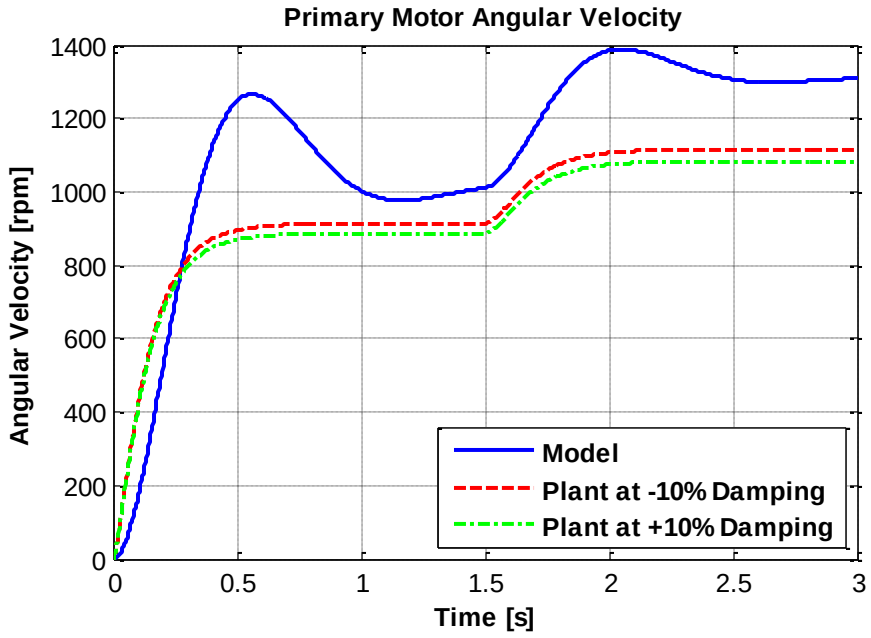

Figure 7.11 Model and plant primary motor angular velocity without controls

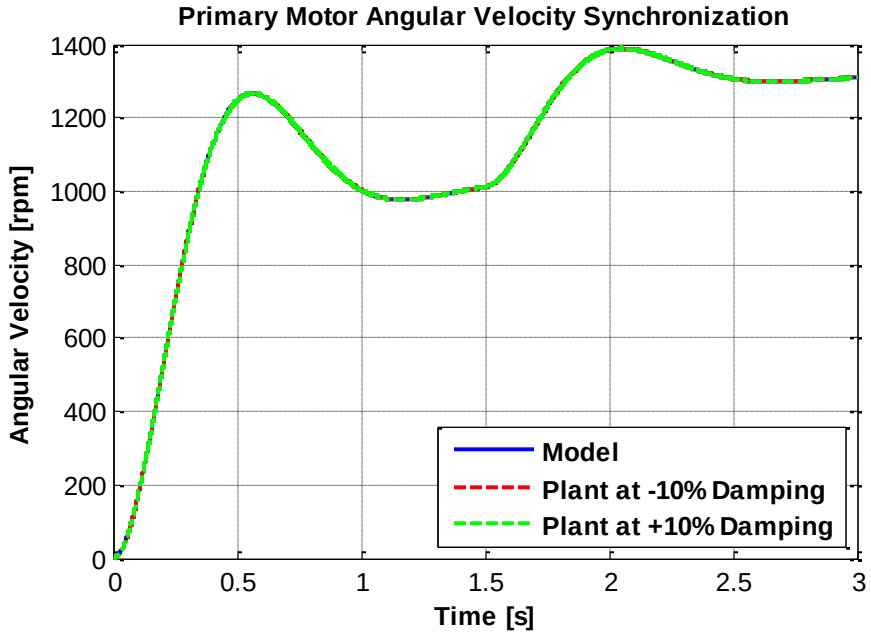

Figure 7.12 Model and plant primary motor angular velocity with controls

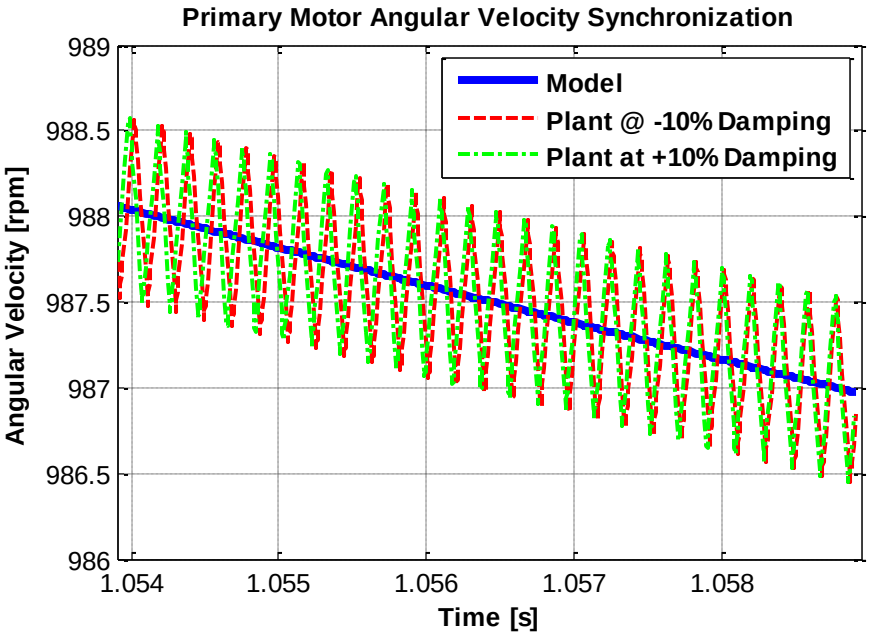

Figure 7.13 A magnified output tracking for a time increment

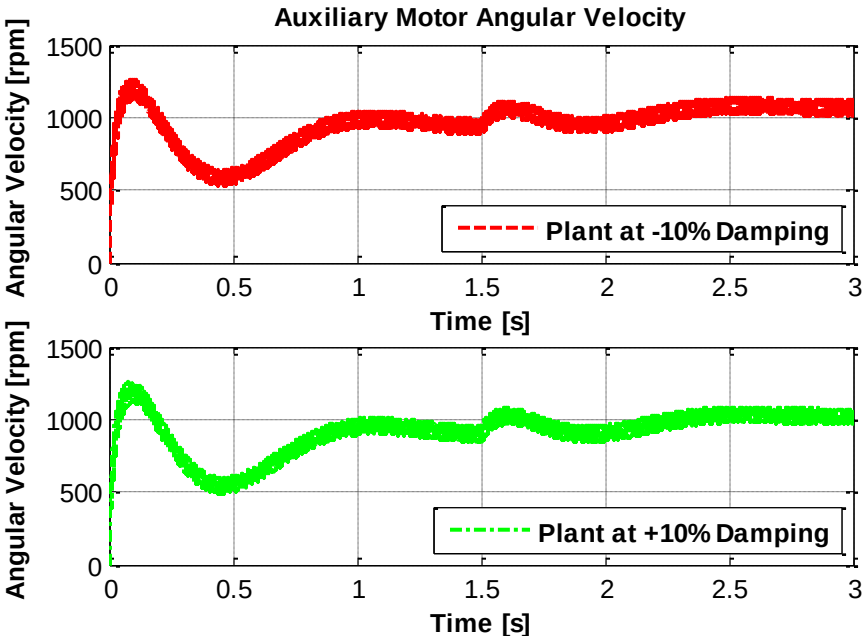

Figure 7.14 Plant Auxiliary motor velocity variation to maintain reference tracking in the primary motor

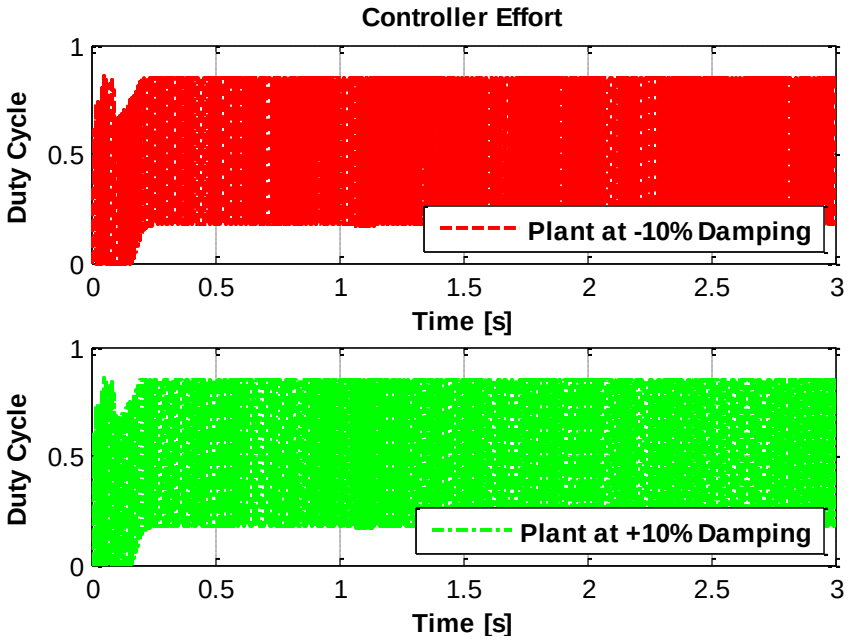

Figure 7.15 Controller effort to maintain model output tracking. The duty cycle is supplied to a 3-way proportional valve to distribute flow between the hydraulic motors in the plant to fulfill angular velocity requirements.

Figure 7.10 displays a step in angular velocity of pump, which is applied to the hydraulic power transmission system. Figure 7.11 demonstrates the simulation results with no control rule applied to the plant. According to the figure, the mathematical model and plant outputs deviate in values due to unknown values and variation of parameters but follow the same pattern and reach to the same state condition.

The tracking performance of the adaptive controller is illustrated in Figures 7.12 and 7.13. As the Figures demonstrate, the plant tracks the reference generated from the model with variation less than ±1 rpm. A close look at the velocity profile determines the accuracy of tracking. The adaptive controller generates a PWM signal with width between %0 and %100 to drive a hydraulic proportional valve and to compensate for hydraulic system uncertainties.

As the flow is controlled to maintain the angular velocity of the main motor, the excess high-pressure fluid is diverted to an auxiliary motor to collect the excess energy. As the control command is applied to track the reference request, the auxiliary motor velocity is illustrated in Figure 7.14.

Figure 7.15 illustrates the control effort to maintain the angular velocity. The control effort is normalized between 0-1 to demonstrate the fully closed and fully open valve conditions respectively. Adaptive controller could achieve a high performance in velocity tracking of a model used in energy transfer of a hydraulic wind power system.

7.1.2 Controller Design for the Nonlinear State-Space Model

This section represents the design of the controller for the nonlinear state-space model of the hydraulic system. The controller is incorporated to maintain the reference primary motor angular velocity. A rate limit (RL) controller is proposed to adjust the position of the proportional valve in fixed-steps to maintain the desired flow distribution for random wind speeds.

7.1.2.1 Rate Limit Controller Design

The intermittent nature of wind imposes fluctuation on the wind power generation and consequently varies the primary hydraulic motor angular velocity. This angular velocity variation results in the fluctuation of the generated electric power. This section introduces a control scheme to mitigate system output fluctuations by applying a control command to the valve to enforce a flow distribution between the hydraulic motors. A rate

limit (RL) controller is introduced to regulate the flow of hydraulic liquid to the main hydraulic motor by adjusting the position of the proportional valve. The flow regulation should maintain a specified angular velocity of the primary motor to retain the frequency of the electricity generated by the electric generator which is coupled with the primary motor at a definite proximity. Figure 7.16 shows the diagram of the RL controller. The RL controller estimates the error between the reference angular velocity and primary pump angular velocity. If the error value is positive, then the controller sends a negative displacement step signal to the valve, to further close the valve to track the reference velocity. If the error value is negative, the controller opens the valve by sending a positive step displacement signals to the valve. The excess flow is directed to the auxiliary motor and the flow energy is captured. Figure 7.17 shows the structure of the RL controller. The step values are designed to maintain system stability while both fast response and error mitigation criteria are fulfilled.

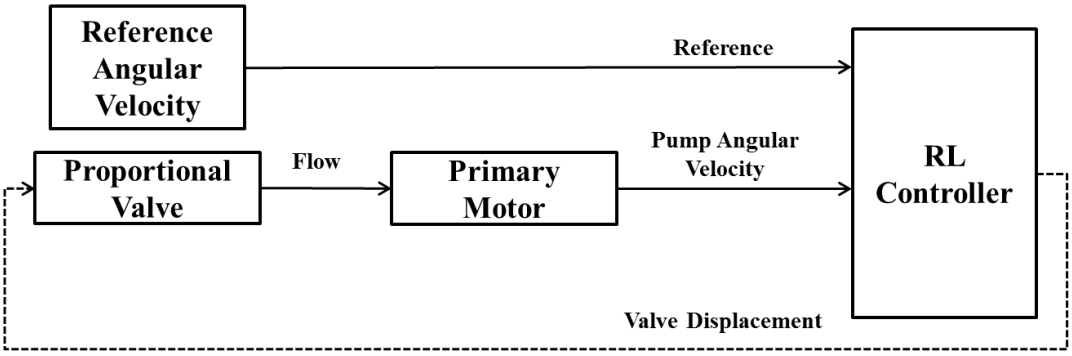

Figure 7.16 The diagram of the RL control closed loop system

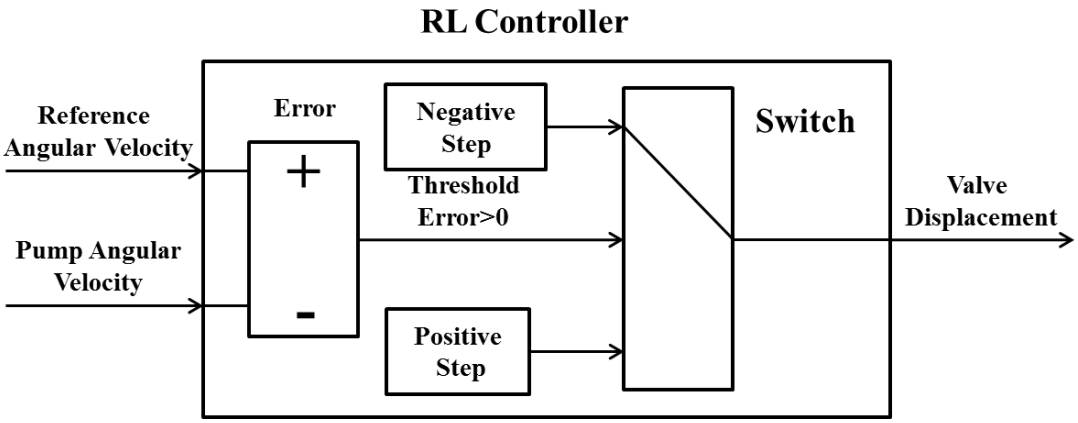

Figure 7.17 The RL controller structure

In order to substantiate the efficiency of the proposed nonlinear state space model of the hydraulic wind power transfer system, a model of the nonlinear state space system was created in MATLAB/Simulink®. A specific pump angular velocity profile was supplied to the simulation model to verify the reference primary motor angular velocity tracking. Table 5.1 illustrates the simulation parameter values and their units.

In simulations, a fixed displacement pump with a displacement of 0.517 in^3/rev supplies hydraulic fluid to a primary motor (Motor A) and an auxiliary motor (Motor B) both with fixed displacements of 0.097 in^3/rev. Figure 7.18 displays the angular velocity profile which is supplied to the hydraulic pump as a step input from 300 rpm to 500 rpm, and from 500 rpm down to 400 rpm. Figures 7.19 to 7.24 show the results of the simulations.

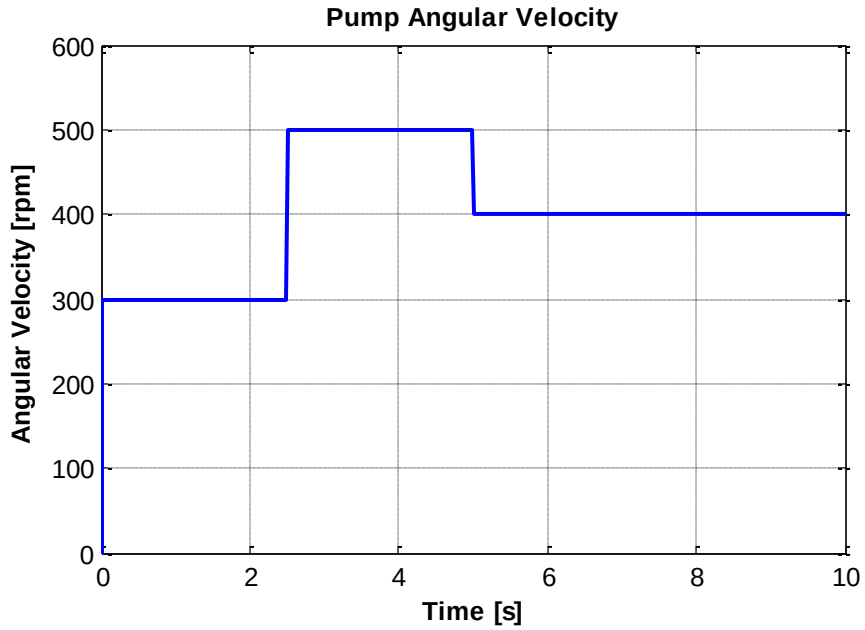

Figure 7.18 Hydraulic pump angular velocity profile

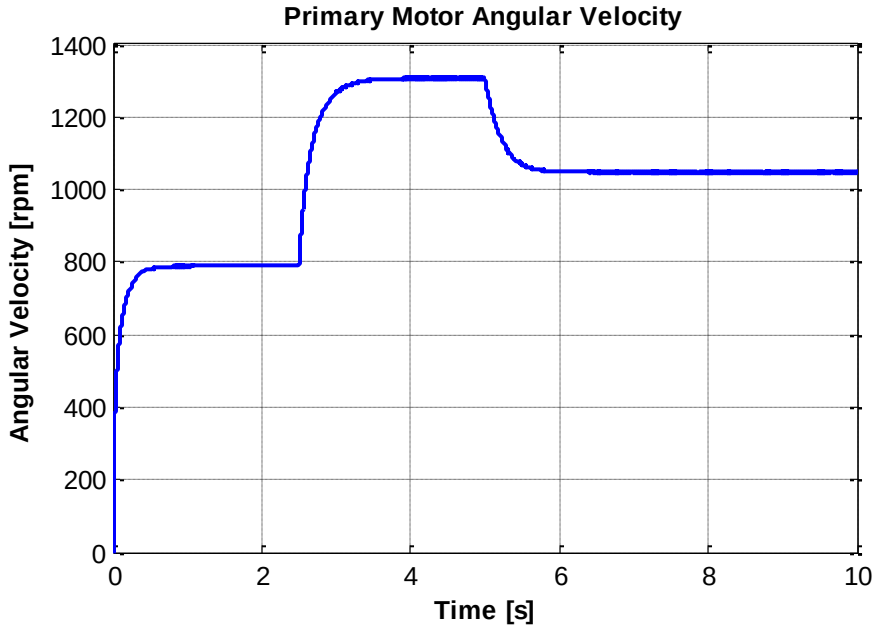

Figure 7.19 Primary motor angular velocity without the control technique

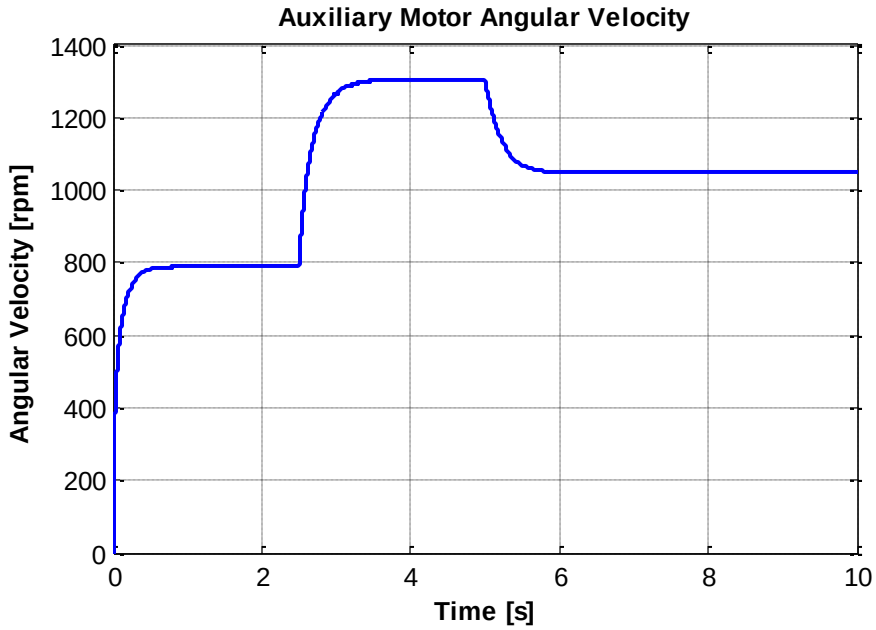

Figure 7.20 Auxiliary motor angular velocity without the control technique

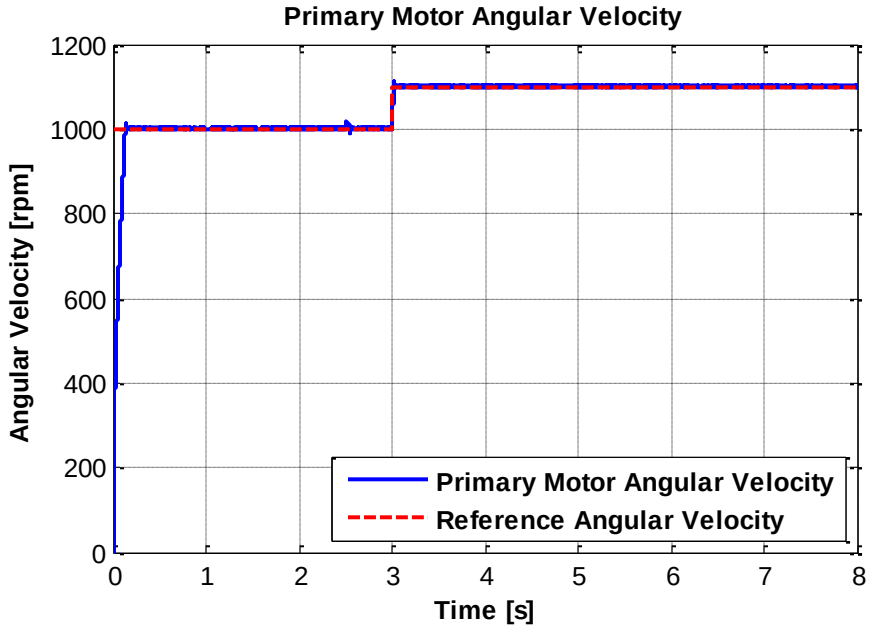

Figure 7.21 Primary motor angular velocity reference tracking

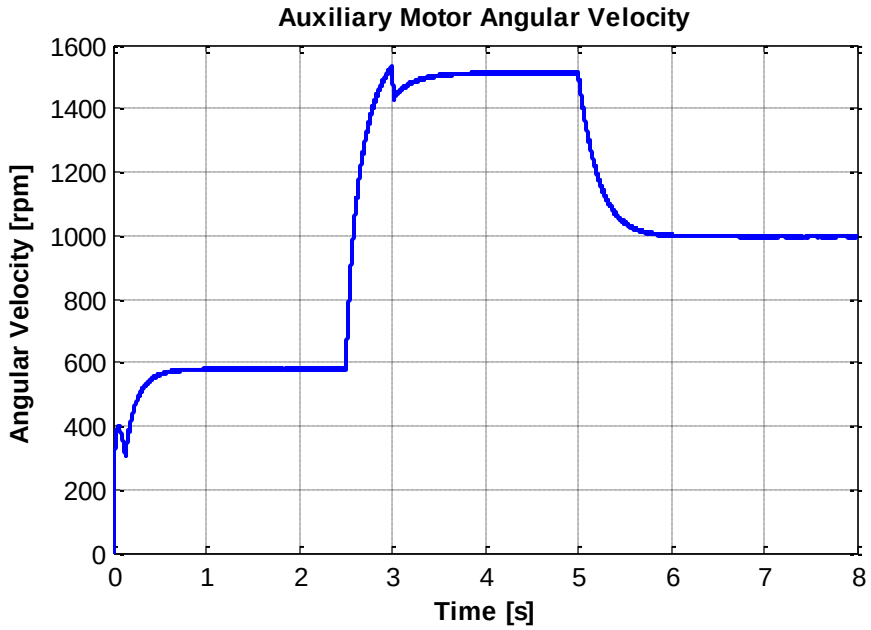

Figure 7.22 Auxiliary motor angular velocity with controls

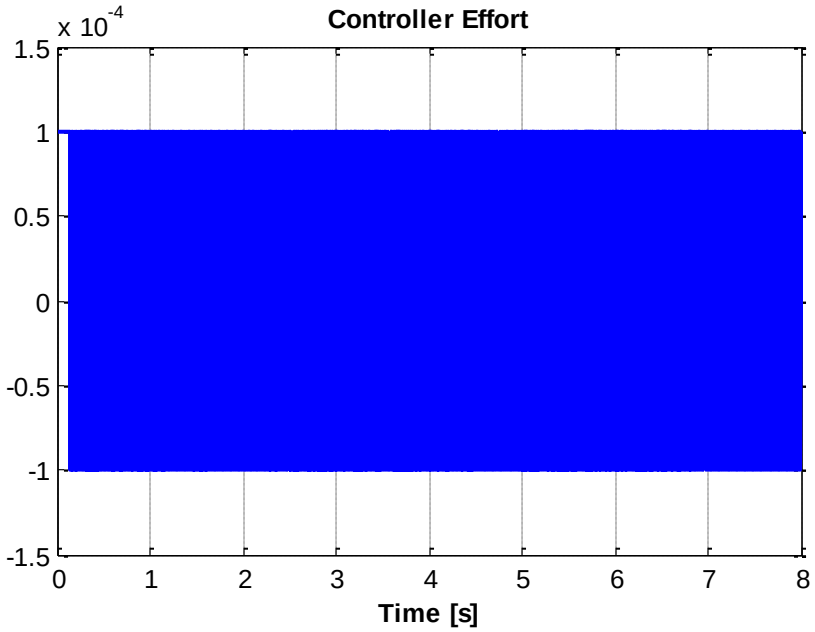

Figure 7.23 Controller effort to maintain reference tracking. The duty cycle is supplied to a 3-way proportional valve to distribute flow between the hydraulic motors in the plant to fulfill angular velocity requirements.

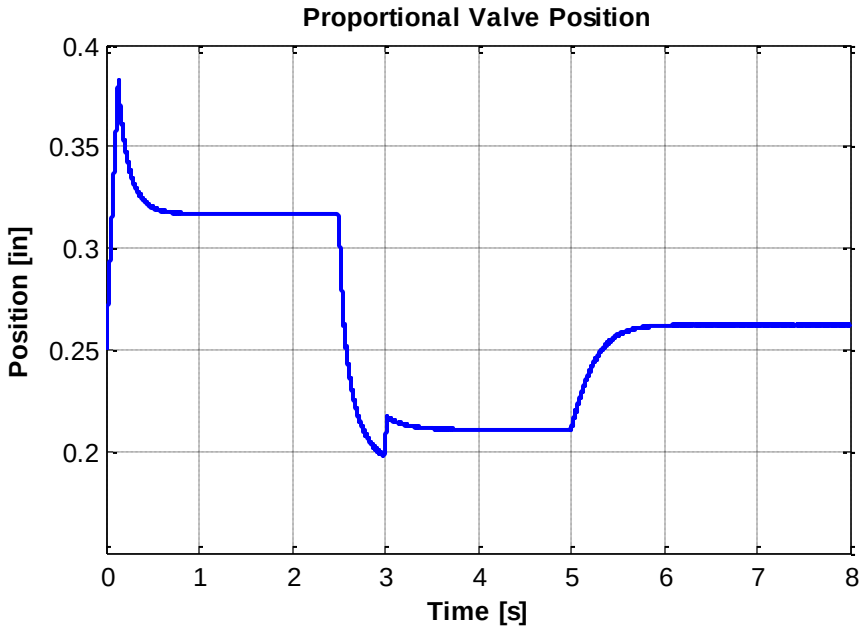

Figure 7.24 Valve position controlled by the RL controller

Figure 7.19 and 7.20 depict the angular velocity of the primary motor and auxiliary motor without the application of the control strategy. In this configuration, the valve position is adjusted to the middle point in which the hydraulic fluid is distributed evenly among the motors. Since the hydraulic motors are geometrically similar, the only considerable dissimilarity between the two is the damping coefficient of the motors which results in a slight divergence of the angular velocities.

Figures 7.21 to 7.22 illustrate the simulation results with application of the control technique. Figure 7.21 depicts the reference angular velocity tracking of the primary motor. The figure verifies the success of the controller to maintain the reference angular velocity and mitigate the steady state error at the motor output. The 0-100% rise time of the response is 0.1324 sec. Since the response displays negligible overshoot, the 2% settling time is similar to the rise time. The excess flow energy is captured by the

auxiliary motor. Figure 7.22 shows the angular velocity variation of the auxiliary motor to accommodate reference tracking of the primary motor angular velocity.

Figure 7.23 displays the controller effort to regulate the valve position to maintain the reference pump angular velocity. Initially the controller opens the valve to accelerate error mitigation and reduce the rise time. The controller further closes the valve maintain the flow.

Figure 7.24 depicts the position of the valve. The valve position is regulated to retain the primary motor angular velocity. The valve is opened to increase the motor angular velocity and is closed to reduce the motor angular velocity.

7.2 Controller Design for the System Prototype

The intermittent nature of wind speed imposes random fluctuation to the output velocity of the electric generator. Consequently, implementation of a control scheme is required to adjust the flow distribution between the primary motor and auxiliary motor to maintain a reference angular velocity.

7.2.1 PI Angular Velocity Controller Design

This section introduces the design and incorporation of a PI control technique to maintain a reference primary motor angular velocity in the experimental prototype. The sensors which are installed in the prototype provide feedback from the system to the controller. The PI controller compares the angular velocity data from the speed sensor with the reference velocity and compensates for the difference by sending a pulse

command to the 3-way proportional valve input to regulate the valve position. The regulation of the valve position varies the flow distribution between the motors and adjusts the primary motor velocity to the reference value. dSPACE is used to collect the data from the sensors and send a corrective signal to the proportional valve.

In experiment, an angular velocity profile is supplied to the hydraulic pump. The reference angular velocity is provided to the controller. Figure 7.25 shows the schematic diagram of the closed loop control system. The PI controller gains are illustrated in Table 7.3. Figures 7.26 to 7.28 demonstrate the results of the angular velocity control of the hydraulic system prototype.

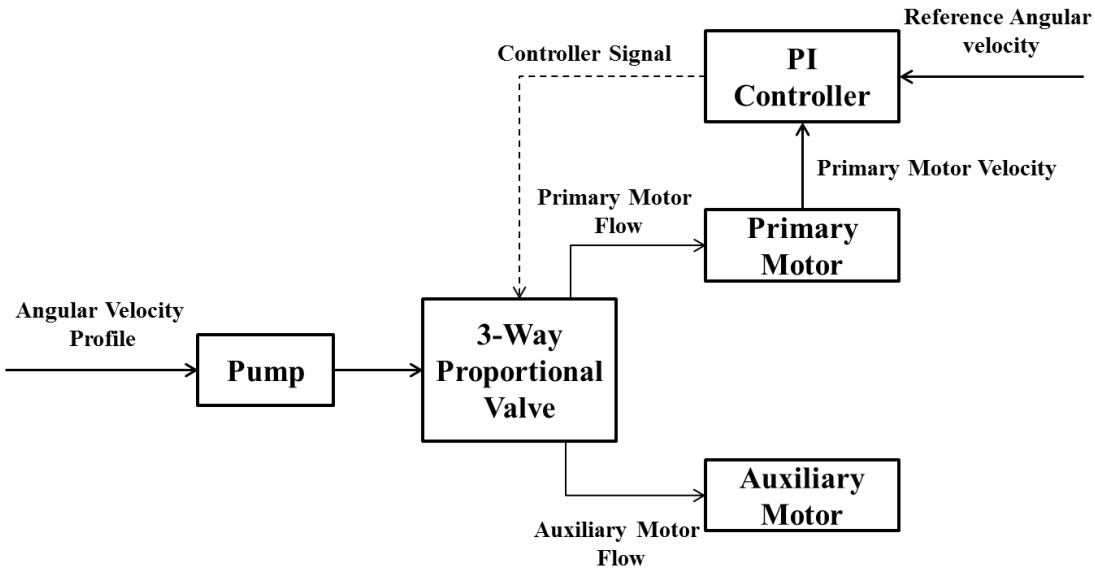

Figure 7.25 Schematic diagram of the closed loop PI control system for the experimental setup

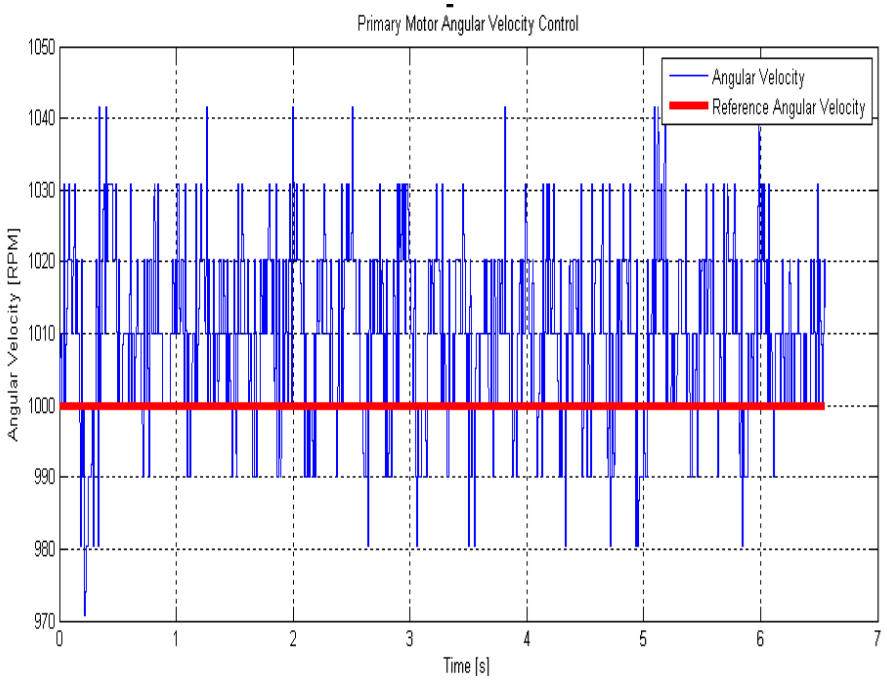

Figure 7.26 Angular velocity control of the primary motor in the experimental setup

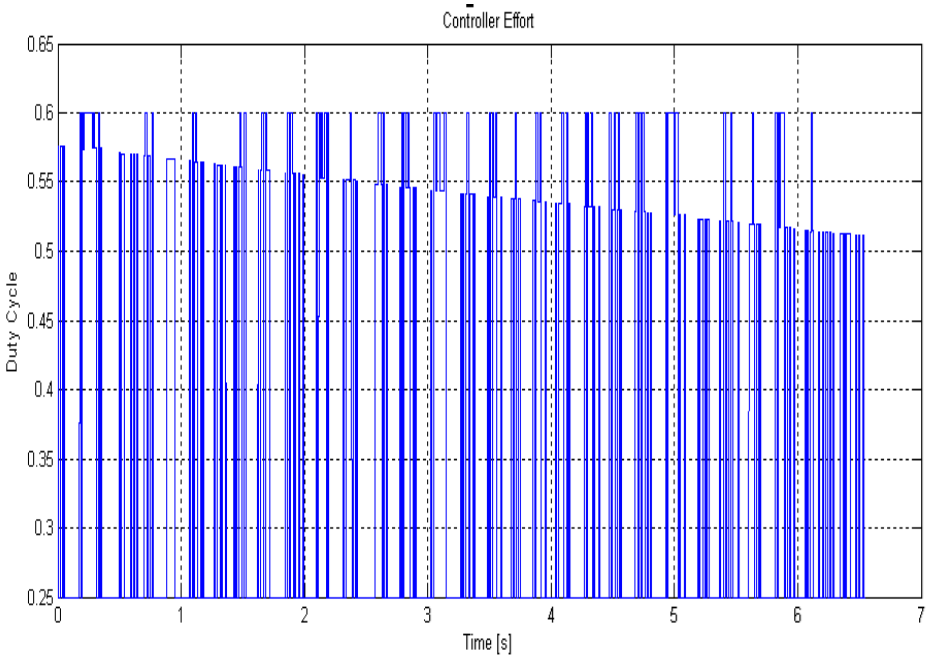

Figure 7.27 PI controller effort to regulate the position of the valve

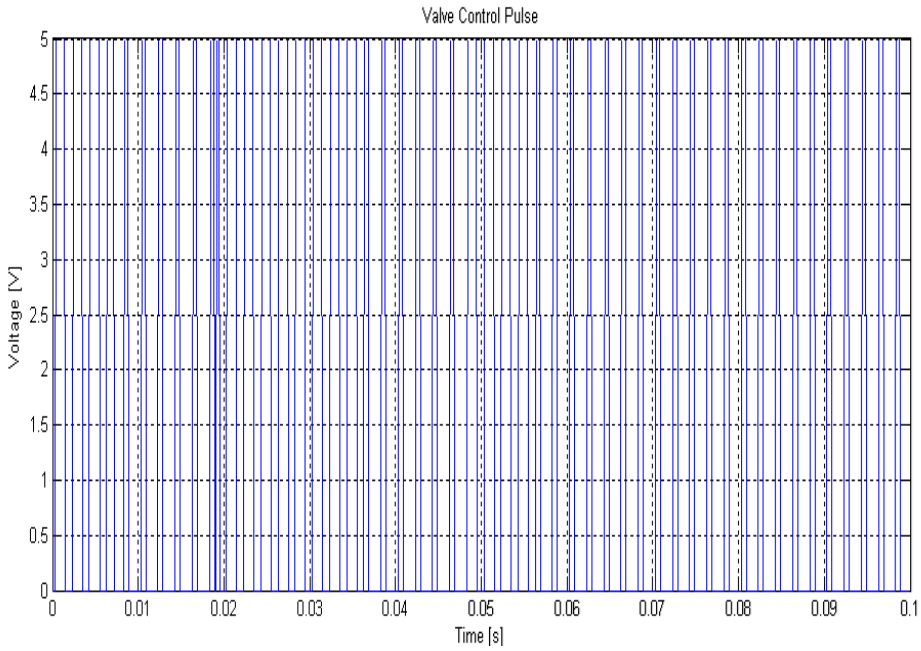

Figure 7.28 PWM signal to the valve input

Figure 7.26 demonstrates the reference angular velocity tracking of the system prototype. The reference angular velocity was adjusted to 1000 rpm and the controller regulated the valve position to maintain the reference velocity tracking. According to this figure, the tracking error was within ±42 rpm.

Figure 7.27 displays the efforts of the PI controller to maintain the reference primary motor angular velocity. The primary motor angular velocity sensor provides the real time speed information to the controller. The speed is compared with the reference value and a control signal is generated to compensate for the difference and to mitigate tracking error.

Figure 7.28 shows the valve input signal. Since the proportional valve is pulse driven, the controller effort is converted to address the valve requirements. The valve

input is a pulse between 0% and 100%, where 0% stands for fully closed and 100% stands for fully opened.

8. FUTURE APPLICATIONS OF THE HYDRAULIC ENERGY TRANSFER

8.1 An Energy Storage Technique for Hydraulic Wind Transfers

Hydraulic wind power transfer systems allow collecting of energy from multiple wind turbines into one generation unit. They bring the advantage of eliminating the gearbox as a heavy and costly component. The hydraulically connected wind turbines provide variety of energy storing capabilities to mitigate the intermittent nature of wind power. This section introduces the hydraulic circuitry and control algorithm for a novel wind energy storage technique. The simulation results demonstrate the successful operation of the storage to maintain the fluid in the system to regulate the generator speed at a predetermined value.

8.1.1 Hydraulic Wind Energy Transfer System with Storage

The hydraulic wind power transfer system consists of a fixed displacement pump driven by the prime mover (Wind turbine) and one or more fixed displacement hydraulic motors. The hydraulic transmission uses the hydraulic pump to convert the mechanical input energy into pressurized fluid. Hydraulic hoses and steel pipes are used to transfer the harvested energy to the hydraulic motors [16].

Figure 8.1 displays a schematic diagram of the wind energy transfer and the energy storage system. As the figure demonstrates, a fixed displacement pump is mechanically coupled with the wind turbine and supplies pressurized hydraulic fluid to two fixed displacement hydraulic motors. The hydraulic motors are coupled with electric generators to produce electric power in a central power generation unit. Since the wind turbine generates a large amount of torque at a relatively low angular velocity, a high displacement hydraulic pump is required to flow high-pressure hydraulics to transfer the power to the generators. The pump might also be equipped with a fixed internal speed-up mechanism. Flexible high-pressure pipes/hoses connect the pump to the piping toward the central generation unit.

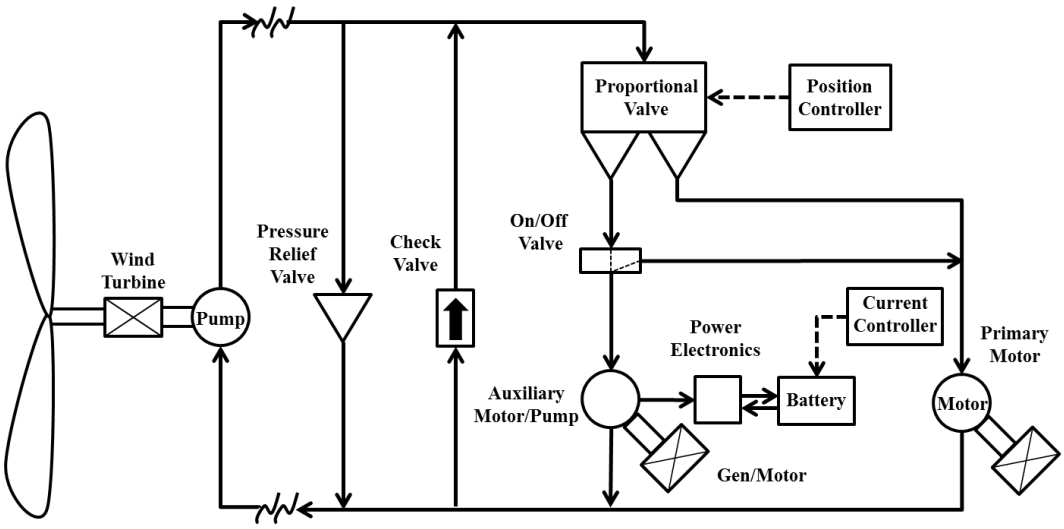

Figure 8.1 Schematic of the high-pressure hydraulic power transfer system. The hydraulic pump is in a distance from the central generation unit.

The hydraulic circuit uses check valves to guarantee the unidirectional flow of the hydraulic flows. A pressure relief valve protects the system components from the

destructive impact of localized high-pressure fluids. These units also provide proper path for the energy storage to circulate the fluid in the system without going through the hydraulic pump at the wind tower. The hydraulic circuit contains a specific volume of hydraulic fluid, which is distributed between hydraulic motors using a proportional valve.

Since the electrical energy produced at the central generation unit could only be supplied to the grid at a specific frequency, a velocity control unit is required to maintain the constant angular velocity at the primary motor-generator. The speed regulation is accomplished by regulating the flow through a proportional valve and directing the excess fluid to the auxiliary motor. The operation of the hydraulic system is split into two categories, namely system operation at high wind and system operation at low wind.

8.1.1.1 System Operation at High Wind

The wind speed fluctuates over time. Therefore utilization of fixed displacement pumps result in flow variation in the system. If the wind speed is higher than the reference that generates 60 Hz voltage in the output, the condition is called high wind. If the excess flow of power and its energy is not captured the generator's frequency will deviate from 60Hz. The proportional valve is regulated such that the required flow is delivered to the primary hydraulic motor, and the excess energy is captured by the auxiliary hydraulic motor. The auxiliary hydraulic motor is coupled with an electric motor/generator. At high wind, the auxiliary hydraulic motor runs the electric generator. The electric generator converts the mechanical energy of the rotating shaft into electric energy and stores it in batteries. The primary motor is coupled to the main generator and

supplies electricity at a specific frequency to the load. Figure 8.2 illustrates the hydraulic circuit of the energy transfer system at high wind. To regulate the amount of energy captured by auxiliary motor a rate limit controller is utilized.

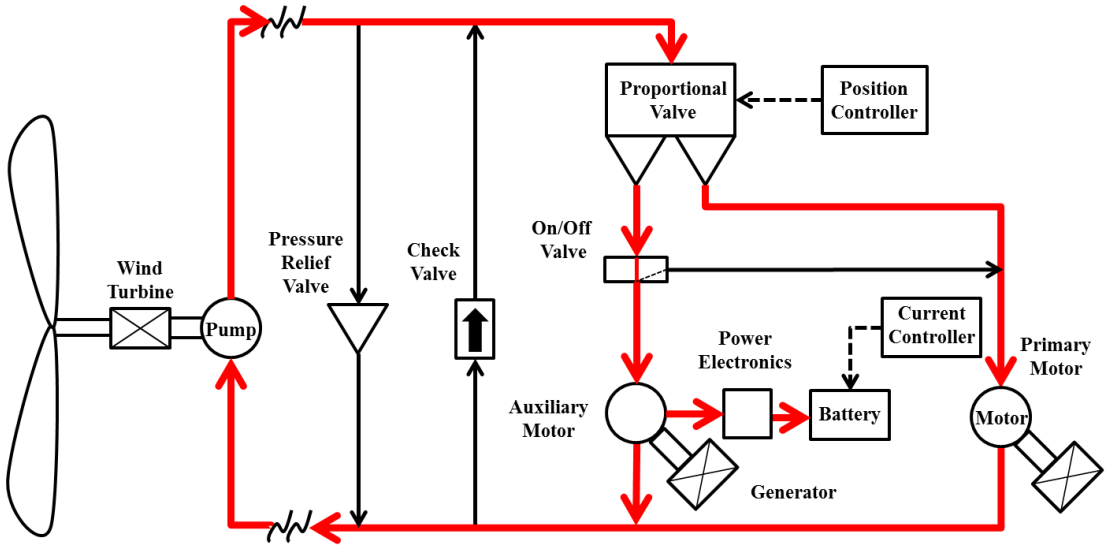

Figure 8.2 Operating configurations of the system at high wind

8.1.1.2 System Operation at Low Wind

If the wind speed drops below a threshold speed, the condition is considered low wind. In this configuration the flow generated by hydraulic pump is not sufficient enough to maintain the reference angular velocity at the primary motor. In order to compensate for the flow deficiency, the energy stored in the storage should be released back to the system. The storage in any form can runs the auxiliary hydraulic pump to generate an augmented pressurized fluid in the system. Figure 8.3 illustrates the system operation at low wind. In this configuration, a PI controller regulates the storage discharge rate such that the main generator maintains the rated frequency.

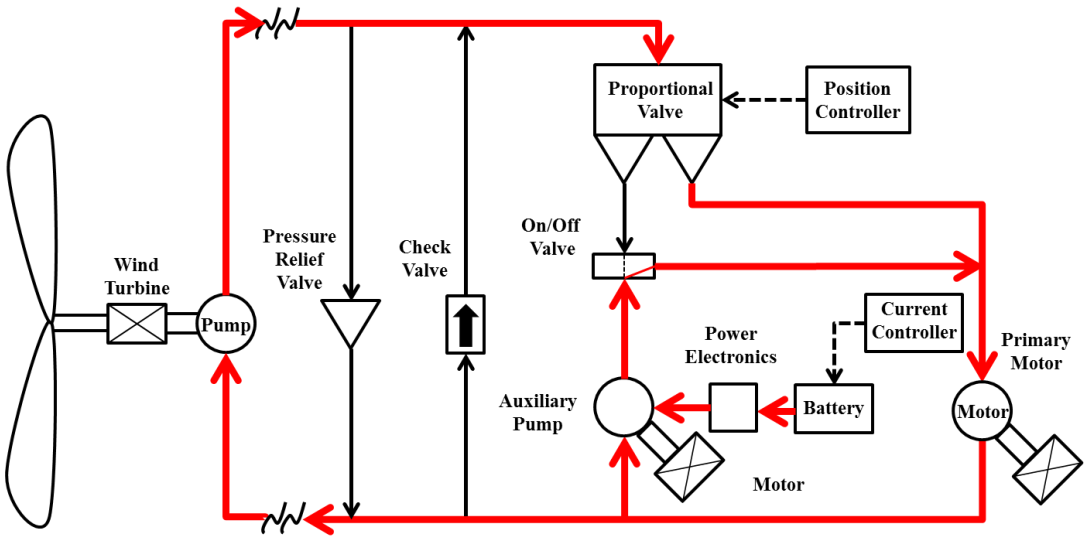

Figure 8.3 Operating configurations of the system at low wind.

8.1.1.3 Storage Dynamic

The general hydraulic circuit incorporates the hydraulic model equations which are introduced in chapter 4. This section augments the storage dynamics to the system. Without loss of generality, in this section we consider the storage as a battery. The excess energy which is captured by the auxiliary motor is transformed to electrical energy through the generator. The charge current is calculated as

$$I_B = \frac{T_{p/m}\omega_{p/m}\eta_{gen}}{V_B} \tag{8.1}$$

where I_B is the battery current, $T_{p/m}$ is the auxiliary pump/motor torque, $\omega_{p/m}$ is the auxiliary pump/motor angular velocity, V_B and is the battery voltage.

The battery state of charge (SOC) which is defined as the percentage of the initial battery capacity is calculated as

$$SOC = \frac{C_i}{C_0} \tag{8.2}$$

where C_i is the available charge of the battery, and C_0 is the nominal capacity of the battery.

The auxiliary motor/pump is coupled with the electric generator/motor. The dependency of the angular velocity of the auxiliary pump to the extracted battery current is expressed such that

$$\omega_{pAux} = kI_B \tag{8.3}$$

where k is the current coefficient of the electric generator which is coupled with the auxiliary pump.

8.1.2 System Operation and Dynamic Model

8.1.2.1 System Operation at High Wind

The overall hydraulic system can be connected as modules to represent the dynamic behavior. Block diagrams of the hydraulic transmission system using MATLAB Simulink are demonstrated in Figures 8.4 and 8.5. The model incorporates the mathematical governing equations of individual hydraulic circuit components. The bulk modulus unit generates the operating pressure of the system.

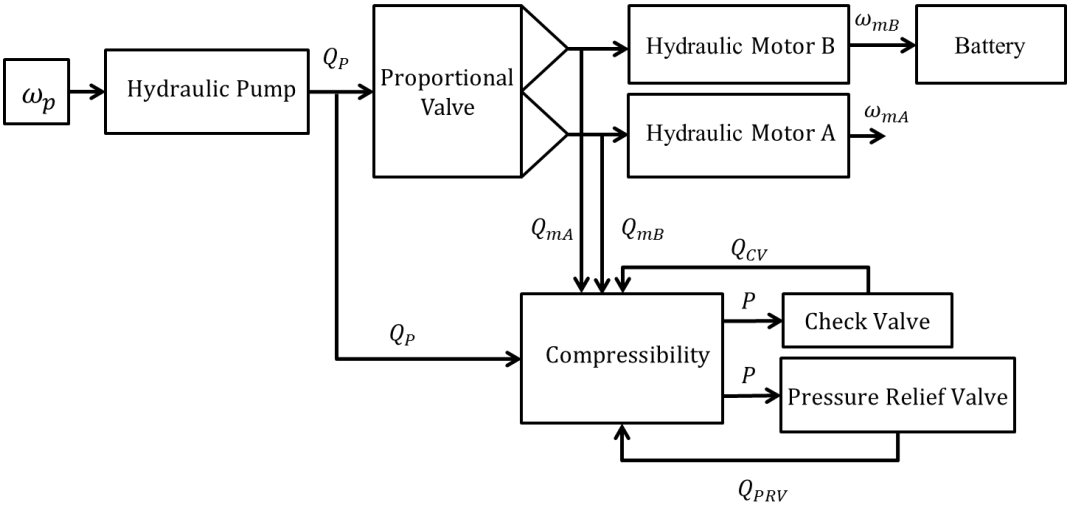

Figure 8.4 Hydraulic transmission schematic diagram at high wind

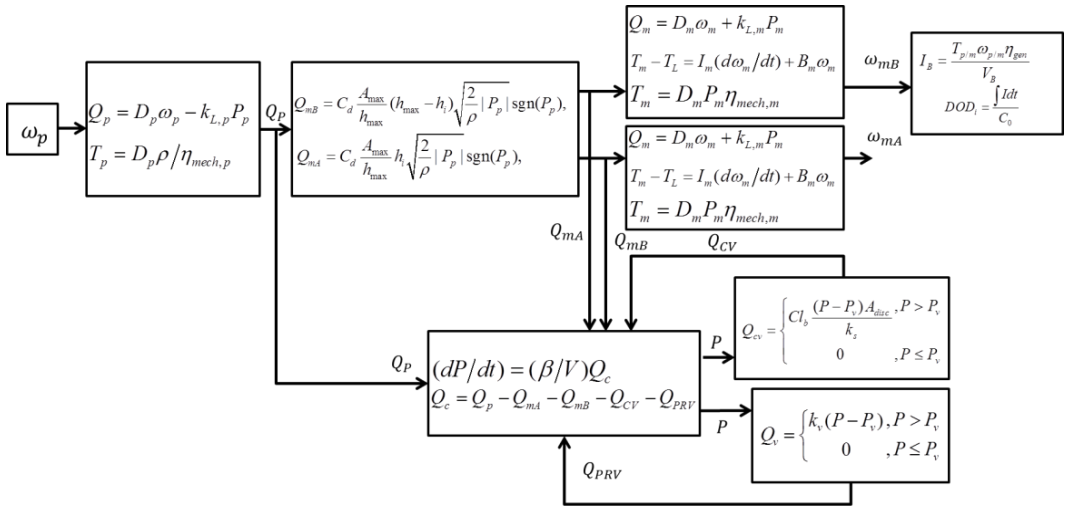

Figure 8.5 Mathematical model of the hydraulic system at high wind

Figure 8.4 depicts a block diagram of the wind energy transfer system in high wind. According to the figure, the wind turbine supplies power at a specific angular velocity to the main hydraulic pump. The hydraulic pump supplies pressurized hydraulic fluid to the proportional valve which the hydraulic fluid between the motors based on the reference primary motor angular velocity. The auxiliary motor captures the surplus

energy of the flow and drives the electric generator to charge electrical storage. The generated electrical energy is stored in a battery through the power electronic converters. The primary motor is coupled with the main generator and supplies electricity to the grid.

Figure 8.5 displays the mathematical model of every hydraulic component in the transmission system. The flows and pressures are calculated for all hydraulic components. The data from the hydraulic circuit is utilized to calculate the flow of energy into the battery.

8.1.2.2 System Operation at Low Wind

The model of the wind energy transfer at low wind is similar to the high wind condition. However, in this configuration, the transfer system is driven by the energy stored in the battery when released back to the system. The current extracted from the battery is regulated to accommodate the primary motor angular velocity demand. The auxiliary motor can be driven as a pump by the electric motor and flows pressurized fluid augmented with the main pump flow. The compressibility block calculates the gauge pressure along the pumps and hydraulic motor terminals. Figures 8.6 and 8.7 show the block diagram of the mathematical model of the hydraulic transfer system at low wind condition.

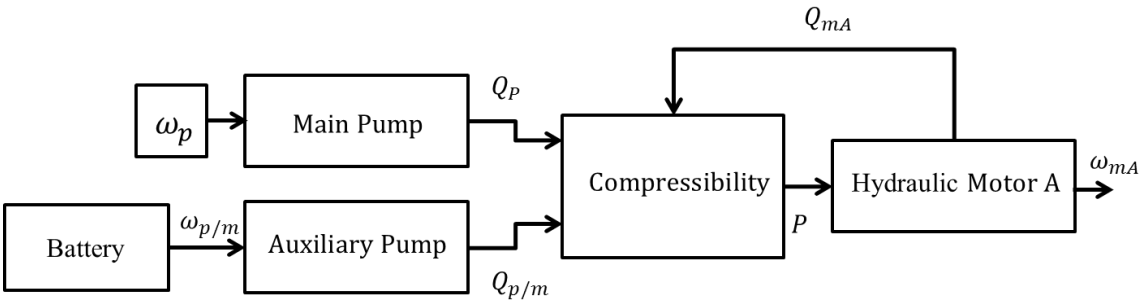

Figure 8.6 Hydraulic transmission schematic diagram at low wind

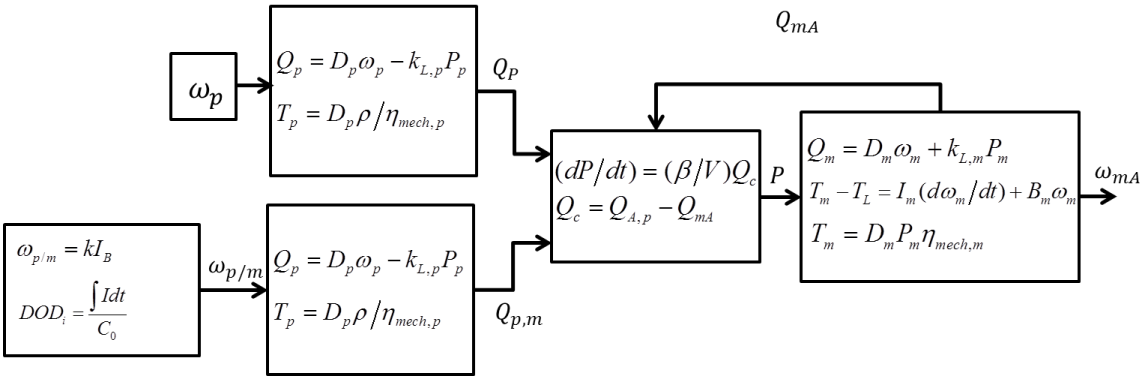

Figure 8.7 Mathematical model of the hydraulic system at low wind

8.1.3 Controller Design

This section introduces the design of the controllers which are required to maintain the reference primary motor angular velocity at both high and low wind conditions. A rate limit controller regulates the position of the proportional valve at the high wind operation to maintain tracking of the reference speed. A PI controller is also utilized to regulate the battery discharge current at low wind operation.

8.1.3.1 Rate Limit Controller Design

The rate limit controller directs the flow of the hydraulic fluid from wind turbine at high wind, and from wind turbine and auxiliary motor at low wind to the main hydraulic motor. The controller adjusts the position of the valve towards the primary motor path to maintain tracking of the reference angular velocity. Figure 8.8 represents the diagram of the rate limit controller.

At the high wind operation, the rate limit controller measures the error between the reference angular velocity and the primary pump angular velocity. If the error value is positive, then the controller sends a number of negative fixed displacement step signals to the valve, to regulate the flow and track the reference velocity. If the error value is negative, the controller opens the valve by sending a fixed positive step displacement signal to the valve. Figure 8.9 shows the structure of the rate limit controller. The step values are designed to maintain system stability while both fast response and error mitigation criteria are fulfilled.

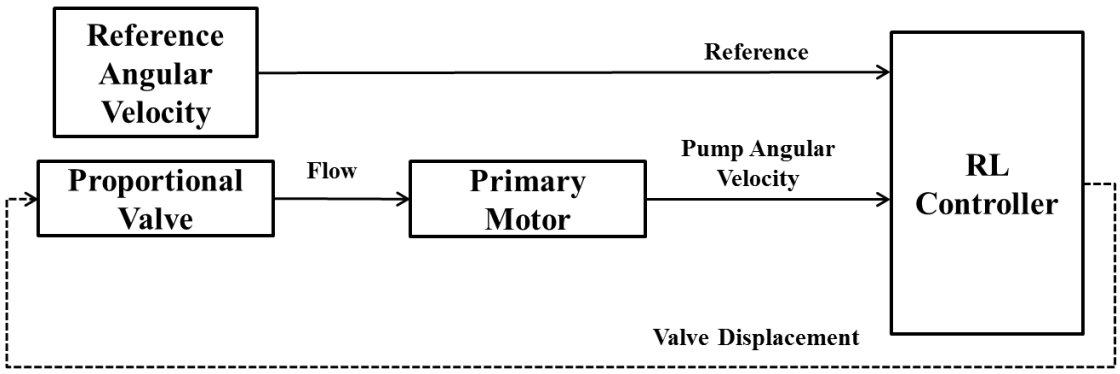

Figure 8.8 The diagram of the rate limit control closed loop system

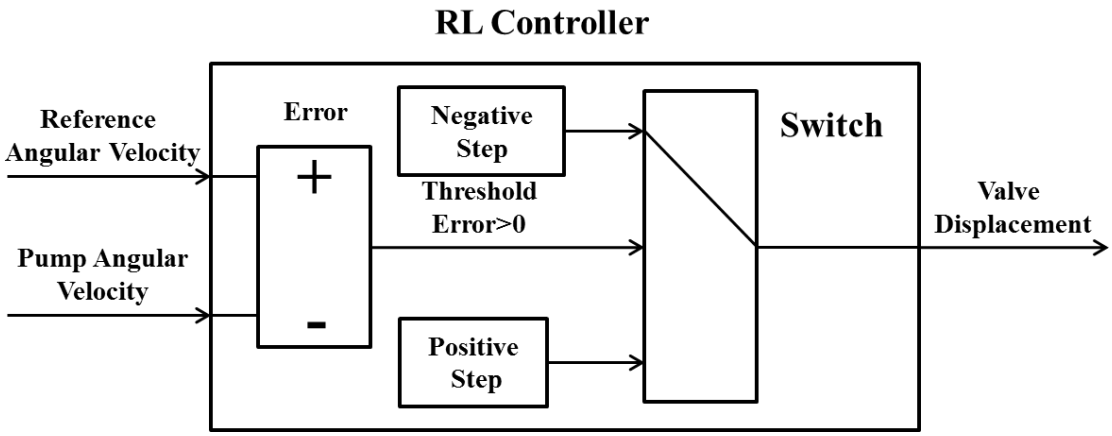

Figure 8.9 The rate limit controller structure

8.1.3.2 PI Controller Design

At low wind conditions and when the battery is being discharged, a PI controller is utilized. In this case, the PI controller regulates the angular velocity of the auxiliary pump to maintain velocity reference of the primary motor. The PI controller regulates the amount of battery discharge current to run the electric motor/generator coupled with the auxiliary pump. Figure 8.10 represents the closed-loop diagram of the PI control system.

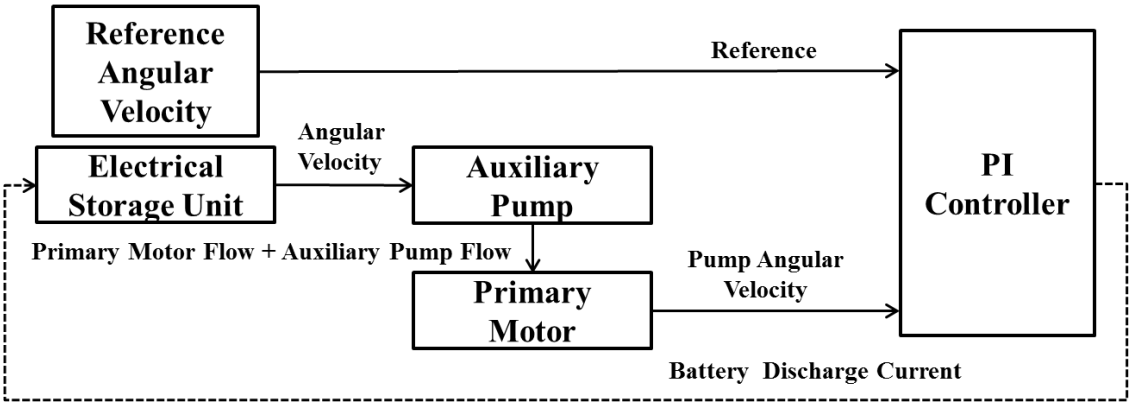

Figure 8.10 The diagram of the PI control closed loop system

The proportional gain adjusts the response time characteristics such as settling time and rise time. At higher proportional gains (within the region of stability) a faster system response is obtained. A proper integral gain mitigates the steady state tracking error.

8.1.4 Simulation Results and Discussions

In this section, the mathematical model of the hydraulic wind energy transfer with the storage unit behavior is simulated and the performance of the control system to maintain the reference angular velocity is evaluated. The simulation parameters are listed in Table 8.1. Figures 8.11 to 8.23 show the results of the simulations from the storage model.

Table 8.1 Simulation parameters for the hydraulic system with the storage technique

Symbol	Quantity	Value	Unit
k	Current Coefficient	10	
V_B	Battery Voltage	12	Volts
C_0	Initial Battery Capacity	31.25	Amp.hr
SOC_0	Initial State of Charge	50	%
	On/off Controller Step Size	0.0001	In
k_p	Proportional Gain	0.001	
k_p	Integral Gain	10	

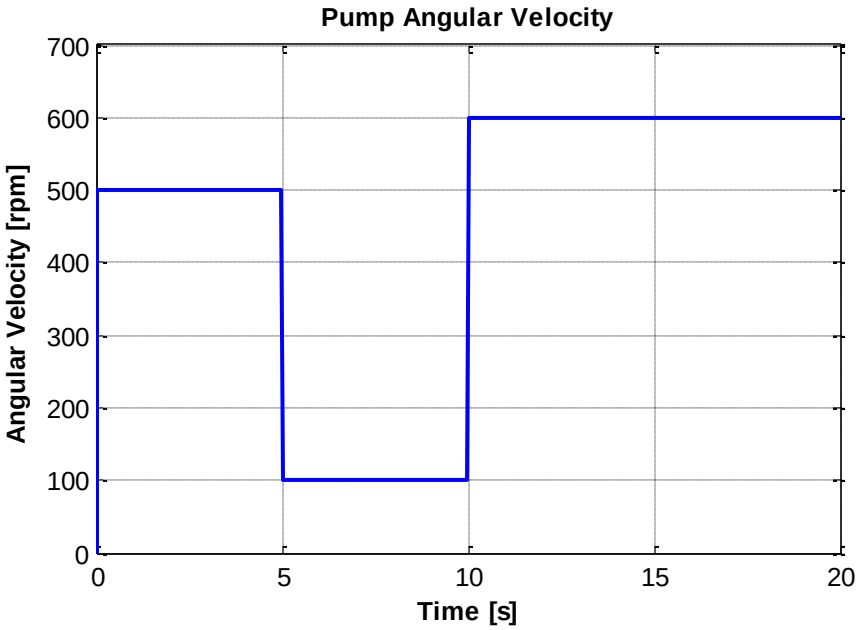

Figure 8.11 Hydraulic pump angular velocity profile

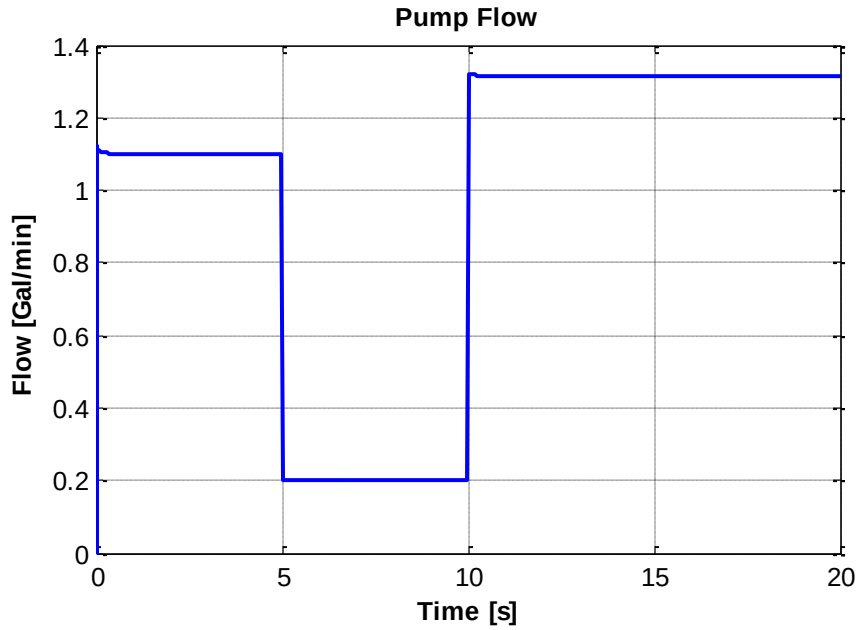

Figure 8.12 Flow generated by the hydraulic pump

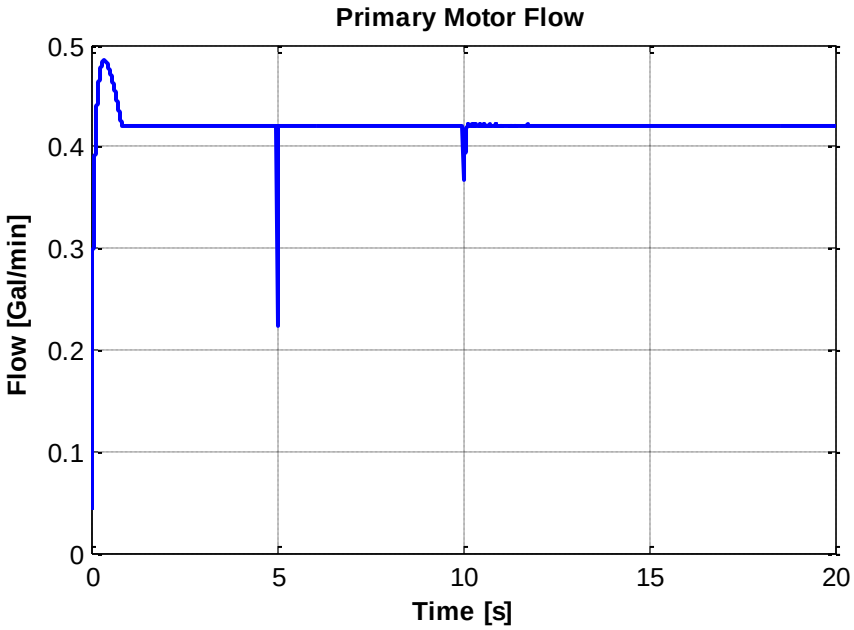

Figure 8.13 Primary motor flow

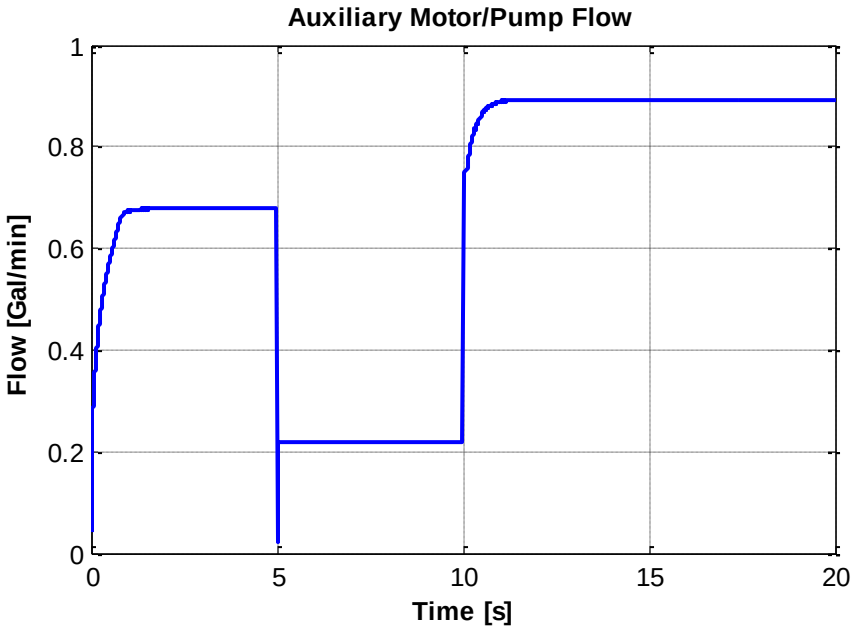

Figure 8.14 Auxiliary motor/pump flow

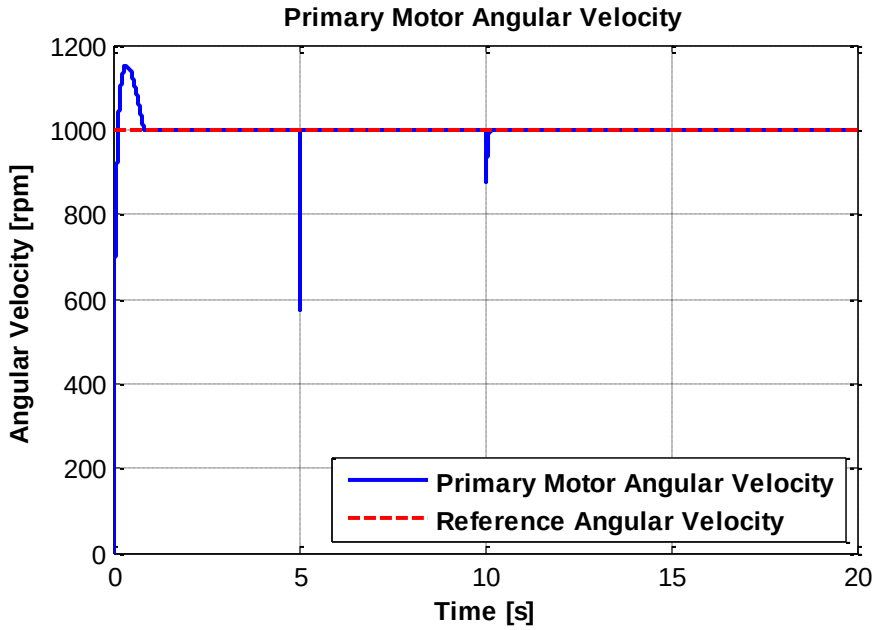

Figure 8.15 Comparison of the primary motor angular velocity and the reference angular velocity

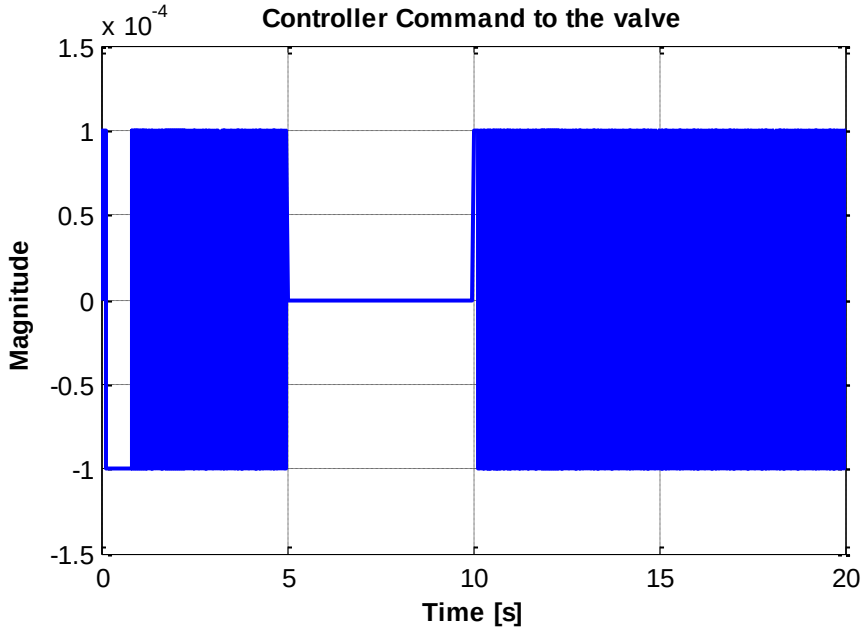

Figure 8.16 Control effort of the rate limit controller to regulate the proportional valve position

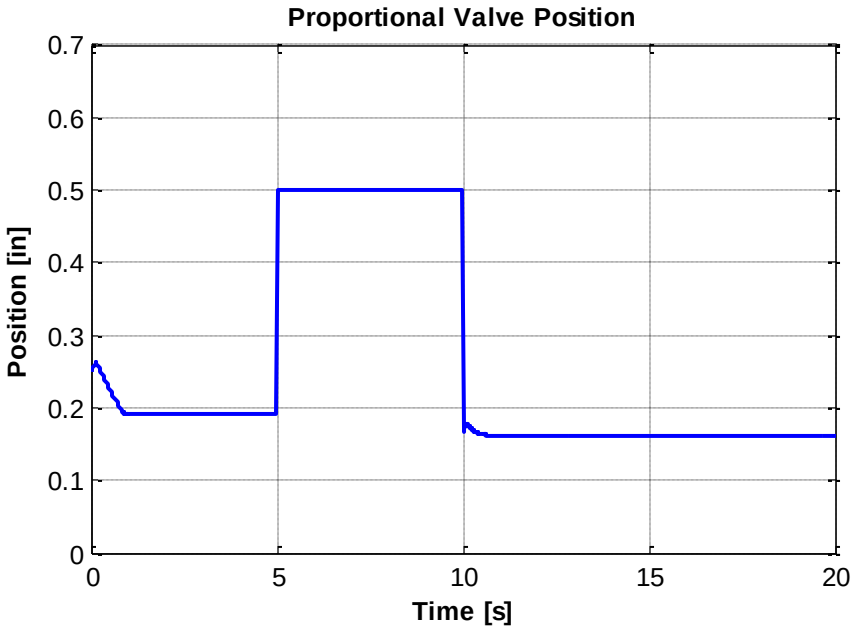

Figure 8.17 Proportional valve position to distribute hydraulic flow between the motors to maintain the reference angular velocity

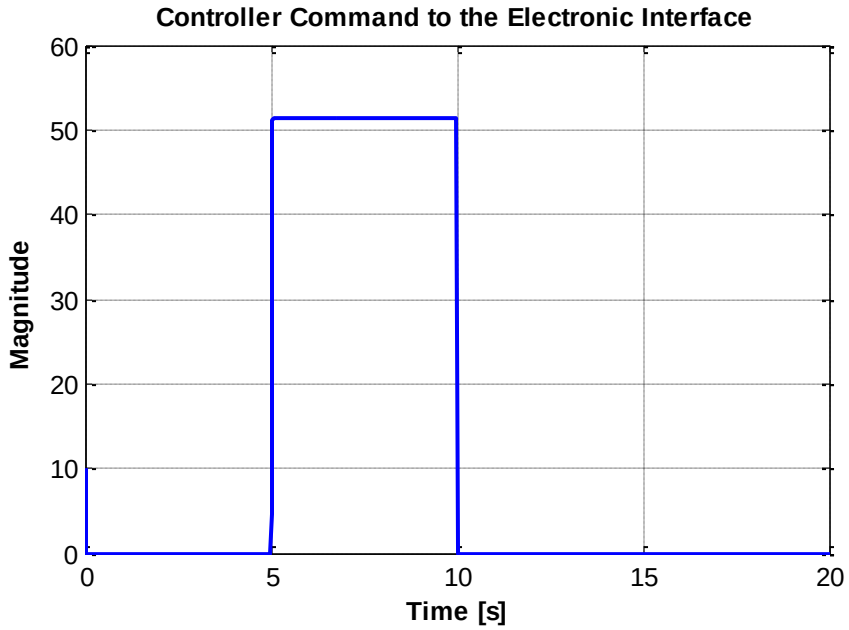

Figure 8.18 Control effort of the PI controller to regulate the discharge current

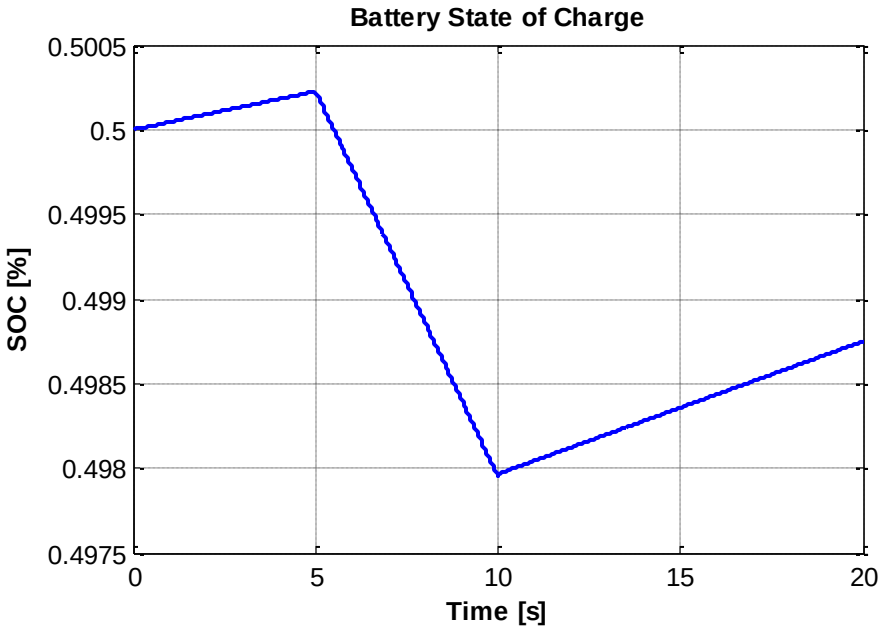

Figure 8.19 Hydraulic transmission system battery state of charge

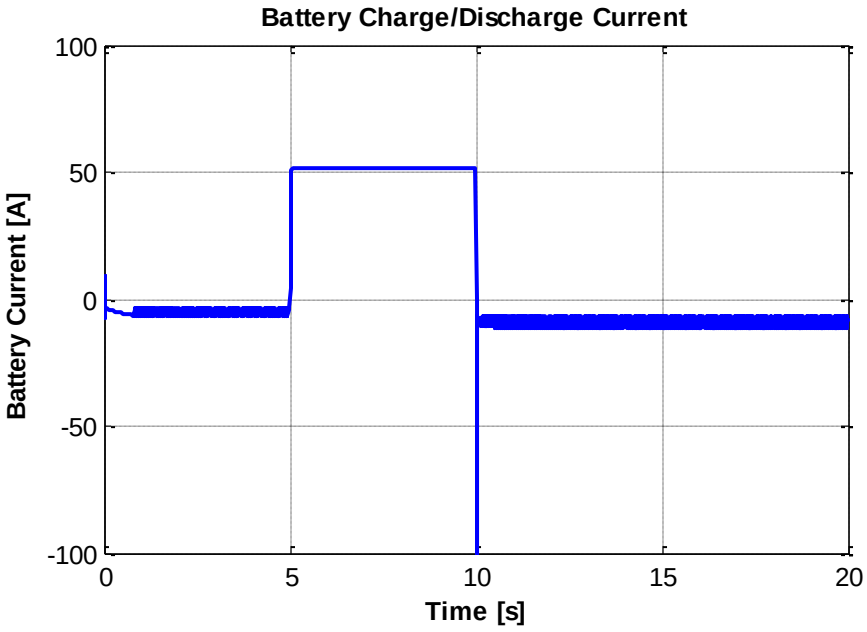

Figure 8.20 Hydraulic transmission battery charge/discharge current

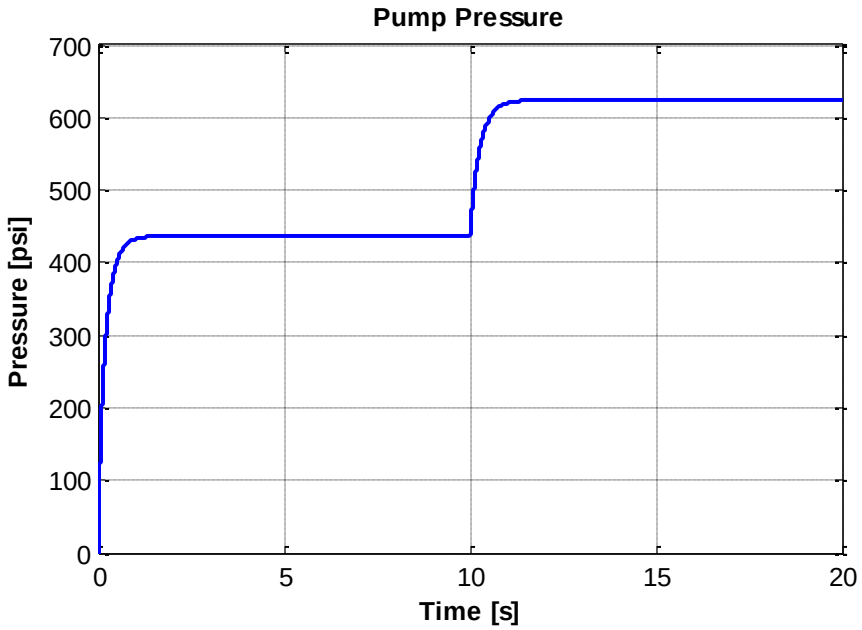

Figure 8.21 Hydraulic pump differential pressure

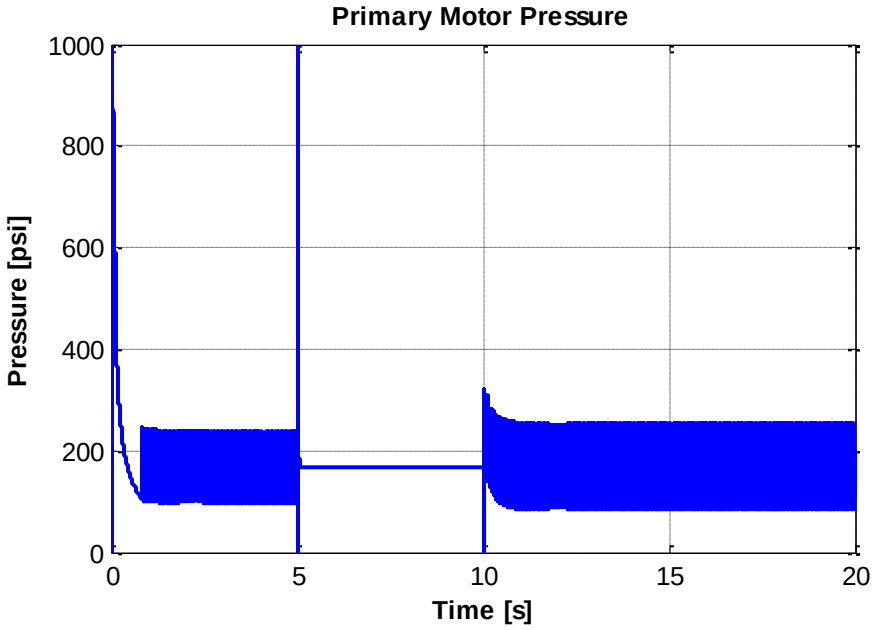

Figure 8.22 Primary motor differential pressure

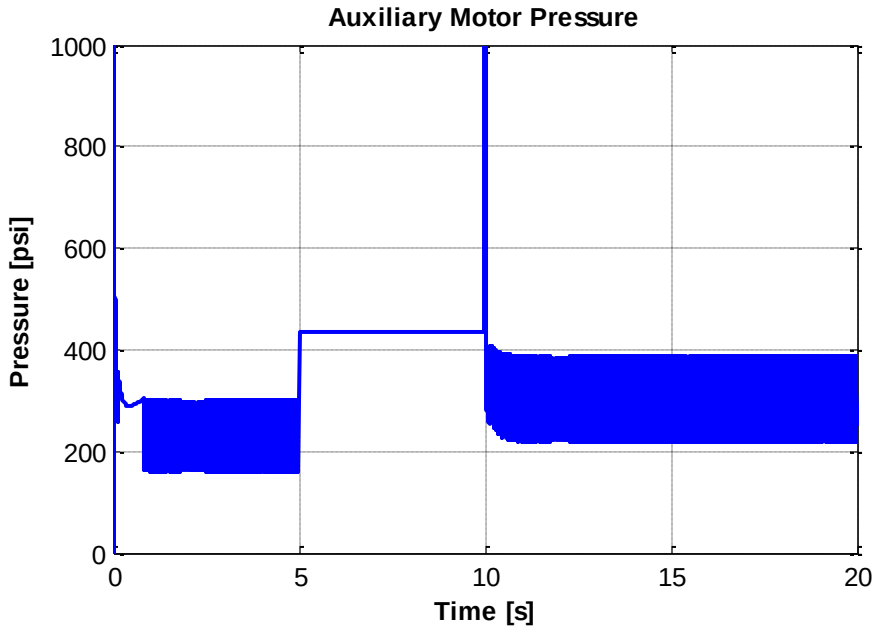

Figure 8.23 Auxiliary motor/pump differential pressure

A constant primary motor angular velocity of 1000 rpm is used as a reference for both the rate limit controller of the proportional valve, and the PI controller for battery current controller. Figure 8.11 illustrates the angular velocity profile which is supplied to the hydraulic transmission system. The angular velocity profile is used to determine the system operating modes both at low wind and at high wind. Initially, a 400 rpm step angular velocity is supplied to the hydraulic pump which simulates the high wind condition. The pump angular velocity is reduced to 100 rpm after 5 seconds to simulate the low wind condition. Then, the angular velocity is increased to 600 rpm to restore the high wind condition at t = 10 sec. According to the hydraulic wind energy transfer configuration (High wind or Low wind), the associated controller generates a control command to maintain the tracking of the reference angular velocity. The transmission system switches between these two configurations based on the wind speed.

Figure 8.12 displays the flow passing through the main pump when the angular velocity profile of Figure 8.11 is applied. According to this figure, the wind speed is initially high enough to maintain the reference primary motor angular velocity, and the pump flow is distributed between the primary and auxiliary motors through the proportional valve. The wind speed drops after 5 seconds and the system switches to the low wind configuration, at which the main pump flow is augmented with the auxiliary pump flow. The high wind conditions will occur in 5 seconds from this event.

Figures 8.13 and 8.14 show the primary motor and auxiliary motor flows. According to these figures, the rate limit controller initially controlled the system flow distribution by regulating the proportional valve position. In this configuration, the auxiliary motor captured the excess flow energy and stored it in a battery though the electric generator. At low wind condition, the PI control regulated the current from the battery and ran the electric motor to compensate for the main pump flow and maintain the reference velocity. According to Figure 12, since the motor angular velocity was proportional to the flow, the controller maintained the fluid flow at a certain rate to maintain the reference velocity. The system switching between these configurations resulted in an instantaneous variation in the system shown as spikes at time 5 and 10 seconds.

Figures 8.14 and 8.15 illustrate the angular velocities of the primary motor and the auxiliary motor/pump. As demonstrated in Figure 8.14, the controller successfully adjusted the valve position at high wind with decremented rate to reduce the flow of main

motor and maintain the required velocity. The simulation results illustrate a rise time of 0.135 sec and an overshoot percentage of 15.2%.

Figure 8.16 illustrates the rate limit control effort to maintain the fluid in the system by regulating the proportional valve position. The controller effort is zero while the system runs in low wind condition between 5 to 10 seconds. The controller effort was either 0.0001 to open the valve or -0.0001 to close the valve. The simulation results demonstrate a high performance system operation.

Figure 8.17 illustrates the position of the proportional valve which was regulated by the rate limit controller. According to the figure, the valve was immediately closed enough from the initial position to reduce the flow of the primary motor at high wind. The valve was completely opened in low wind to direct the entire flow towards the primary motor path and augment with the auxiliary motor flow.

Figure 8.18 illustrates the effort of the PI controller in discharging the battery. The controller effort was zero when the system was in high wind condition. As soon as the wind condition changed to low wind speed, the PI controller adjusted the battery discharge current to maintain the primary motor angular velocity. The charging process was determined by the amount of fluid redirected from the proportional valve to the auxiliary motor. Figure 8.19 shows the battery state of charge variation as the system operation mode changed. As the figure illustrates, the SOC increased in high wind condition. Figure 19 illustrates battery charge/discharge current controlled by the PI. The current is negative during charge cycles and positive when the battery is being discharged.

The figure demonstrates a high performance control of the battery charge and discharge process.

Figures 8.21 to 8.23 display the variation of the differential pressures of the hydraulic components of the system. The pump gauge pressure changes very steady since the input angular velocity of the pump varies very steadily. Nevertheless, the motors gauge pressure constantly fluctuates due to frequent variation of the flow distribution. The pressures only become stable at high wind condition where the auxiliary pump supplies a constant flow to the primary motor.

8.2 Modeling and Control of a Hybrid-Hydraulic Electric Vehicle

Hybrid propulsion systems are ideal candidates for regenerative energy in vehicular technology. A typical hybrid propulsion system has two or more power sources of which at least one can store and reuse energy. The benefits derived from using such a system are superior fuel economy compared to similar conventional vehicles, emission reductions, and fuel cost savings. Moreover, the application of hybrid drivetrains reduces the reliance on fossil fuels [52].

Regenerative braking systems use vehicle's kinetic energy to generate and store electrical energy in a battery in hybrid electric vehicles. However, the principal shortcoming of a regenerative brake system is the necessity to generate and store closely similar electric current to the one generated from the power source [53]. Only a small portion of the vehicle's kinetic energy is recaptured and stored in vehicle battery via regenerative braking [54, 55].

Various configurations of a hydraulic energy storage based hydraulic propulsion system have been investigated in [56]. This section has classified these hydraulic storage system into three categories namely, pure hydrostatic, hydro-mechanical and power assist systems. Another study [57-58] reports 79% improvement of the fuel economy of a hydraulically assisted hybrid vehicle in urban driving.

Although proven reliable, mechanical transmission systems are subject to frictional losses negatively impacting overall vehicle efficiency. Several power transmission techniques are developed to address the friction loss issue. These techniques include a hydraulic hybrid transmission system which is developed by the Artemis Intelligent Power Company [59]. Additionally, variable displacement hydrostatic transmission systems provide a solution to the encountered problem with the losses [60]. These hydraulic transmission systems offer the benefit of a continuously Variable Transmission (CVT), which is the infinite effective gear ratio. These infinite shifting ratios of the power transmission system allow less energy losses and better fuel efficiency in vehicles.

The application of gearless hydraulic power transmission systems has shown promise in wind energy transfer technology [20-24]. Moreover, the elimination of the gearbox from such systems results in increased life span and reduced maintenance cost of the wind turbine towers. Other benefits of this technique include high-energy transfer rate achievement and reduction of the size of the power electronics.

This section integrates the regenerative hybrid vehicle system and gearless hydraulic transmission system to address both energy requirements of a hybrid vehicle and friction energy losses in the mechanical transmission system. A regenerative gearless HEV driveline is introduced through a hydraulically connected power transmission system. A dynamic model of the hydraulic transmission system is created. A rate limit controller is designed to control the displacement of the proportional valve which distributes the flow between the motors, while a PI controller is designed to control the discharge current from the battery to run the auxiliary pump.

8.2.1 Hybrid Hydraulic Transmission System Design

The hydraulic transmission system for HEVs is designed to provide motion by using two main sources of power as range extender Internal Combustion Engine (ICE) and from Battery storage devices. The hydraulic circuit consists of a fixed displacement pump driven by the prime mover (range extender) and two fixed displacement hydraulic motors namely the primary motor and the auxiliary motor [22]. The schematic diagram of a hydraulic transmission system is illustrated in Figure 8.24. A fixed displacement pump is mechanically coupled with the range extender (ICE) and supplies pressurized hydraulic fluid to two fixed displacement hydraulic motors. The main hydraulic motor is coupled with the differential to transfer the power of the hydraulic fluid to wheels, while the auxiliary motor is coupled with a generator to produce electric power and charge the batteries. Flexible high-pressure pipes/hoses provide power transfer path from the source to the wheels. Safety devices such as pressure-relief valves and check valves protect the

system from high pressure. Directional flow valves and proportional valves are used to direct and regulate the fluid in the system both in electric and gasoline configurations.

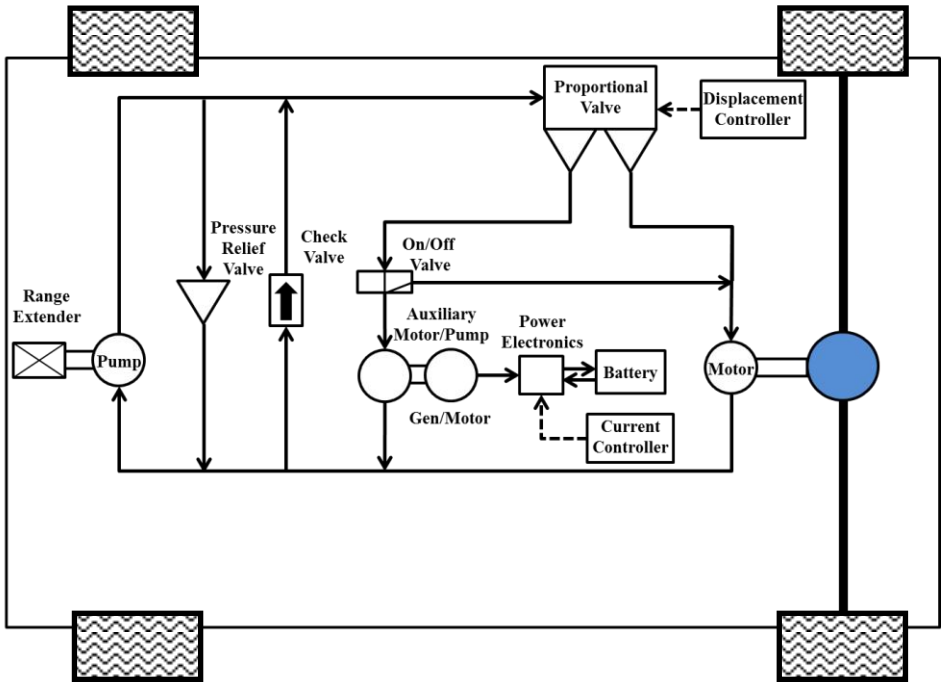

Figure 8.24 Schematic diagram of the gasoline configuration of the transmission system

The vehicle can accelerate as more fluid is provided from the pump. A proportional valve regulates the fluid flow to the motors to maintain the driver speed commands. Therefore it needs to be translated into proper valve position or battery discharge power rating. The storage unit receives the energy of the excess flow captured at the gasoline configuration in form of electric power stored in batteries. The stored energy is released back to the system when the vehicle is running in full electric configuration.

8.2.1.1 Gasoline Configuration

Figure 8.25 depicts the gasoline configuration of the transmission system at a high engine efficiency operating point. When the vehicle is running on gasoline, the main hydraulic pump is coupled to the range extender and high pressurized fluid is directed to the primary motor and auxiliary motor/pump through a proportional valve. The valve position is adjusted such that the driver speed command is maintained at the primary motor. The primary motor drives the wheels, while the auxiliary motor captures the excess flow energy to charge the battery through a generator. The benefit of this technique is to run the ICE at the highest efficiency operating condition.

8.2.1.2 All-electric Configuration

Figure 8.26 displays the full electric configuration of the transmission system. All-electric mode of operation occurs when there is enough energy stored in the battery, or the operation of ICE is not efficient due to the driver's specific speed request. When the vehicle is running in all-electric mode, the proportional valve is closed to exclude the main pump from the hydraulic circuit. Instead, the auxiliary motor/pump is driven by the battery to directly drive the primary motor to run the wheels. The current extracted from the battery is regulated such that the driver speed command is tracked by the primary motor.

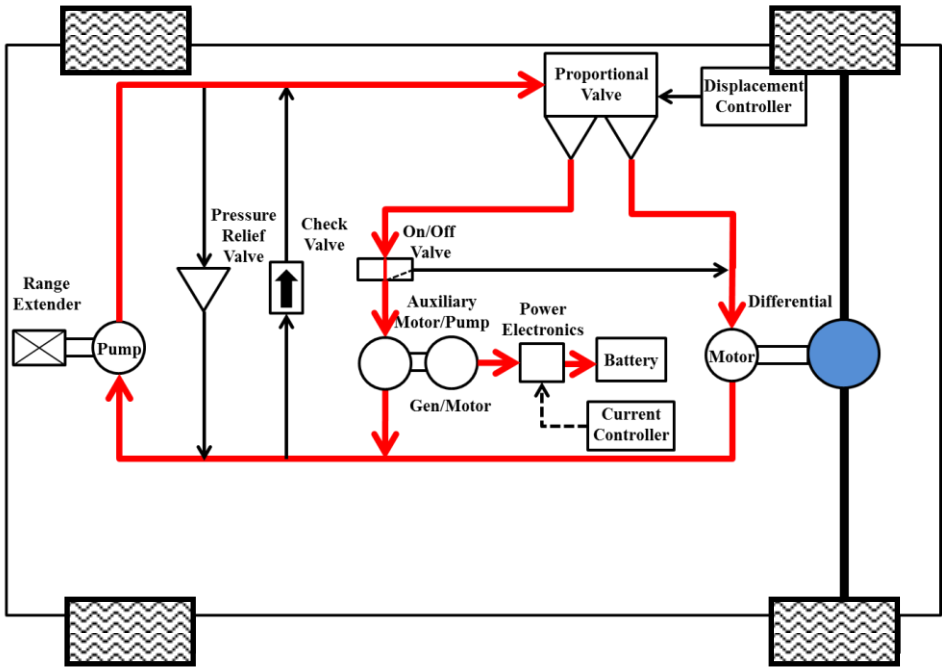

Figure 8.25 Schematic diagram of the gearless power transmission system with the storage unit

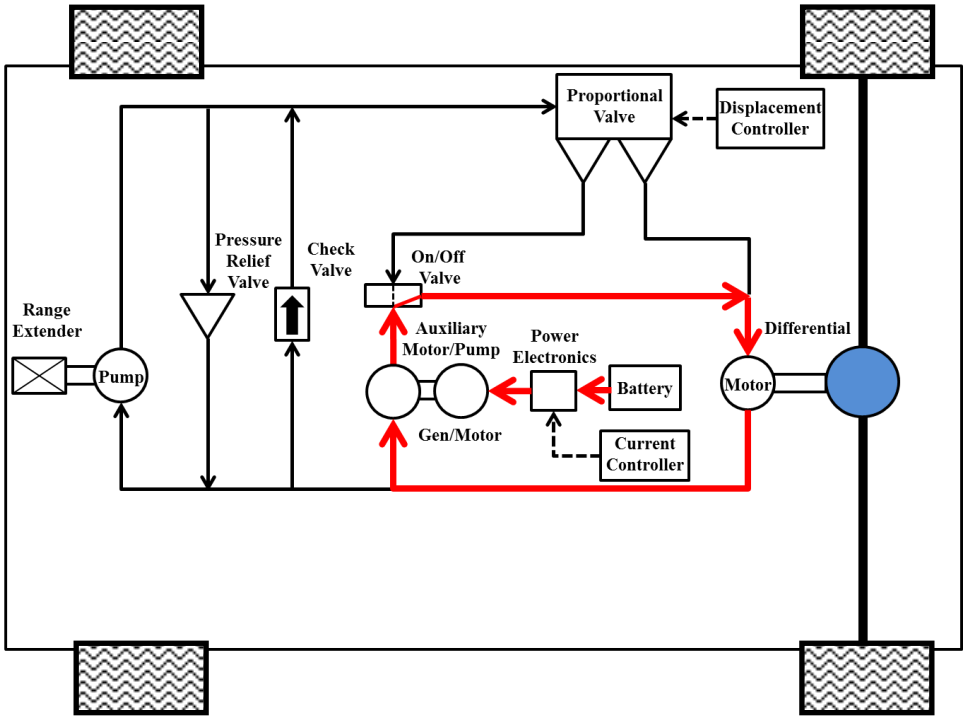

Figure 8.26 Schematic diagram of the full electric configuration of the transmission system

8.2.2 System Operation and Dynamic Model

This section introduces the dynamic model of the hydraulic transmission system. The overall hydraulic model is similar to the one which is displayed in Chapter 3. The battery model is similar to Section 8.1.1.3. Subsequently, the models of the gasoline configuration and all-electric configuration are represented.

8.2.2.1 Gasoline Configuration

In this configuration, the vehicle is driven by the range extender at high engine efficiency. The overall hydraulic system can be connected as modules to represent the dynamic behavior. Block diagrams of the hydraulic transmission system using MATLAB Simulink are demonstrated in Figures 8.27 and 8.28. The model incorporates the mathematical governing equations of individual hydraulic circuit components. The bulk modulus unit generates the operating pressure of the system.

Figure 8.27 depicts a block diagram of the vehicle transmission system in the gasoline configuration. According to the figure, the range extender supplies power at a specific angular velocity to the main hydraulic pump. The hydraulic pump supplies pressurized hydraulic fluid to the proportional valve. The valve distributes the hydraulic fluid between the motors based on the driver speed command. The auxiliary motor captures the surplus energy of the flow. The auxiliary motor runs the electric generator which is coupled with and the generator converts the mechanical energy of the hydraulic fluid to electrical energy. The generated electrical energy is stored in a battery through

the power electronics. The primary motor is coupled with the differential and runs the wheels.

Figure 8.28 displays the mathematical model of every hydraulic component in the transmission system. The flows and pressures are calculated for every hydraulic component. The data from the hydraulic circuit is utilized to calculate the flow of energy into the battery.

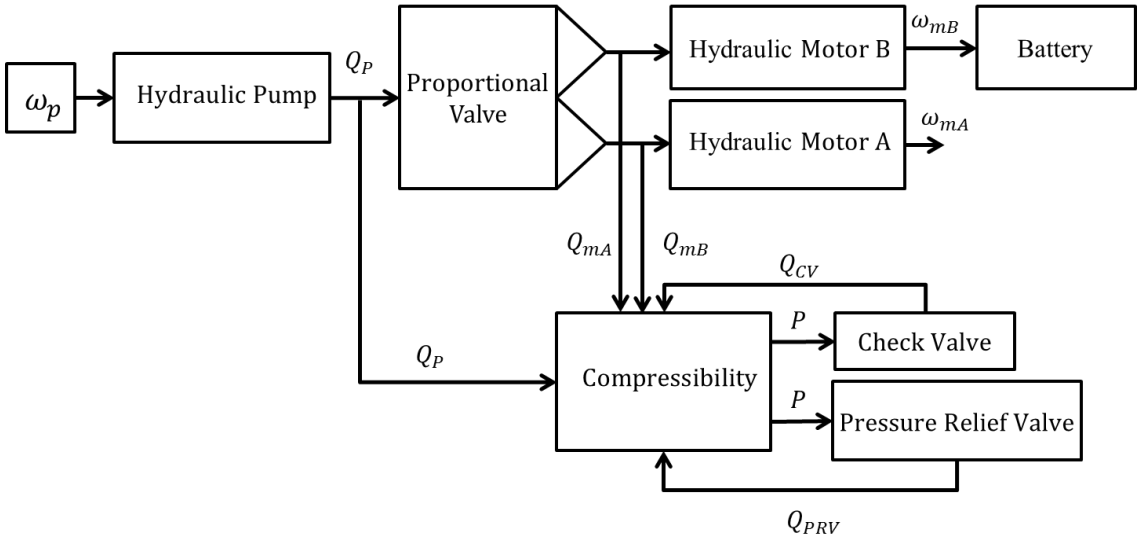

Figure 8.27 Hydraulic transmission schematic diagram in gasoline configuration

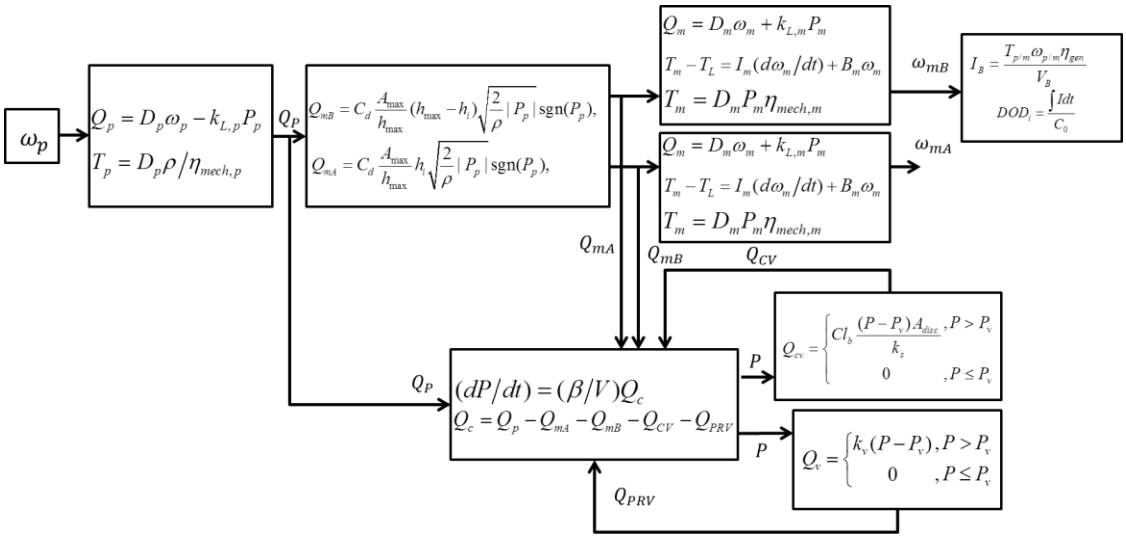

Figure 8.28 Simulink model of the hydraulic transmission system in gasoline configuration

8.2.2.2 All-electric Configuration

The model of the electric configuration is represented similar to the gasoline configuration. In this configuration, the vehicle is driven by the battery at low engine efficiency. The current extracted from the battery is regulated to accommodate the driver speed demand. The current is supplied to the electric motor which is coupled with the auxiliary pump. The auxiliary motor can be driven as pump by the electric motor and flows pressurized fluid which is directed to the primary hydraulic motor. The compressibility block calculates the gauge pressure along the auxiliary pump and hydraulic motor terminals. The primary motor is coupled with the differential and runs the wheels. Figure 8.29 and 8.30 show the block diagram of the mathematical model of the hydraulic transmission in all-electric configuration.

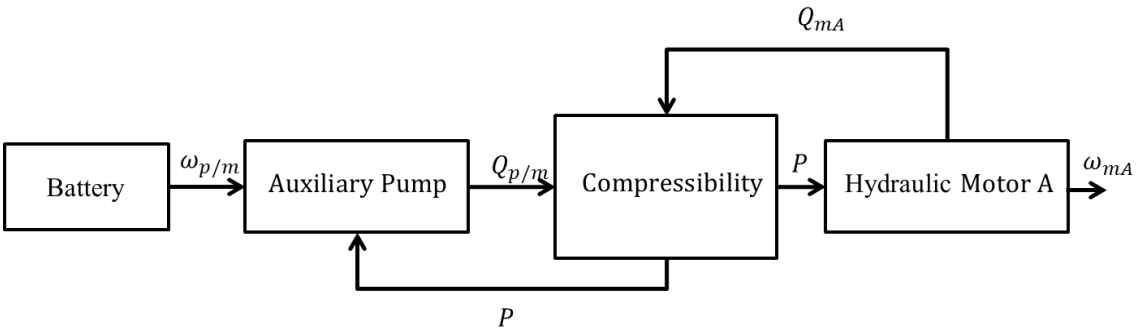

Figure 8.29 Hydraulic transmission schematic diagram in electric configuration

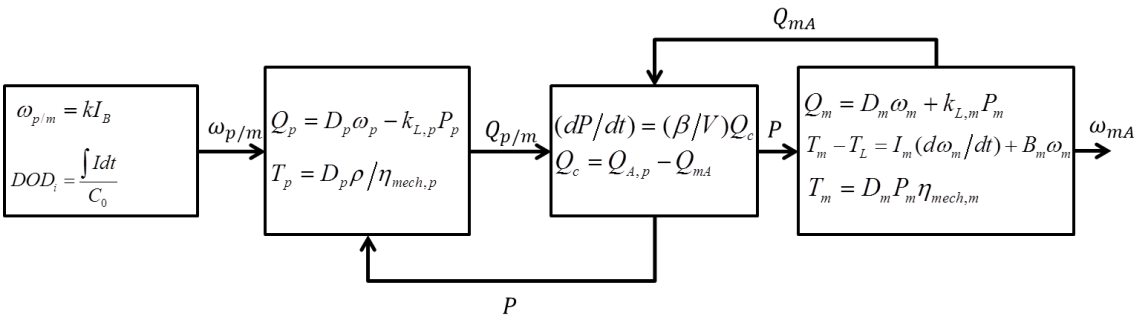

Figure 8.30 Simulink model of the hydraulic transmission system in electric configuration

8.2.3 Controller Design

This section introduces the design of the controllers which are required to accommodate the driver speed command during both gasoline and all-electrical configurations. A (RL) controller regulates the position of the proportional valve in the gasoline configuration to maintain tracking of the driver speed command. A PI controller is also designed and implemented to regulate the battery charge/discharge current in the all-electric mode to maintain driver velocity command tracking.

8.2.3.1 Rate Limit Controller Design

The RL controller directs the flow of the hydraulic fluid to the main hydraulic motor. The controller adjusts the position of the valve towards the primary motor path to maintain tracking of the driver velocity command. Figure 8.31 represents the diagram of the RL controller.

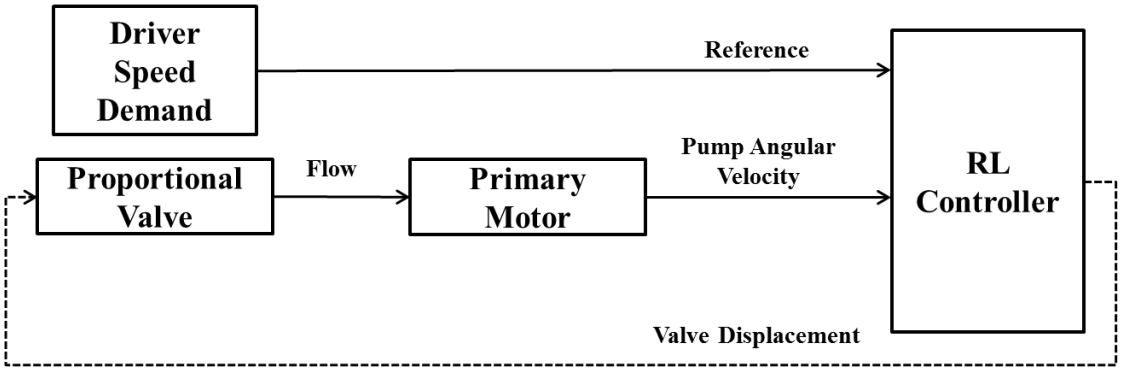

Figure 8.31 The diagram of the RL control closed loop system

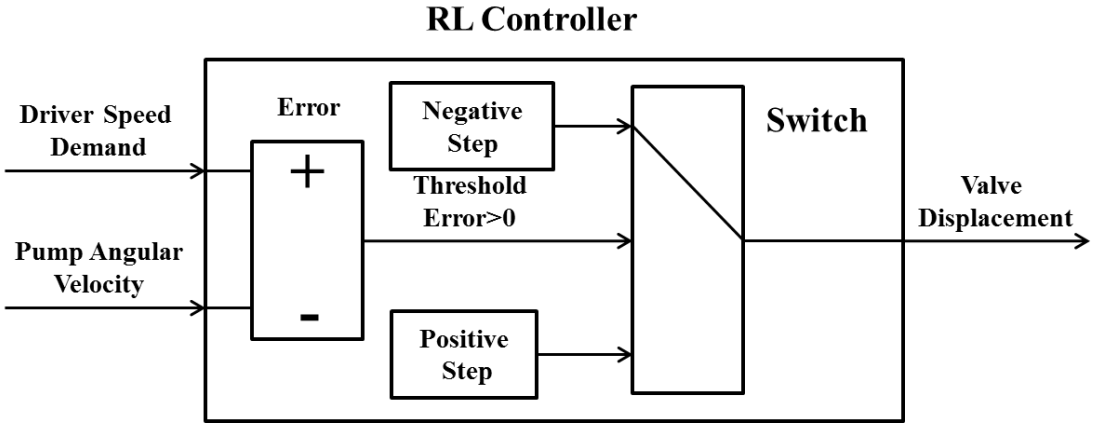

Figure 8.32 The RL controller structure

In the gasoline ICE configuration, the RL controller estimates the error between the reference angular velocity and primary pump angular velocity. If the error value is

positive, then the controller sends a negative displacement step signal to the valve, to further close the valve to track the reference velocity. If the error value is negative, the controller opens the valve by sending a positive step displacement signals to the valve. The excess flow is directed to the auxiliary motor and the flow energy is captured. The electric generator which is coupled with the motor transforms the mechanical energy into electrical energy and stores it in the battery. Figure 8.32 shows the structure of the RL controller. The step values are designed to maintain system stability while both fast response and error mitigation criteria are fulfilled.

8.2.3.2 PI Controller Design

The RL controller is excluded from the control system when the powertrain system switches to all-electric configuration. In this case a PI controller regulates the system operation such as the angular velocity of the auxiliary pump. The reference command for this controller is generated by driver as velocity demand. The PI controller regulates the amount of battery discharge current to run the electric motor/generator coupled with the auxiliary pump. Figure 8.33 represents the diagram of the PI control system.

The proportional gain adjusts the response time characteristics such as settling time and rise time. At higher proportional gains (within the region of stability) a faster system response is obtained. A proper integral gain mitigates the steady state tracking error.

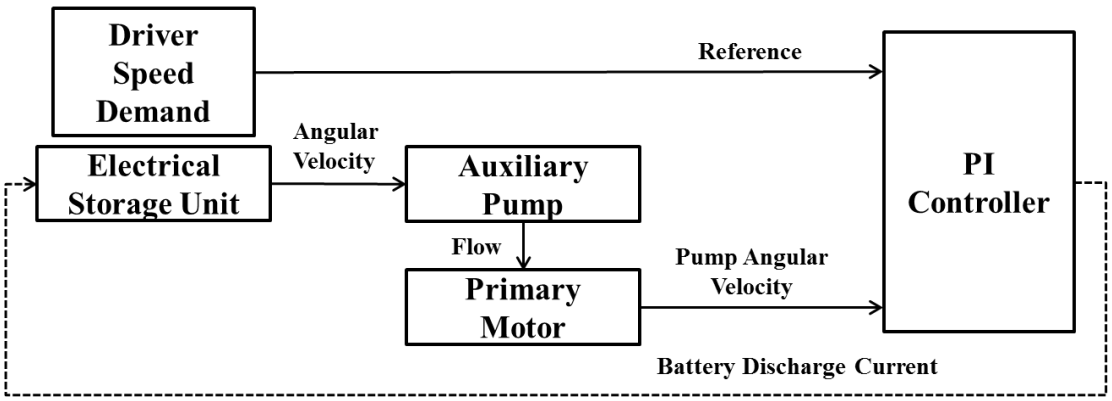

Figure 8.33 The diagram of the PI control closed loop system

8.2.4 Simulation Results and Discussions

In this section, the mathematical model of the hydraulic transmission behavior is simulated and the effectiveness of the control system is evaluated. The simulation parameters are listed in Table 8.2.

Figure 8.34 illustrates the FTP-75 driving cycle which is used as the driver speed demand reference for both RL controller of the hydraulic proportional valve, and the PI battery power management controller. The angular FTP-75 driving cycle is used to determine the system operating modes. According to the vehicle operating configuration (Gasoline or Electric), the associated controller (RL or PI) generates a control command to maintain the tracking of the reference angular velocity. The vehicle switches between these two configurations based on the ICE efficiency threshold which is correlated with the vehicle speed. In general, ICE engines are very inefficient in lower speeds; hence, the system is all-electric if the engine efficiency drops below a certain efficiency threshold. The engine is turned off under this configuration. If the engine efficiency exceeds the threshold, the vehicle switches to gasoline ICE configuration. The efficiency threshold is

adjusted to the point at which the vehicle speed is 20 Mph. Figures 8.34 to 8.45 illustrate the simulation results of the hybrid-hydraulic electric vehicle.

Table 8.2 Simulation parameters for the Hybrid-Hydraulic Electric Vehicle model

Symbol	Quantity	Value	Unit
D_p	Pump Displacement	0.517	in^3/rev
D_{mA}	Primary Motor Displacement	0.097	in^3/rev
D_{mB}	Auxiliary Motor/Pump Displacement	0.097	in^3/rev
I_{mA}	Primary Motor Inertia	0.0014	$kg.m^2$
I_{mB}	Auxiliary Motor Inertia	0.0014	$kg.m^2$
B_{mA}	Primary Motor Damping	0.0026	N.m/(rad/s)
B_{mB}	Auxiliary motor Damping	0.0022	N.m/(rad/s)
$K_{L,p}$	Pump Leakage Coefficient	0.17	
$K_{L,mA}$	Primary Motor Pump Leakage Coefficient	0.1	
$K_{L,mB}$	Auxiliary Motor Pump Leakage Coefficient	0.001	
η_{total}	Pump/Motor Total Efficiency	0.90	
η_{vol}	Pump/Motor Volumetric Efficiency	0.95	
η_{gen}	Generator Efficiency	0.95	
β	Fluid Bulk Modulus	183695	psi
ρ	Fluid Density	0.0305	lb/in^3
υ	Fluid Viscosity	7.12831	cSt
k	Current Coefficient	10	
V_B	Battery Voltage	12	Volts
C_0	Initial Battery Capacity	31.25	Amp.hr
SOC_0	Initial State of Charge	50	%
	RLS Controller Step Size	0.0001	In
k_p	Proportional Gain	0.001	
k_i	Integral Gain	5	
	Vehicle Speed Threshold	20	Mph

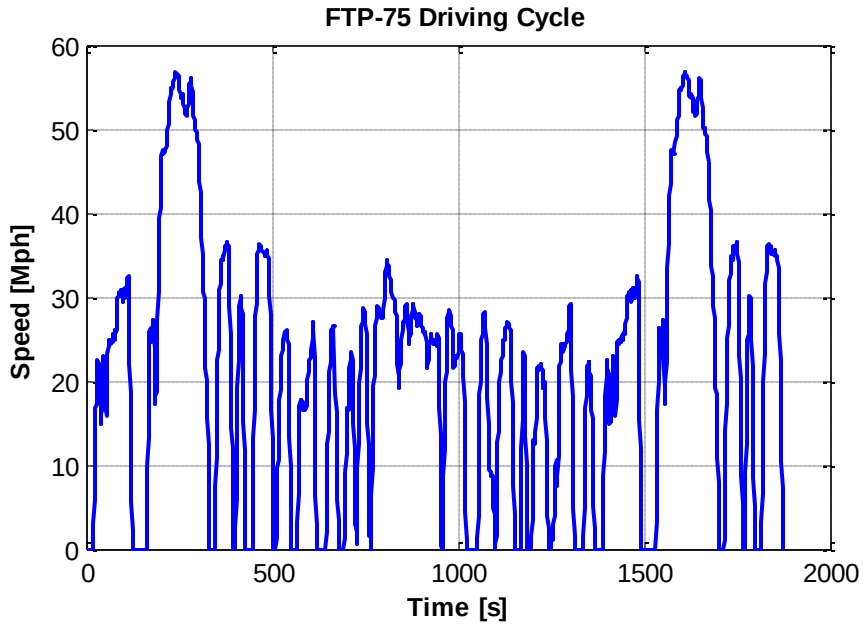

Figure 8.34 Driver angular velocity demand profile

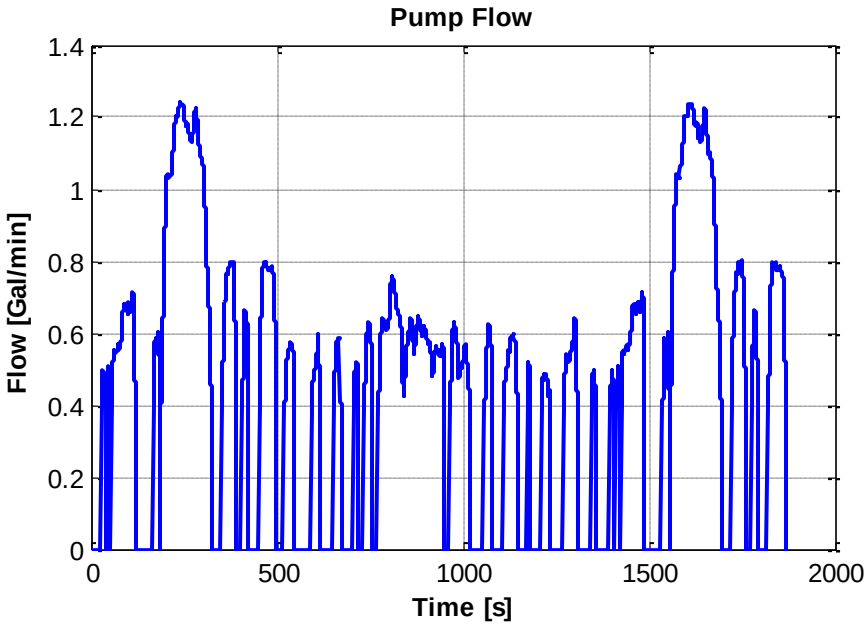

Figure 8.35 Hydraulic transmission system flow generated from main pump

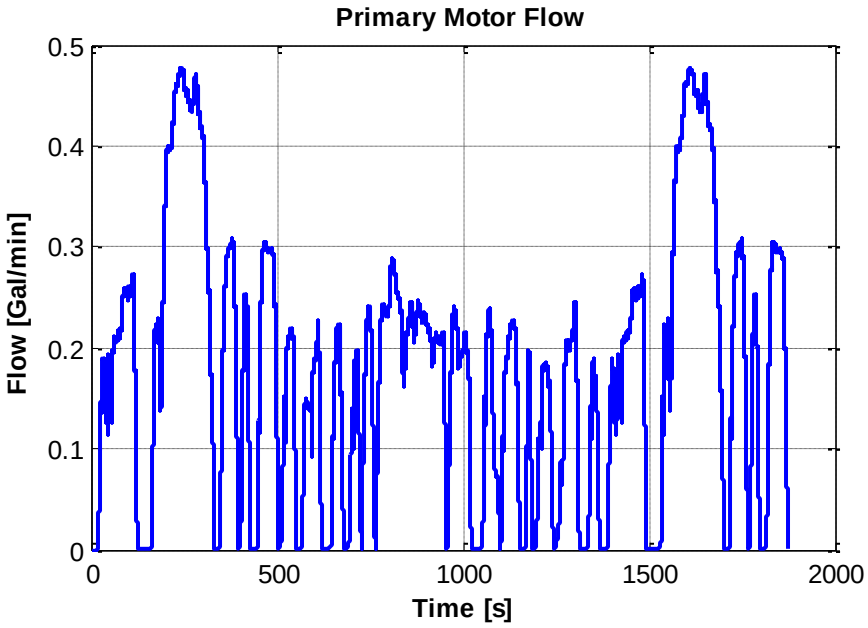

Figure 8.36 Hydraulic transmission system primary motor flow

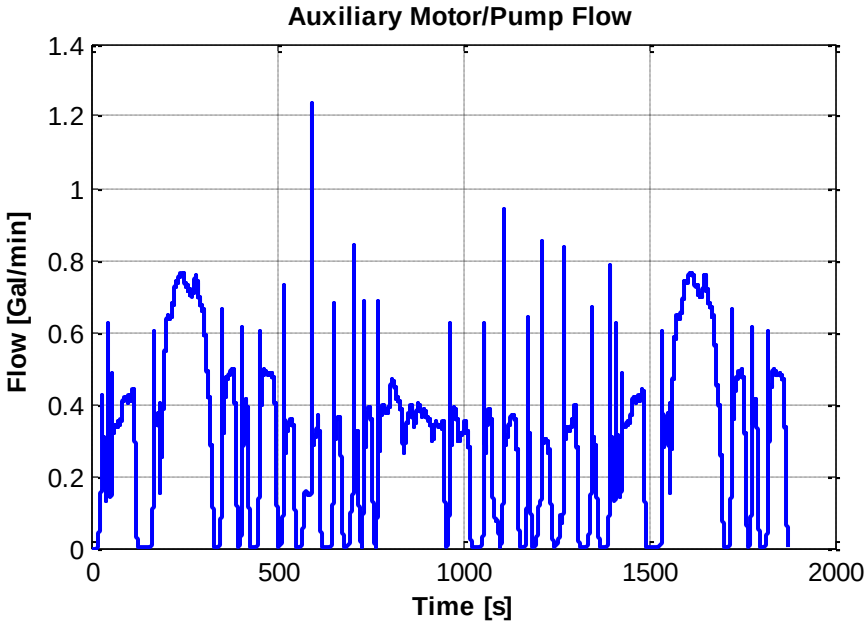

Figure 8.37 Hydraulic transmission system auxiliary motor flow

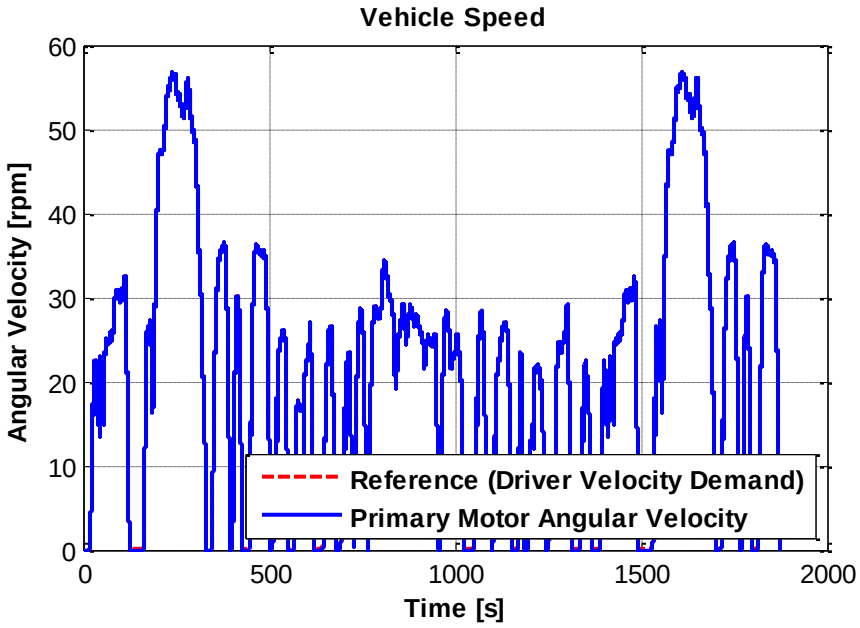

Figure 8.38 Comparison of the primary motor angular velocity and the driver speed demand

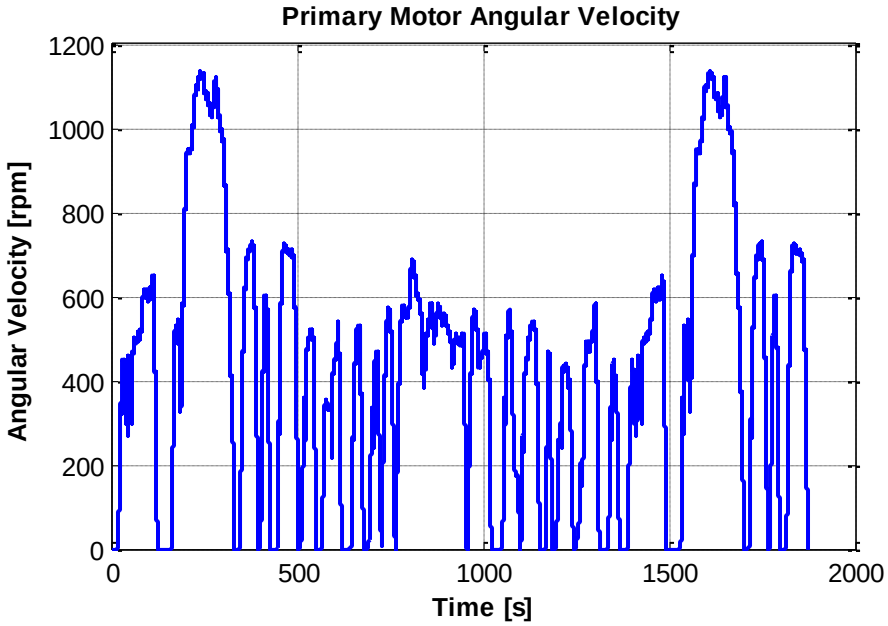

Figure 8.39 Hydraulic transmission primary motor angular velocity

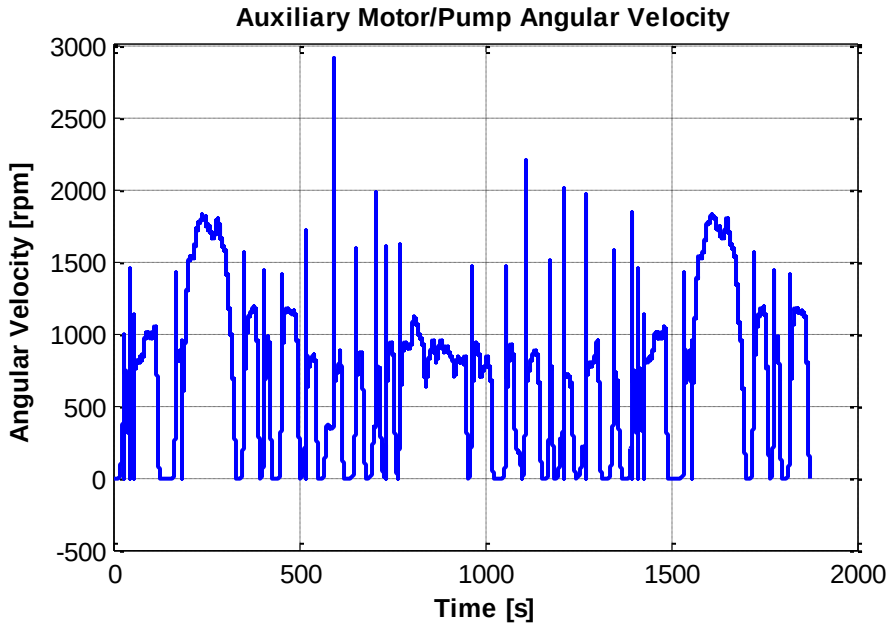

Figure 8.40 Hydraulic Transmission Auxiliary motor/pump angular velocity

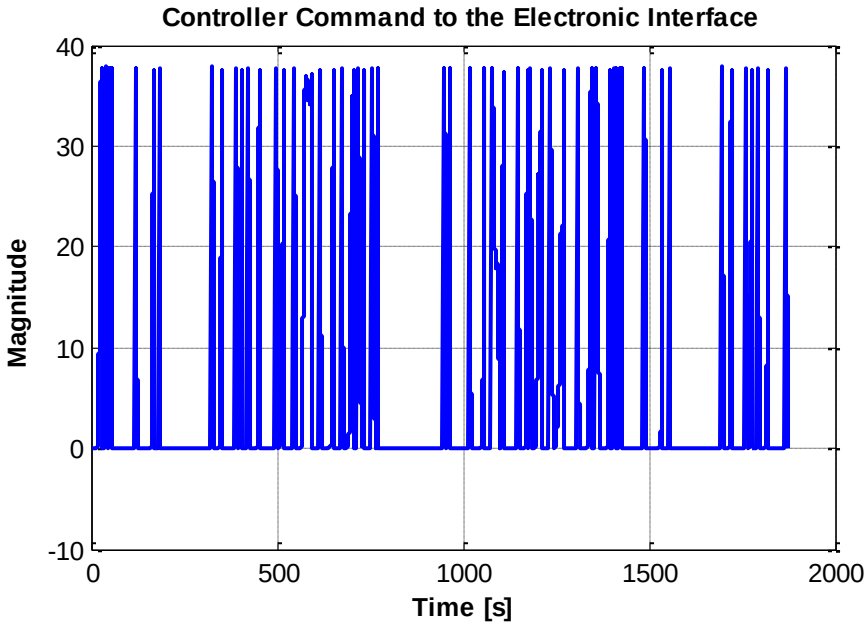

Figure 8.41 Control effort of the PI controller

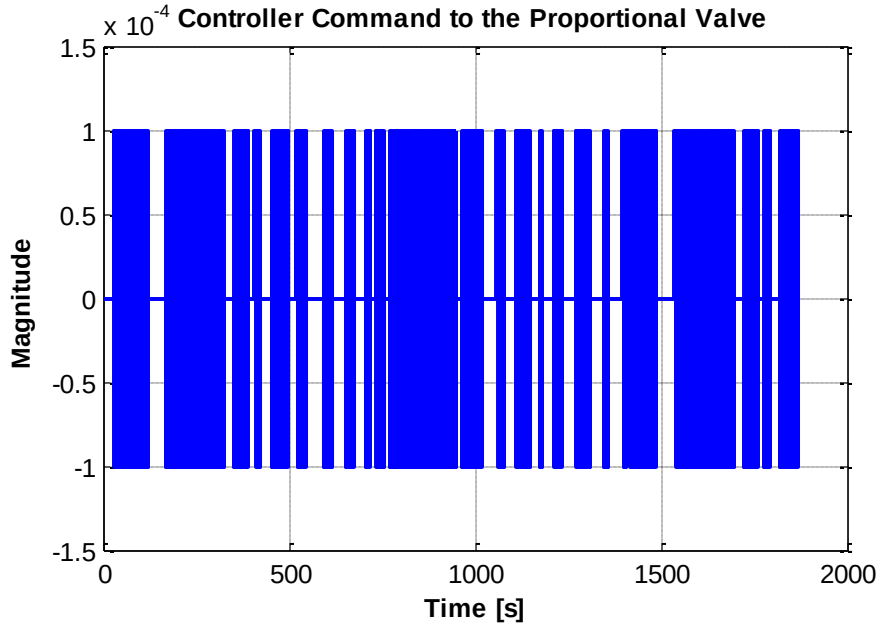

Figure 8.42 Control effort of the RL controller

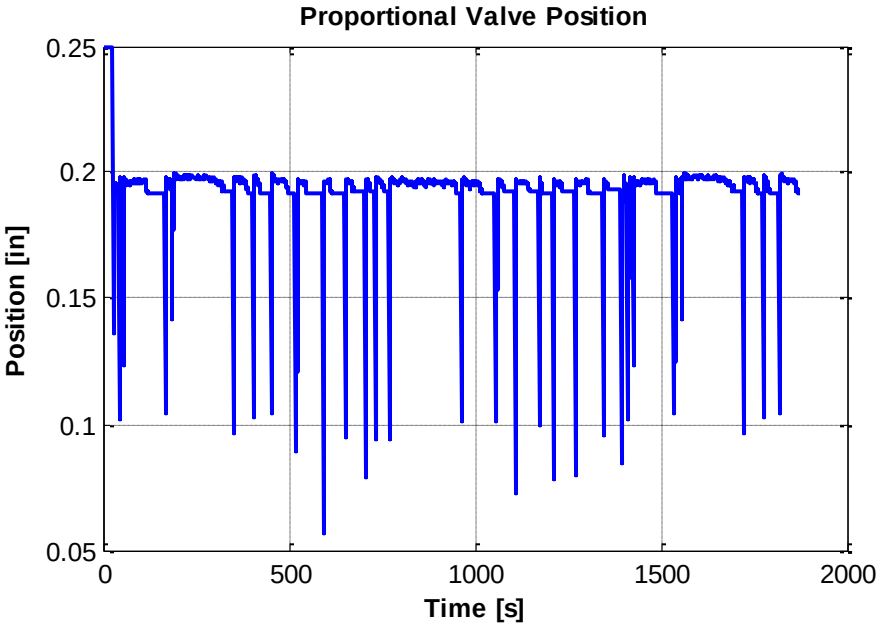

Figure 8.43 Proportional Valve position regulation by the RL controller

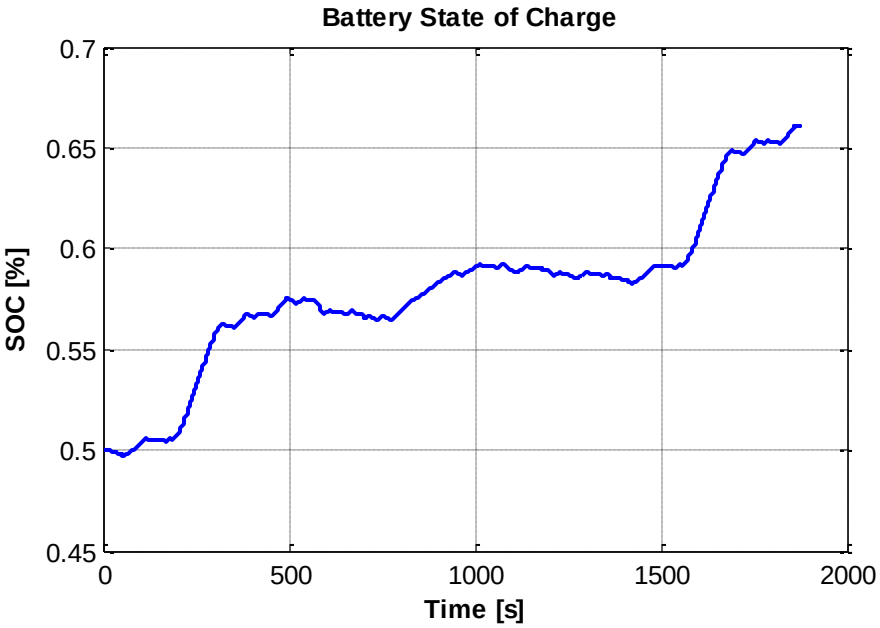

Figure 8.44 Hydraulic transmission battery charge/discharge current

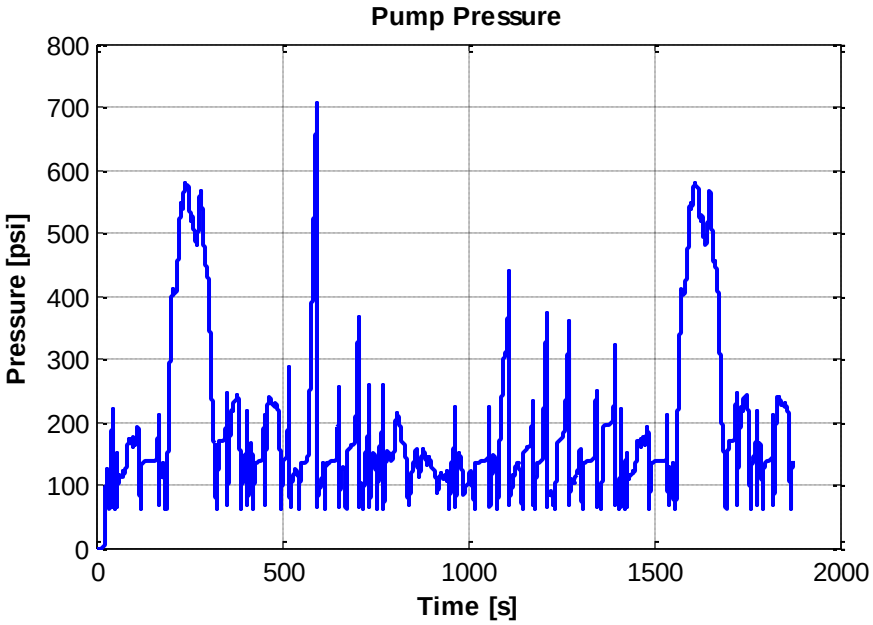

Figure 8.45 Pump differential pressure

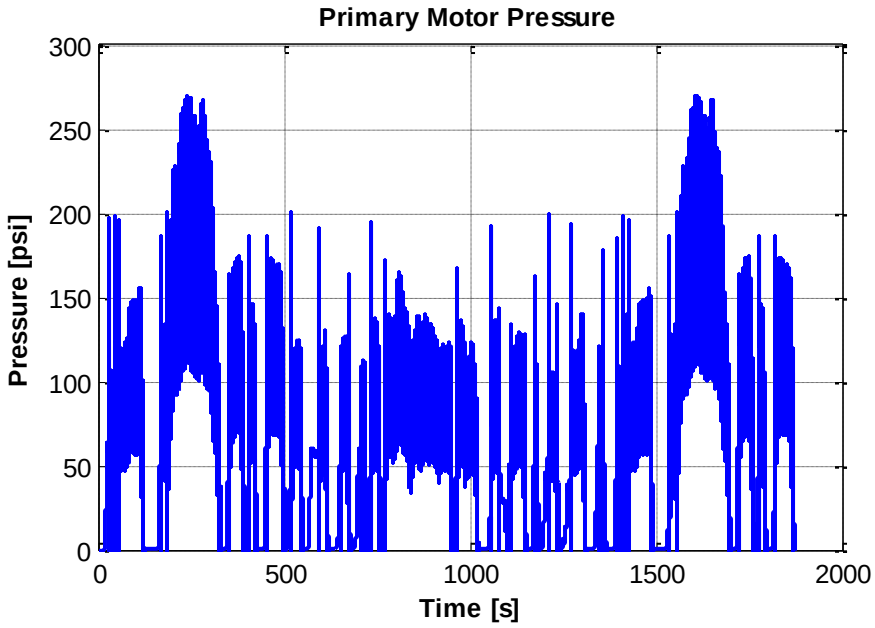

Figure 8.46 Primary motor differential pressure

Figure 8.35 displays the flow passing through the main pump when the FTP-75 driving cycle of Figure 8.34 is applied. According to this figure, when the vehicle speed is lower than 20 Mph, the engine was shut down and the main pump was excluded from the hydraulic circuit. When the engine efficiency exceeded a threshold value, the system switched to ICE gasoline configuration. Consequently, the main pump started circulating the hydraulic flow in the system. Occasionally, in vehicle deceleration, the engine efficiency fell below the target efficiency and the pump was bypassed to run in all-electric mode.

Figures 8.36 and 8.37 show the primary motor flow and auxiliary motor flow. According to these figures, the sum of the hydraulic motor flows equals the pump flow in gasoline configuration. In electric configuration, the auxiliary pump provides the required flow to track the driver speed demand solitary, consequently the primary motor and

auxiliary pump have similar flow values. The peaks in Figure 8.37 denote the vehicle stop and go situations at which the vehicle runs in electric configuration. As soon as the vehicle begins accelerating from the full stop condition, the PI discharge current controller sends an instantaneous discharge command to accelerate the vehicle to the driver speed demand.

Figure 8.38 depicts the FTP-75 driving cycle tracking. The figure demonstrates close tracking of the reference speed demand in both high engine efficiency conditions at which the RL controller regulated the 3-way proportional valve position, and low engine efficiency conditions where the PI controller adjusts the energy released from the battery .

Figures 8.39 and 8.40 illustrate the angular velocities of the primary motor and the auxiliary motor/pump. Since the hydraulic motors have equal displacements, they both have similar output angular velocity values while running in full electric mode. The auxiliary motor received more fluid in gasoline ICE configuration depending on the driver demand. Figure 3.40 shows a spike at the switching time from ICE to all-electric configurations. This was generated as a result of operating system initial conditions.

Figure 8.41 illustrates the PI control effort to maintain the fluid in the system by discharging the battery. The controller effort was zero while the vehicle was running in the gasoline configuration. Otherwise, the controller adjusts the battery discharge current to address driver speed demand.

Figure 8.42 illustrates the effort of the RL controller. The controller effort was zero when the vehicle was running in all-electric mode. As soon as the powertrain

switched to gasoline configuration, the RL controller adjusted the displacement of the valve by generating incremental positive and negative valve displacement steps to regulate the flow directed from the proportional valve to the hydraulic motors. The simulation results demonstrated the high performance system operation.

Figure 8.43 depicts the valve position regulation by the RL controller. The valve was excluded from the hydraulic circuit in all-electric configuration. In gasoline configuration the valve position was regulated to track the driver velocity command. The spikes in the figure denote the stopping point of the vehicle where the transferred energy to the primary motor was minimized to decelerate the vehicle.

Figure 8.44 shows the battery state of charge variation as the vehicle operation modes change. As the figure illustrates, the SOC increased when the ICE was running in the proposed driving cycle of Figure 8.34 and the battery was discharged while running in electric configuration. Figures 8.45 and 8.46 display the differential pressure of the main pump and the gauge pressure of the primary motor.

LIST OF REFERENCES

LIST OF REFERENCES

[1] T. Senjyu, R. Sakamoto, N. Urasaki, H. Higa, K. Uezato, and T. Funabashi, "Output Power Control of Wind Turbine Generator by Pitch Angle Control Using Minimum Variance Control," *Electrical Engineering in Japan*, vol. 154, no. 2, 2006.

[2] J. G. Slootweg, H. Polinder, and W. L. Kling "Dynamic Modelling of a Wind Turbine with Doubly Fed Induction Generator," *IEEE Power Engineering Society Summer Meeting*, 2001.

[3] J. G. Slootweg, S. W. H. de Haan, H. Polinder, and W. L. Klimg, "General Model for Representing Variable Speed Wind Turbine in Power System Dynamics Simulations," *IEEE Transaction on Power Systems*, vol. 183, no. 1, February 2003.

[4] Y. Lei, A. Mullane, G. Lightbody, and R. Yacamini, "Modeling of Wind Turbine with a Doubly Fed Induction Generator for Grid Integration Studies," *IEEE Transaction on Energy Conservation*, vol. 21, no. 1, March 2006.

[5] "Wind Energy by 2030 – Increasing Wind Energy's Contribution to U.S. Electricity Supply," *U.S. Department of Energy*, May 2008.

[6] http://www.awea.org/pubs/factsheets/Market_Update.pdf. Last Accessed April 2012.

[7] S. Eriksson, H. Bernhoff, and M. Leijon, "Evaluation of Different Turbine Concepts for Wind Power," *Renewable and Sustainable Energy Reviews*, vol. 12, issue 5, pp. 1419-1434, June 2008.

[8] A. Ragheb and M. Ragheb, "Wind Turbine Gearbox Technologies," *Proceedings of the 1st International Nuclear and Renewable Energy Conference (INREC10)*, Amman, Jordan, March 2010.

[9] K. Dasgupta, "Analysis of a Hydrostatic Transmission System Using Low Speed High Torque Motor," *Mechanism and Machine Theory*, vol. 35, pp. 1481-1499, Oct 2000.

[10] http://www.acadianahydraulic.com/apage/63976.php. Last Accessed April 2012.

[11] G. A. Sohl and J. E. Bobrow, "Experiments and Simulations on the Nonlinear Control of a Hydraulic Servosystem," *IEEE Transactions on Control Systems Technology*, vol. 7, pp. 238-247, Mar 1999.

[12] S. Habibi and A. Goldenberg, "Design of a New High-Performance Electrohydraulic Actuator," *IEEE-Asme Transactions on Mechatronics*, vol. 5, pp. 158-164, Jun 2000.

[13] S. G. Kim, J. H. Kim, and W. S. Lee, "Hydraulic System Design and Vehicle Dynamic Modeling for Development of a Tire Roller," *International Journal of Control, Automation, and Systems*, vol. 1, no. 4, Dec 2003.

[14] Z. Jedrzykiewicz, J. Pluta, and J. Stojek, "Application of the MATLAB – Simulink Package in the Simulation Tests on Hydrostatic Systems," *Acta Montanistica*, vol. 1, pp. 29-36, 1998.

[15] B. Ji-Zhong, X. Ai-Guo, Y. Xin-Hua, and Z. Li-Kun, "Simulation Model of Hydraulic Turbine Speed Control System and Its Parameters Identification Based on Resilient Adaptive Particle Swarm Optimization Algorithm," *Power and Energy Engineering Conference (APPEEC)*, pp. 1-4, March 2010.

[16] K. Wu, et al., "Modelling and Identification of a Hydrostatic Transmission Hardware-in-the-Loop Simulator," *International Journal of Vehicle Design*, vol. 34, pp. 52-64, 2004.

[17] R. Zhang and A. Alleyne, "A Model Reference Load Controller with Adaptation Using a Two Stage Pressure Relief Valve," *in Plastics*, 2nd ed. vol. 3, J. Peters, Ed. New York: McGraw-Hill, 1964, pp. 15–64.

[18] S. Habibi and A. Goldenberg, "Design of a New High Performance ElectroHydraulic Actuator," *Proceedings of the 1999 IEEE/ASME International conference on Advanced Intelligent Mechatronics*, September 19-23, 1999, Atlanta, USA.

[19] A. V. Akkaya, "Effect of Bulk Modulus on Performance of a Hydrostatic Transmission Control System," *Sadhana*, vol. 31, Part. 5, October 2006, pp. 543-556.

[20] S. Hamzehlouia, A. Izadian, A. Pusha, and S. Anwar, "Controls of Hydraulic Wind Power Transfer," *IECON 2011 37th Annual Conference of the IEEE Industrtial Electronics Society*, pp. 2475-2480, 2011.

[21] A. Pusha, A. Izadian, S. Hamzehlouia, N. Girrens, and S. Anwar, "Modeling of Gearless Wind Power Transfer," *IECON 2011 37th Annual Conference of the IEEE Industrtial Electronics Society*, pp. 3176-3179, 2011.

[22] A. Izadian, "Central Wind Turbine Power Generation," US Patent Application, US2010/061972.

[23] S. Hamzehlouia and A. Izadian, "Modeling of Hydraulic Wind Power Transfers," *PECI 2012*.

[24] S. Hamzehlouia and A. Izadian, "State-Space Representation of a Hydraulic Wind Power Transfer," *EIT 2012*.

[25] S. Gao and N. Zhang "A Review of Different Methodologies for Solving the Problem of Wind Power's Fluctuation*," International Conference on Sustainable Power Generation and Supply (SUPERGEN '09),* pp. 1-5, 2009.

[26] G. C. Carrilo, A. E. Feijoo, J. Cidras, and J. Gonzalez, "Power Fluctuation in an Isolated Wind Plant," *IEEE Transaction on Energy Conversion*, vol. 19, no. 1, March 2004.

[27] P. Sorensen, N. A. Cutululis, A. V. Rodriguez, L. E. Jensen, J. Hjerrild, M. H. Donovan, and H. Madsen, "Power Fluctuations from Large Wind Farms," *IEEE Transaction on Power Systems*, vol. 22, no. 3, August 2007.

[28] B. Ji-zhong, X. Ai-guo, Y. Xin-hua, and Z. Li-kun, "Simulation Model of Hydraulic Speed Control System and Its Parameters Identification Based on Resilient Adaptive Particle Swarm Optimization Algorithm," *Power and Energy Engineering Conference (APPEEX)*, Asia-Pacific, pp. 1-4, March 2010.

[29] M. R. Sirouspour and S. E. Salcudean, "On the Nonlinear Control of Hydraulic Servo-Systems." *Proceedings of the 2000 IEEE International Conference on Robotics & Automation*, San Francisco, pp. 1276-1282, April 2000.

[30] P. H. Chang and S-J Lee, "A Straight-line Motion Tracking Control of Hydraulic Excavator System," *Journal of Mechatronics*, vol. 12, pp. 119-138, 2002.

[31] K. Hulhatala, "Modeling of a Hydrostatic Transmission – Steady-State, Linear, and Non-Linear Models," *Acta Polytechnica Scandinavica,* no. 123, pp. 9-101, 1996.

[32] F. P. Wijnheijmer, "Modeling and Hydraulic Servo System," Master's Thesis, Eindhoven Technical University, 2005.

[33] M. F. Rahmat, M. Rozali, N. A. Wahab, Zulfatman, and K. Jusoff, "Modeling and Controller Design of an Electro-Hydraulic Actuator System," *American Journal of Applied Science*, vol. 7, issue 8, pp. 1100-1108, 2010.

[34] M. V. Gorbeshko. "Development of Mathematical Models for the Hydraulic Machinery of Systems Controlling the Moving Components," *Hydrotechnical Constructio,* vol. 3, no. 12. 1997.

[35] http://www.mathworks.com/help/toolbox/physmod/hydro/ref/fixeddisplacementpump.html. Last Accessed April 2012.

[36] http://www.mathworks.com/help/toolbox/physmod/hydro/ref/hydraulicmotor.html. Last Accessed April 2012.

[37] G. Licsko, A. Champneys, and C. Hos, "Dynamical Analysis of a Hydraulic Pressure Relief Valve," *Proceedings of the World Congress on Engineering 2011*, vol. 2, July 1-3, 2009, London, U.K.

[38] A. Pandula and G. Halasz, "Dynamic Model for Simulation of Check Valves in Pipe Systems," *Periodica Polytechnica, Mech. Eng. Series*, vol. 46/2, pp. 91-100, 2002.

[39] Y. Hou, L. Li, P. He, Y. Zhang, and L. Chen, "Shock Absorber Modeling and Simulation Based on Modelica," *Proceedings of the 8th International Modelica Conference*, issue 063, pp. 843-846, March 20-22, 2011.

[40] http://www.mathworks.com/mason/tag/proxy.html?dataid=12968&fileid=63032. Last Accessed April 2012.

[41] K. Ogata, *Modern Control Engineering*, 5th Edition, Prentice Hall, 2010.

[42] A. Esposito, *Fluid Power with Application*, 7th Edition, Prentice Hall, 2009.

[43] S. M. Prabhu, J. Wendlandt, J. Glass, and T. Egel, "Multi-Domain Modeling and Simulation of an Electro-Hydraulic Implement System," *SAE 2006 Commercial Vehicle Engineering Congress and Exhibition*, 2006.

[44] http://www.mathworks.com/help/toolbox/physmod/hydro/ref/fixeddisplacementpump.html. Last Accessed April 2012.

[45] Z. Y. Zhao, M. Tomizuka, and S. Isaka, "Fuzzy Gain Scheduling of PID Controllers," *IEEE Transaction on Systems, Man, and Cybernetics*, vol. 23, no. 5, September/October 1993.

[46] J. Faitli, "Pressure Loss Calculation Model for Well-Graded Solid-23Liquid Pipe Flows on the Basis of Systematic Pilot Plant Investigations," *Intellectual Service for Oil and Gas Industry: Analysis, Solution, Co-Perspectives Proceedings of Ufa State Petroleum Technical University and the University of Miskolc*, Ufa 2000th.

[47] A. Izadian, J. Dawson, and P. Famouri, "Drift Reduction of MEMS Gyroscopes Using an Input-Output Lyapunov Based Adaptive Controller," *American Control Conference*, Seattle, WA, June 2008.

[48] A. Izadian and P. Famouri, "Reliability Enhancement of Micro Comb Resonators under Fault Conditions," *IEEE Transaction on Control System Technology*, vol. 16, no. 4, July 2008, pp 726-734.

[49] A. Izadian, "Automatic Control and Fault Diagnosis of MEMS Lateral Comb Resonators," PhD Dissertation, West Virginia University, College of Engineering and Mineral Resources, 2008.

[50] J. J. E. Slotine and W. Li, *Applied Nonlinear Control*, Upper Saddle River: Prentice Hall, 1991.

[51] P. Ioannou and B. Fidan, *Adaptive Control Tutorial*, Philadelphia, PA: SIAM, 2006.

[52] http://www.afdc.energy.gov/afdc/vehicles/electric_benefits.html. Last Accessed April 2012.

[53] http://engineering.wikia.com/wiki/Regenerative_braking. Last Accessed April 2012.

[54] I. Husain, *Electric and Hybrid Vehicles – Design Fundamentals*, 2nd Edition, CRC Press, 2011

[55] M. Ehsani, Y. Gao, and A. Emadi, *Modern Electric, Hybrid Electric, and Fuel Cell Vehicles – Fundamentals, Theory, and Design*, 2nd Edition, CRC Press, 2010.

[56] L. O. Hewko and T. R. Weber, "Hydraulic Energy Storage Based Hybrid Propulsion System for A Terrestrial Vehicle," *Energy Conversion Engineering Conference*, vol. 4, pp. 99-105, August 1990.

[57] P. Wu, N. Luo, F. J. Fronczak, and N. H. Beachley, "Fuel Economy and Operating Characteristics of a Hydropneumatic Energy Storage Automobile," *SAE* Paper No. 851678, 1985.

[58] S. W. BTollefson, N. H. Beachley, and F. J. Fronczak, "Studies of an Accumulator Energy Storage Automobile Design with a Single Pump/Motor," *SAE* Paper No. 851677, 1985.

[59] http://www.gizmag.com/hydraulic-hybrid-transmission-artemis/11118/. Last Accessed April 2012

[60] http://pigeonsnest.co.uk/stuff/trilink/trilink.html. Last Accessed April 2012.

APPENDICES

Appendix A List of Simulation Parameters

```
clc
close all
clear all

%Pump

Dp=0.517; %(in^3/rev)%Pump_displacement
PVeff=0.95; %Pump_Volumetric_efficiency
PTeff=0.90; %Pump_Total_efficiency
PPnom=3000; %(psi) %Pump_Nominal_pressure
Pwnom=4000; %(rpm) %Pump_Nominal_angular_velocity
Pvisc_nom=5; %(cSt) %Pump_Nominal_kineMotortic_viscosity
w_p=560; %(rpm) %Pump_ref_speed
Rho=844*0.000036127; %(lb/in^3) %Fluid_Density
visc=15.9869; %(cSt) %Fluid_Viscosity
KP_Leakage=Dp*Pwnom*(1-PVeff)*Pvisc_nom*Rho/(PPnom*visc*Rho); %Pump
Leakage Coefficient

%Motors

DmA=0.097; %(in^3/rev) %Motor_displacement
DmB=0.097; %(in^3/rev) %Motor_displacement
MVeff=0.95; %Motor_Volumetric_efficiency
MTeff=0.90; %Motor_Total_efficiency
MPnom=3000; %(psi) %Motor_Nominal_pressure
Mwnom=2000; %(rpm) %Motor_Nominal_angular_velocity
Mvisc_nom=5; %(cSt) %Motor_Nominal_kineMotortic_viscosity
I_mA=0.0005; %(kg/m^2) %Motor Inertia
B_mA=0.0026;%0.0026; %(Nm/(rad/s)) %Damping Coefficient %0.0020
I_mB=0.0005; %(kg/m^2) %Motor Inertia
B_mB=0.0022;%0.0022; %(Nm/(rad/s)) %Damping Coefficient %0.0019
KM_Leakage=DmA*Mwnom*(1-MVeff)*Mvisc_nom*Rho/(MPnom*visc*Rho); %Pump
Leakage Coefficient
KMB_Leakage=DmB*Mwnom*(1-MVeff)*Mvisc_nom*Rho/(MPnom*visc*Rho);
TL=0; %N.m

%Compressibility

SG=0.94;
Gamma=62.4*0.88;
Rho=844*0.000036127; %(lb/in^3) %Fluid_Density
Visc=15.9869; %(cSt) %Fluid_Kinematic_Viscosity
B=183695; %(psi) %Fluid Bulk Modulus
L=10; %(m) %Pipe_Length
D=(3/8); %(in) %Pipe_Diameter
A=pi*(D/2)^2;
g=32.174; %in/s^2;
V=55; % (in^3)
```

```
%Check Valve

P_0=1500; % (psi) Cracking Pressure
C=0.2; % Flow Coefficient 0.04 for one motor, 0.2 for two motors
A_disc=0.7; % (in^2) Area of the disc
I_b=(sqrt(A_disc/pi)*2*pi); % (in) disc perimeter
k_s=10; % (N/m) Spring stiffness

%PRV

Kzb=2.2;
P_b=3000;

%2-Way Directional Valve

A_max=1; %(in^2)
h_max=0.5; %(in)
C_d=1.5; %2.8 was the initial adjustment
x_0=h_max/2; %0 for adaptive%(in)

%MRAC
U_L=1000;
L_L=-1000;
```

Appendix B Linear State-Space Model

```
clc
close all
clear all


%State Space
u=1;
a11=-B/V*(KM_Leakage+KP_Leakage+KM_Leakage)/231;
a12=-B/V*DmA/231;
a13=-B/V*DmB/231;
a21=DmA/(I_mA*2*pi);
a22=-B_mA/I_mA;
a23=0;
a31=DmB/(I_mB*2*pi);
a32=0;
a33=-B_mB/I_mB;

A2=[a11 a12 a13;
    a21 a22 a23;
    a31 a32 a33];

B2=[B/V*Dp;
    0;
    0]/231;

C2=eye(3,3);

D2= zeros(3,1);
```

Appendix C Experimental Data Generation

```
close all
clear all
clc

%%
DATA=xlsread('mot1_2_300_400_3.csv');
DATA=DATA(17:end,:);

%%
clc

I=0.0014;
Time_E=DATA(:,1);
Flow_MA_E=DATA(:,2);
Flow_MB_E=DATA(:,3);
Speed_MA_E=DATA(:,4);
Speed_MB_E=DATA(:,5);
Flow_PB_E=DATA(:,6);
Pressure_E=DATA(:,8);
Speed_PB_E=DATA(:,9);
S_Time=Time_E(2)-Time_E(1);
```

Appendix D Least Square Method for Parameter Configuration

```
%% Least Square
%Motor A
X1=[Speed_MA_E Pressure_E];
Y1=231*Flow_MA_E;
Mot1=X1\Y1;
DmA=Mot1(1);
KM_Leakage=Mot1(2);

%Motor B
X2=[Speed_MB_E Pressure_E];
Y2=231*Flow_MB_E;
Mot2=X2\Y2;
DmB=Mot2(1);
KMB_Leakage=Mot2(2);

%Pump
X3=[Speed_PB_E Pressure_E];
Y3=231*Flow_PB_E;
Pump1=X3\Y3;
Dp=Pump1(1);
KP_Leakage=Pump1(2);
```

Appendix E Linear State-Space Model Stability Analysis

```
%Stability
SYS=ss(A2,B2,C2,D2);
TF=tf(SYS)

%Poles and Zeros
P1=pole(TF(1))
Z1=zero(TF(1))

P2=pole(TF(2))
Z2=zero(TF(2))

P3=pole(TF(3))
Z3=zero(TF(3))

%Bode Plot
figure
bode(TF(1))
grid on
title('FRF for the Transfer Function between x_1 and u'...
    ,'fontsize',11,'FontWeight','b')
hd = findall(gcf,'type', 'axes');
set(cell2mat(get(hd,'Xlabel')),'fontsize',11,'FontWeight','b')
set(cell2mat(get(hd,'Ylabel')),'fontsize',11,'FontWeight','b')
figure
bode(TF(2))
grid on
title('FRF for the Transfer Function between x_2 and u'...
    ,'fontsize',11,'FontWeight','b')
hd = findall(gcf,'type', 'axes');
set(cell2mat(get(hd,'Xlabel')),'fontsize',11,'FontWeight','b')
set(cell2mat(get(hd,'Ylabel')),'fontsize',11,'FontWeight','b')

figure
bode(TF(3))
grid on
title('FRF for the Transfer Function between x_3 and u'...
    ,'fontsize',11,'FontWeight','b')
hd = findall(gcf,'type', 'axes');
set(cell2mat(get(hd,'Xlabel')),'fontsize',11,'FontWeight','b')
set(cell2mat(get(hd,'Ylabel')),'fontsize',11,'FontWeight','b')
```

Appendix F Sample Plotting Code

```
clc
close all

%Pump Flow
figure

plot(Time_E,Flow_PB_E,'LineWidth',2)

hold on

plot(Time,Qp,'--r','LineWidth',2)

grid on

title('Pump Flow','fontsize',10,'fontweight','b')
xlabel('Time [s]','fontsize',10,'fontweight','b')
ylabel('Flow [Gal/min]','fontsize',10,'fontweight','b')
Leg1=legend('Experiment','Mathematical');
set(Leg1,'fontsize',10,'fontweight','b','Location','southeast')

%Motor A Flow
figure
plot(Time_E,Flow_MA_E,'LineWidth',2)

hold on

plot(Time,QmA,'--r','LineWidth',2)

grid on

title('Primary Motor Flow','fontsize',10,'fontweight','b')
xlabel('Time [s]','fontsize',10,'fontweight','b')
ylabel('Flow [Gal/min]','fontsize',10,'fontweight','b')
Leg1=legend('Experiment','Mathematical');
set(Leg1,'fontsize',10,'fontweight','b','Location','southeast')

%Motor B Flow
figure
plot(Time_E,Flow_MB_E,'LineWidth',2)

hold on

plot(Time,QmB,'--r','LineWidth',2)

grid on

title('Auxiliary Motor Flow','fontsize',10,'fontweight','b')
```

```
xlabel('Time [s]','fontsize',10,'fontweight','b')
ylabel('Flow [Gal/min]','fontsize',10,'fontweight','b')
Leg1=legend('Experiment','Mathematical');
set(Leg1,'fontsize',10,'fontweight','b','Location','southeast')

%Differential Pressure
figure
plot(Time_E,Pressure_E,'LineWidth',2)

hold on

plot(Time,P,'--r','LineWidth',2)

grid on

title('Pump Differential Pressure','fontsize',10,'fontweight','b')
xlabel('Time [s]','fontsize',10,'fontweight','b')
ylabel('Pressure [psi]','fontsize',10,'fontweight','b')
Leg1=legend('Experiment','Mathematical');
set(Leg1,'fontsize',10,'fontweight','b','Location','southeast')

%Motor A Speed
figure
plot(Time_E,Speed_MA_E,'LineWidth',2)

hold on

plot(Time,WmA,'--r','LineWidth',2)

grid on

title('Primary Motor Angular Velocity','fontsize',10,'fontweight','b')
xlabel('Time [s]','fontsize',10,'fontweight','b')
ylabel('Angular Velocity [rpm]','fontsize',10,'fontweight','b')
Leg1=legend('Experiment','Mathematical');
set(Leg1,'fontsize',10,'fontweight','b','Location','southeast')

%Motor B Speed
figure
plot(Time_E,Speed_MB_E,'LineWidth',2)

hold on

plot(Time,WmB,'--r','LineWidth',2)

grid on

title('Auxiliary Motor Angular
Velocity','fontsize',10,'fontweight','b')
xlabel('Time [s]','fontsize',10,'fontweight','b')
ylabel('Angular Velocity [rpm]','fontsize',10,'fontweight','b')
Leg1=legend('Experiment','Mathematical');
```

```
set(Leg1,'fontsize',10,'fontweight','b','Location','southeast')

%Pump B Speed
figure
plot(Time_E,Speed_PB_E,'LineWidth',2)

grid on

title('Pump Angular Velocity','fontsize',10,'fontweight','b')
xlabel('Time [s]','fontsize',10,'fontweight','b')
ylabel('Angular Velocity [rpm]','fontsize',10,'fontweight','b')
Leg1=legend('Experiment','Mathematical');
set(Leg1,'fontsize',10,'fontweight','b','Location','southeast')
```

Appendix G Simulink Model Block Diagrams

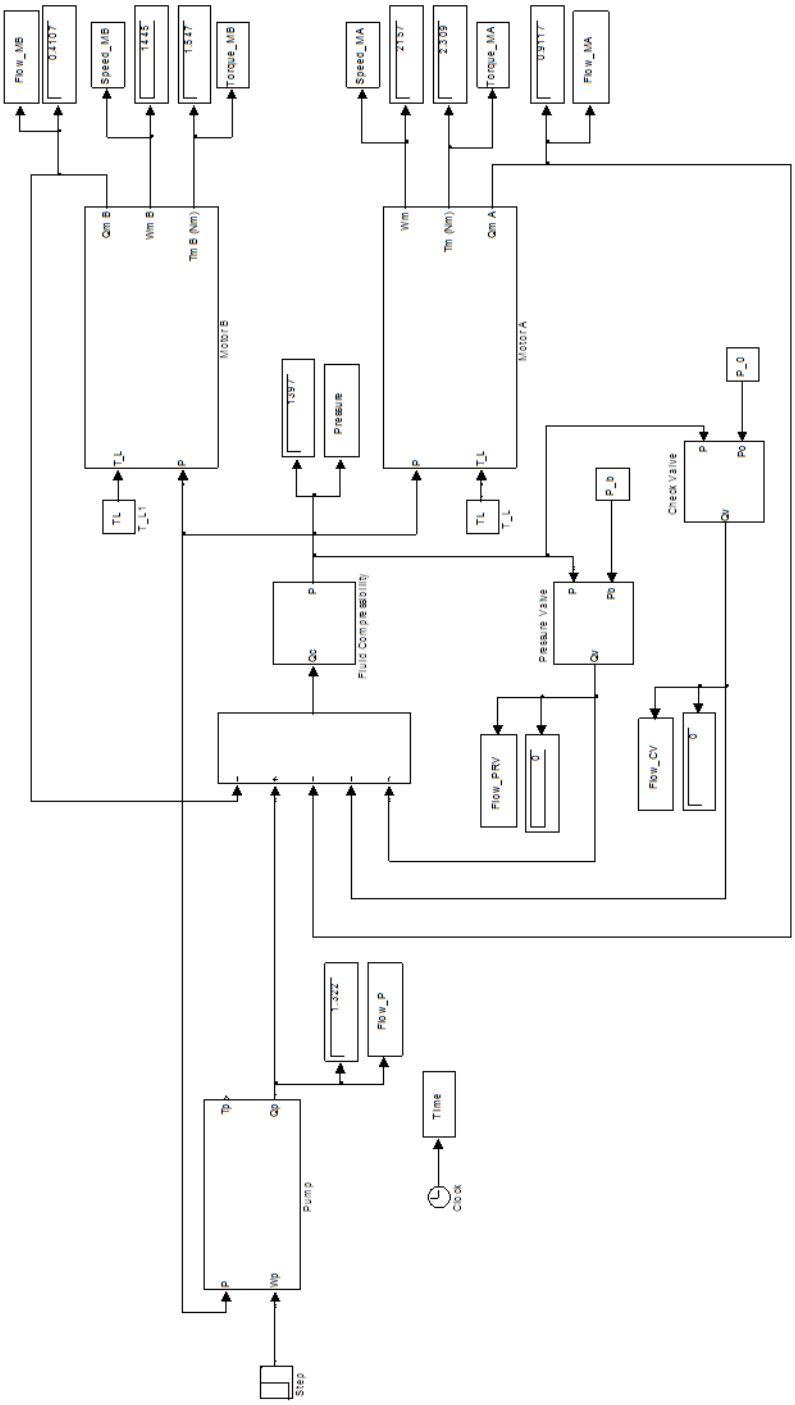

Figure A.1 Simulink model of the mathematical model (ODE) of the hydraulic system

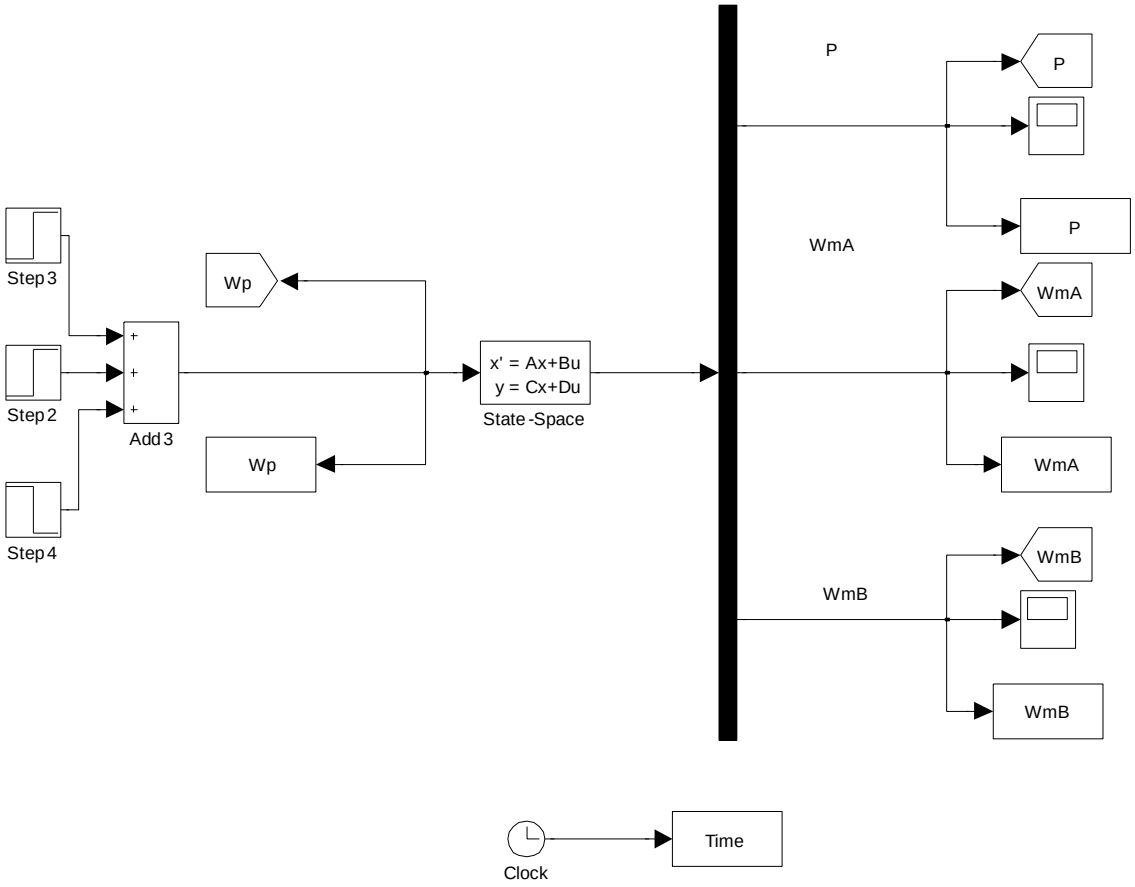

Figure A.2 Simulink model of the linear state-space model of the hydraulic system

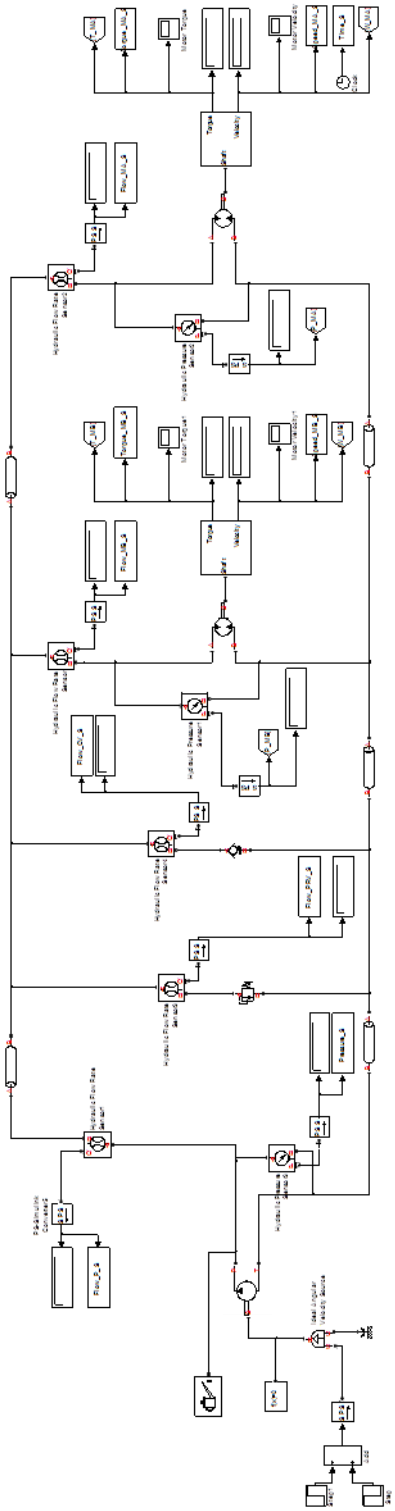

Figure A.3 SimHydraulics model of the hydraulic system